From the holdings of the Department of Special Collections , Princeton University Library, Princeton, NJ

These documents are either in the public domain, or can only be used for educational and research purposes (Fair use) as per U.S. Copyright law (text below). By accessing this file, all users agree that their use falls in the public domain or within fair use as defined by the copyrightlaw. We do not charge any permission or usage fees for the publication of images of material inour collections, including those provided by Princeton University Library, via our website, catalog, or directly from staff.For more information regarding copyright, credit, and citation please review the information onthe Copyright, Credit and Citation Guidelines page of our website.
https://library.princeton.edu/special-collections/policies/copyright-credit-and-citation-guidelines. If you have any questions, including how to order higher-quality images from the collection, contact Special Collections Public Services via our Ask Us! Form. https://library.princeton.edu/special-collections/ask-us

---

Doctoral Dissertations, 2011-2026 Psychology

2020

INVESTIGATING STRUCTURAL PLASTICITY AND PERINEURONAL NETS IN THE HIPPOCAMPUS AND DORSAL STRIATUM

Briones, Brandy Angeline

Princeton, NJ : Princeton University

---

http://arks.princeton.edu/ark:/88435/dsp01xw42nb95b

U.S. Copyright law: The copyright law of the United States (Title 17, §108, United States Code) governs the making of photocopies or other reproductions of copyrighted material. Under certain conditions specified in the law, libraries and archives are authorized to furnish a photocopy or other reproduction. One of these specified conditions is that the photocopy or reproduction is not to be used for any purpose other than private study, scholarship, or research. If a user makes a request for, or later uses, a photocopy or reproduction for purposes in excess of fair use that user may be liable for copyright infringement. This institution reserves the right to refuse to accept a copying order if, in its judgment, fulfillment of the order would involve a violation of copyright law. https://www.copyright.gov/title17/title17.pdf

INVESTIGATING STRUCTURAL PLASTICITY AND PERINEURONAL NETS IN THE HIPPOCAMPUS AND DORSAL STRIATUM

Brandy Angeline Briones

A DISSERTATION PRESENTED TO THE FACULTY

OF PRINCETON UNIVERSITY

IN CANDIDACY FOR THE DEGREE

OF DOCTOR OF PHILOSOPHY

RECOMMENDED FOR ACCEPTANCE BY

THE DEPARTMENT OF PSYCHOLOGY

Adviser: Elizabeth Gould

September 2020

© Copyright by Brandy Angeline Briones, 2020. All rights reserved.

ABSTRACT

My dissertation investigates hippocampus and dorsal striatum-dependent plasticity, specifically, to better understand inhibitory neurons and perineuronal nets (PNNs), specialized extracellular matrix structures. These structures have been studied extensively within the developing visual cortex and are typically thought of as restraints on structural and synaptic plasticity, but it is unknown what role, if any, inhibitory neurons and PNNs play in regions exhibiting high degrees of experience-dependent plasticity throughout adulthood.

In the hippocampus, I investigated adult-born granule cell (abGC) projections onto GABAergic inhibitory parvalbumin (PV+) interneurons, many of which are PNN+, and discovered that abGC mossy fiber boutons are more often associated with PV+PNN+ interneurons. These results, while unexpected, suggest a more complex region-specific role for PNNs in the adult mammalian brain. To further investigate this possibility, I turned to the dorsal striatum, a region I have demonstrated exhibits experience-dependent dendritic spine plasticity of inhibitory medium spiny neurons (MSNs). To better understand how PNNs influence inhibitory signaling and linked behaviors, I examined PNNs in the dorsomedial striatum (DMS) of four mouse models of behavioral inflexibility and excessive repetitive behavior. Across all models, I observed consistent over-expression of PNNs surrounding PV+ interneurons, further implicating PNN involvement in mechanisms of inhibitory plasticity. I also found that reducing PNNs diminishes excessive repetitive behaviors. To characterize the effects of increased PNNs on inhibitory signaling, I investigated electrophysiological and structural properties of DMS MSNs. Mice with increased PNNs showed decreased MSN dendritic spines and altered inhibitory signaling compared to healthy controls, and while reduction of DMS PNNs altered inhibitory signaling, it did not “normalize” it. These findings additionally suggest that an overabundance of PNNs in the DMS prevents adaptive disengagement from repetitive behaviors, potentially through abnormal inhibitory signaling, but further studies are required to identify the mechanisms by which PNNs might gate this behavior.

These studies taken together demonstrate that PNNs play complex roles that differ depending on brain region; hippocampal PNNs participate in structural plasticity via connectivity from abGCs, and conversely, DMS PNNs are related to mechanisms of behavioral rigidity in mouse models of excessive repetitive behaviors.

Table of Contents

Abstract.....iii

Acknowledgements vi

Chapter 1: Structural plasticity in the hippocampus..... 1

Chapter 2: Structural plasticity in the striatum 20

Chapter 3: Adult-born granule cell mossy fibers preferentially target parvalbumin-positive interneurons surrounded by perineuronal nets 45

Chapter 4: Investigating the role of perineuronal nets and striatal plasticity in mouse models with excessive repetitive behaviors 76

Concluding Remarks 105

References..... 107

ACKNOWLEDGEMENTS

I have had a tremendous amount of support throughout this journey and would like to express my gratitude to all who have made this possible. The culmination of this work has been a concerted effort, and I am thankful to so many for encouraging me to complete this dissertation and receive my doctorate.

First, I would like to thank my PhD advisor, Dr. Elizabeth Gould, for everything she has done to support me and help me succeed. Liz, I cannot even begin to tell you how much of a positive impact you have had on my life. I have learned and grown so much under your guidance and will no doubt continue to learn from you even after I leave the lab. Thank you for inspiring me to be a thoughtful and diligent scientist, giving me the confidence to experiment and be curious, and encouraging me through all the highs and lows that I have experienced along the way. I feel so lucky to have you as my graduate research mentor, and even luckier to have you as a friend.

Many thanks to all the past and present Department of Psychology and Princeton Neuroscience Institute staff, students, and faculty for providing me with a supportive community and many cherished memories. Especially, thank you to my thesis committee members, Dr. Ilana Witten, Dr. Tim Buschman, and Dr. Jordan Taylor, for all your thoughtful input on my experiments and dissertation, and even more so, for the friendly conversations we have shared across the years. I am so appreciative for the opportunities to collaborate with your labs; this work would not have been possible otherwise. Ilana, thank you for being my secondary advisor, it has been wonderful getting to be a part of the fun Witten lab outings – thank you for including me. Thank you to my oral committee members, Dr. Casey Lew-Williams and Dr. Jonathan Pillow. You both have been an integral part of my graduate school experience; thank you for always taking the time to check-in with me and making me feel like I belonged. Thank you to Dr. Esteban Engel and Dr. Heather Cameron for your input, collaboration, and expertise throughout the retrovirus-labeled new neuron project, this project would not have been possible without you.

To my past and present lab mates and collaborators, you all have made my experience in the lab a truly memorable one. First, I would like to thank undergraduate researchers, Uma, Vincent, Amanda, and Miah, for working tirelessly on the work presented in this dissertation, I am

so proud and honored to have gotten the opportunity to mentor you all. Amanda, thank you for always bringing a smile to my face, for your friendship and dedication, and importantly, for helping me learn how to be a better researcher and mentor. Miah, thank you for your inspiration and contributions to these projects, much of this work would not have been possible without you. I am so grateful for our friendship, from neuroscience to volleyball you are truly impressive. I look forward to hearing about your graduate research at Berkeley. To my collaborators, Tom, Camden, and Alex, thank you for putting in so much time and effort to make these projects possible. To Emma, Renée, Blake, Pierre-Antoine, and Anna, our WaWa, Nassau, and other miscellaneous outings have been crucial to my sustained work ethic. Thank you all for your friendship, help, and encouragement, it has been an absolute pleasure to work with all of you and I wish you all the very best as you continue your graduate research. Gary, thank you for teaching me everything I know about linear mixed effects models and coding in R. To the Gould lab postdocs, Elise and Sahana, our time together has overlapped essentially my entire time as a graduate student. I thank you both very much for your support and for all the memories we have shared along the way, from game nights to baking cupcakes, there has never been a dull moment. Thank you to my cohort, Jessie, Mai, Aaron, Cam, Angela, and Nina, and all the friends I have made here at Princeton for making my experience such an enjoyable one.

Big thanks to my friends: Maya, I never would have imagined that graduate school would bring me such a special friendship as ours, you are an incredible neuroscientist, and I am grateful to have a role model like you. Liz and Cosmo, you two were the best roommates; always there to help brighten my days, eat good food, play volleyball and so many other games, at times when I needed to break from work. Tyler and Jamal, thank you for inspiring me to try new things and always being a source of comic relief. Weston, thank you for being there, for going on endless adventures with me, for collaborating with me, for all the support and encouragement when I needed it most – a true friend and one I will forever cherish. To my cat Thorndike, while you will never be able to read this, you are the purest, fluffiest, and best companion I have had through this entire journey.

To my loving family – Mom, Dad, and Dean – you all mean the world to me. Thank you for always being there for me even though, physically, we have been far apart. I could not have made it to this point in my life without your love and support. I know at times life has been tough, but even through it all you have always made time for me: visited me, helped me move, our many phone calls, and sent care packages. Thank you and much love to my enormous extended family, you all are a special bunch. Last, but not least, a special thank you to my Grandparents for their constant encouragement, support and love, and letting me know that I am your favorite granddaughter. Thank you all for making this experience a truly remarkable one. I hope that I can give back as much, to each and every one of you, as has been given to me.

Reflecting on these past six years, I am moved with overwhelming feelings of gratitude. With each learning moment, I have grown more and more, and come to realize that I know less and less.

Life is so fluid that one can only hope to capture the living moment, to capture it alive and fresh…without destroying that moment.

The possession of knowledge does not kill the sense of wonder and mystery. There is always more mystery.

– Anaïs Nin

CHAPTER 1: STRUCTURAL PLASTICITY IN THE HIPPOCAMPUS

Adapted from Briones BA, Gould E. (2019) Neurogenesis and Stress, Handbook of Stress vol 3: Stress, Physiology, Biochemistry and Pathology. Chapter 7 – Adult Neurogenesis and Stress. Jan 18; 79-92.

Chapter Introduction

This chapter highlights adult neurogenesis, an important form of neuronal plasticity that is involved in the sculpting of and reorganization of inhibitory circuits throughout the lifespan. It has been demonstrated that the generation and integration of newborn neurons are greatly affected, both positively and negatively, by changes in the systems' internal and external environment through changes in circulating hormones and physiological stress response, acute and chronic stressors, enriched environment, exercise, and learning, to name a few. Gaining a better understanding of the processes and factors that alter inhibitory neurons and their connections may provide added insight into what roles non-neuronal structures, such as perineuronal nets (PNNs), might play in inhibitory plasticity. While this chapter primarily focuses on hippocampal plasticity and adult neurogenesis, I have provided some preliminary evidence suggestive of striatal neurogenesis in the adult rodent brain, albeit at a significantly lower rate than that of the hippocampus. However, these differences may be evidence suggestive of brain region-specific mechanisms of plasticity, a question that I will dive into deeper in the studies presented in later chapters.

Adult Neurogenesis

The hippocampus is a highly plastic region displaying an unusual amount of structural plasticity throughout the lifespan, including the addition of entirely new neurons into the preexisting circuitry, a process termed adult neurogenesis. The hippocampus functions on a dorsal-ventral axis (see reviews by Fanselow and Dong, 2010; Moser and Moser, 1998). Dorsal subregions of the hippocampus are important for spatial and episodic memory encoding (Moser et al., 1993, 1995), whereas ventral areas are involved in stress-related regulatory functions involving amygdalar circuits and the hypothalamic-pituitary axis (Bannerman et al., 2003; Kim and Fanselow, 1992; McHugh et al., 2011). The hippocampus-focused studies throughout this

dissertation will focus primarily on dorsal areas of the hippocampus, namely the dorsal dentate gyrus (see **Fig S3.1** for example anatomical representations).

A significant portion of my dissertation work has focused on the production of new neurons in the dentate gyrus of the hippocampus. This process occurs in three distinct phases across differing time points, including: gestation, the early postnatal period, and adulthood. During gestation, new neurons are born in the ventricular zone and migrate across the hippocampal rudiment to populate the embryonic dentate gyrus (Altman and Bayer, 1990; Schlessinger et al., 1975). During the postnatal period, progenitor cells migrate into the dentate gyrus and continuously produce new neurons, specifically new granule cells, which then help to form the granule cell layer (Altman and Bayer, 1990; Schlessinger et al., 1975). In young adulthood, these progenitor cells lie on the border of the granule cell layer and hilus, a region known as the subgranular zone (SGZ), of the hippocampus. The progenitor cells divide, and their daughter cells differentiate into new granule cells throughout adulthood, but at a slower rate with advanced age (Seki and Arai, 1995).

It has been well established that new neurons in the dentate gyrus receive synaptic input (Kaplan and Bell, 1984; Kaplan and Hinds, 1977; van Praag et al., 2002; Toni et al., 2007), extend axons into the mossy fiber pathway (Hastings and Gould, 1999; Stanfield and Trice, 1988), and establish functional synapses with hilar interneurons, mossy cells, and pyramidal cells of the CA2 and CA3 regions (Toni et al., 2008). This circuit organization serves to form a feedforward inhibitory circuit (Marín-Burgin et al., 2012; Song et al., 2013), playing a functional role in dentate gyrus-dependent learning and memory (Akers et al., 2014; Gould et al., 1999a), pattern separation (Sahay et al., 2011), and exploration and context encoding of novel environments (Danielson et al., 2016; Kheirbek et al., 2012). Neurogenesis is a highly dynamic process, consisting of multiple modifiable stages, and because it occurs throughout the lifespan, it is susceptible to modification by experience. In this section, I will highlight how experience affects adult neurogenesis and hippocampal-dependent behaviors.

The development of the CAG-GFP retrovirus labeling technique has allowed for increased temporal and structural resolution to visualize hippocampal newborn neuron connectivity (Zhao et al., 2006). The stages of abGC maturation were described in that study as follows: 1) mitotic cells begin differentiating, polarization, migration, and initial axonal dendritic growth (< 4 days post infection). 2) Dendrites and axons extend, axon fibers arborize and reach the CA3 area (1-2 weeks post infection (wpi). 3) Dendritic spine growth occurs, and dendrites and axons continue to grow (2-8 wpi). 4) Structural modifications on spines and synapses, dependent on experience and environment (3-18 wpi). I utilized this technique in the research study described in Chapter 3.

There is evidence to support adult neurogenesis in both the SVZ and hippocampus across multiple mammalian species. I had found preliminary evidence suggestive of newborn neurons in the rat striatum (see image examples in **Fig 1.1**), a finding that has also been reported by others in humans, rabbits, and rats (Dayer et al., 2005; Ernst et al., 2014; Luzzati et al., 2006). However, because this phenomenon seems to occur at a much lower rate in the striatum than in the hippocampus, and because it has not been extensively studied, I will focus on the hippocampus and how adult neurogenesis is impacted by environment-dependent experiences in this chapter.

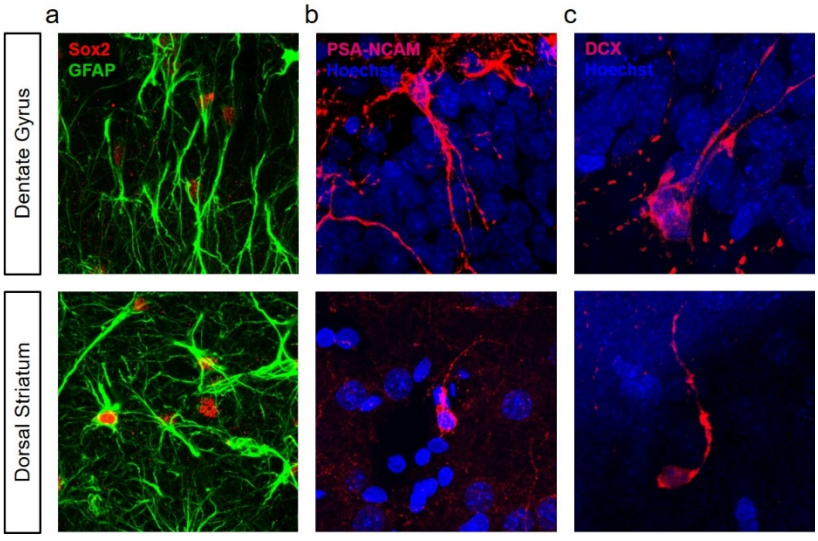


Figure 1.1 Positive evidence for cells with immature neuronal characteristics in the hippocampus and striatum. (**a**) Expression of progenitor cell marker Sox2 in the adult rat dorsal striatum (bottom) is similar to expression in the DG (top). (**b-c**) Markers of 3+ week old immature neurons, PSA-NCAM (middle) and DCX (right), express similarly in DG and dorsal striatum.

Species differences in adult hippocampal neurogenesis

In addition to having been reported in birds (Alvarez-Buylla et al., 1988; Barnea and Nottebohm, 1994; Ling et al., 1997) and reptiles (Pérez-Cañellas and García-Verdugo, 1996; Perez-Sanchez et al., 1989; Yanes et al., 1990), adult neurogenesis has been reported in the hippocampus of a large number of mammalian species, including mice, voles, rats, hamsters, squirrels, chipmunks, guinea pigs, rabbits, hedgehogs, pigs, sheep, opossum, foxes, cats, dogs, minks, ferrets, tree shrews, marmosets, squirrel monkeys, and macaques (Amrein and Slomianka, 2010; Gould et al., 1997, 1998, 1999b; Hwang et al., 2007; Leuner et al., 2007; Simon et al., 2005) (**Fig. 1.2**). Early reports searching for adult neurogenesis in bats failed to find positive evidence; however, subsequent studies showed that the process of capturing bats reduces the expression of doublecortin (DCX), an immature neuron marker, which is commonly used to assess adult neurogenesis. Once this was controlled for, it was shown that several species of bats do indeed exhibit evidence of adult neurogenesis in the hippocampus (Chawana et al., 2014; Gatome et al., 2010). Since capture is a significant stressor, and stress is known to inhibit adult neurogenesis (Bain et al., 2004; Heine et al., 2004; Malberg and Duman, 2003), it seems that the earlier reports were likely false negatives. Altogether, adult neurogenesis has been demonstrated in over 30 species of mammals (Amrein and Lipp, 2009).

Most studies investigating adult hippocampal neurogenesis in different species did not compare across species within a given experiment. Thus, the comparisons made across species are frequently confounded by the fact that different markers, procedures, and visualization techniques were used. Additionally, the animals across experiments did not have the same life experiences (including stress levels), which greatly impact neurogenesis. Yet, broadly these studies indicate that species differ in their rates of adult hippocampal neurogenesis. For example, high numbers of new neurons are consistently demonstrated in the hippocampus of young adult rats compared to what has been reported in the hippocampus of young adult macaques. This may arise from species-related differences that impact the selection of appropriate techniques for investigating new neurons. It is also possible that young adult macaques exhibit relatively lower

rates of neurogenesis, because these animals are born in a more mature state than rats. Because infant macaques are considerably more precocious than are newborn rat pups, by the time they reach adulthood, they are likely farther along in the developmental trajectory than rats in adulthood. Age-related decline in adult hippocampal neurogenesis is well accepted and seems highly conserved across species (**Fig. 1.2**). However, if differences in the rate of age-related decline are not adjusted for in comparisons across species, they will differ in their apparent rates of adult neurogenesis. Notwithstanding the potential differences in rates of adult neurogenesis in the hippocampus between species, the large number of species in which adult neurogenesis has been demonstrated raises the possibility that this is a feature of all mammalian brains, including those of humans. Since humans are considerably more altricial than macaques, it seems plausible that they would display a relatively higher rate of adult neurogenesis.

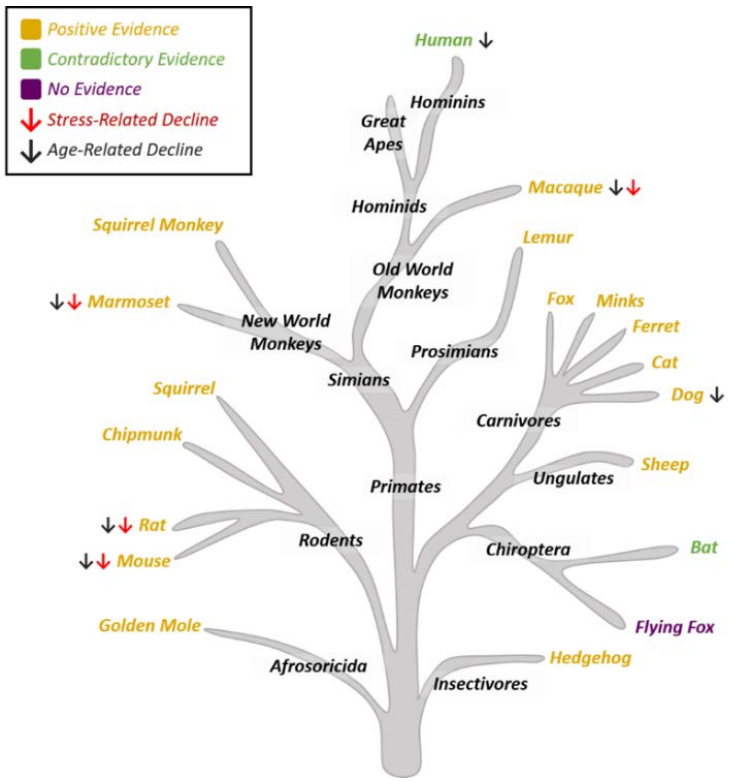


Figure 1.2 Partial phylogenetic tree depicting mammals with positive, contradictory, or lack of evidence for adult neurogenesis in the hippocampus. Overall, this evidence suggests that adult neurogenesis is a common phenomenon of the hippocampus across mammalian species. Animals showing positive evidence are depicted in gold, those for which contradictory evidence exists are shown in green, and those that have not been investigated are shown in purple. Species for which age-related decline and stress-induced decline in adult neurogenesis have been reported are indicated with colored down arrows. Species not included in this tree but for which positive evidence exists, include: voles, hamsters guinea pigs, rabbits, pigs, opossums, and tree shrews.

The question of whether adult neurogenesis exists in the human hippocampus has received a considerable amount of attention over the past decades (Boldrini et al., 2018; Dennis et al., 2016; Eriksson et al., 1998; Knoth et al., 2010; Pereira et al., 2007; Sorrells et al., 2018; Spalding et al., 2013). Some researchers have suggested that the continual addition of new neurons is not compatible with maintaining stable memories over the long lifespan of humans (Akers et al., 2014); however, computational studies suggest that adult neurogenesis is highly consistent with some of the cognitive capabilities displayed by humans (Aimone et al., 2010). The experimental evidence for adult neurogenesis in the hippocampus has been contradictory. Twenty years ago, the first convincing report of adult neurogenesis in the human hippocampus was published, demonstrating robust neurogenesis even in older humans dying of cancer (Eriksson et al., 1998). This initial study was followed by several reports corroborating these findings using direct and indirect methods to measure adult neurogenesis (Boldrini et al., 2018; Knoth et al., 2010; Pereira et al., 2007; Spalding et al., 2013). Some groups have failed to find evidence for adult hippocampal neurogenesis using traditional immunohistochemical methods (Dennis et al., 2016; Sorrells et al., 2018), which puts the positive findings into question. In response to these lack of findings, experts in the field have emphasized the importance of tissue collection and processing methodologies (Kempermann et al., 2018; Moreno-Jiménez et al., 2019). All of these studies have examined biopsy and/or autopsy tissue. Since the biopsy samples were all obtained from people with abnormal hippocampi, typically as a result of a hippocampal seizure focus, it is difficult to assess negative or positive data resulting from these studies. Often before surgery is performed, people with epilepsy already have significant hippocampal sclerosis with considerable reactive gliosis. Negative evidence could be the result of a depletion of resident progenitors or excessive glia inhibiting ongoing neurogenesis. Positive evidence might arise from damage-induced neurogenesis, which has been reported in rodent species (Gould and Tanapat, 1997; Jin Kunlin et al., 2004; Parent, 2003; Parent et al., 1997). With regard to autopsy samples, there are several important issues to consider. The first is postmortem interval, which is often considerable (over 2 days), and has been shown to negatively

impact histological measures, including DCX staining (Boekhoorn et al., 2006; Swaab and Uylings, 1988). The next is the lifestyle of the individual, which may have included experiences known to reduce adult neurogenesis (see below).

Additional concerns include human-specific technical problems, such as the possibility that immature neuron markers may not be the same across species and the presence of high levels of autofluorescent lipofuscin in the adult human brain, which may obscure positive staining or produce false positives. These concerns, taken together with contradictory papers in the literature using the same methods (**Table 1.1**), suggest that replicability and reproducibility are dependent on precise methodology and transparency in reporting and sharing of methods. A recent publication from the Llorens-Martín lab effectively demonstrates the importance of proper controls and careful methodologies to study postmortem human tissue (Moreno-Jiménez et al., 2019). Using these proper controls, these investigators found convincing evidence for adult neurogenesis in the human hippocampus. An innovative study was done looking at the age of neurons in postmortem brain tissue using an isotope of carbon, ^{14}C, as a birth dating method, given the presence of this isotope in the atmosphere during the time of nuclear bomb testing. While this study provides evidence for adult neurogenesis in the human hippocampus, it has been criticized because of large variability across individuals and its dependence on using adults living during a specific time period (Spalding et al., 2013). In addition, given that the data were obtained from postmortem samples, confounds related to the cause of death, lifestyle, and postmortem interval must be considered. Definitive evidence of adult neurogenesis in the human hippocampus likely requires technical innovations, such as *in vivo* imaging, which allows for the identification of new neurons in healthy individuals living “proneurogenic” lifestyles. A previous paper moved in this direction using cerebral blood volume in the dentate gyrus as a proxy for evidence of adult neurogenesis (Pereira et al., 2007) and found indirect evidence for increased neurogenesis in adult humans after physical exercise, an experience that is known to increase neurogenesis in adult rats and mice (van Praag et al., 1999; Rhodes et al., 2003). This work, amongst others, reaffirms adult neurogenesis as a robust phenomenon in the dentate gyrus of

mammalian species. Notwithstanding the controversy about whether adult neurogenesis occurs in the human hippocampus, a considerable number of studies have investigated the regulation of new neuron formation in the hippocampus of experimental animals by experience.

	Research Group	Brain Region(s) Analyzed	Technique(s) and/or Markers Used	Evidence	Subjects
Positive	Eriksson et al., 1998	Dentate gyrus, SVZ	Immunohistochemistry: BrdU-labeling, combinend with neuronal markers NeuN, calbindin, NSE	BrdU+ NeuN+, BrdU+ Calbindin+labeling, and BrdU+NSE+ staining in the dentate gyrus, only.	Postmortem tissue from BrdU-treated cancer patients (57-72yrs)
	Pereira et al., 2007	Hippocampal subregions	In vivo imaging of cerebral blood volume using MRI with a contrast agent	Bran region specific exercise-induced increase in blood volume similar to what is observed in rodents with incresed adult neurogenesis	Healthy, living young-middle aged adults (21-45 yrs)
	Knoth et al., 2010	Dentate gyrus	Immunohistochemistry: immature neuronal marker DCX	DCX+ cells in the dentate gyrus	Postmortem tissue (fetal-100yrs); many causes of death
	Spalding et al., 2013	Dentate gyrus	^{14}C labeling of neurons measured by accelerator mass spectroscropy	^{14}C labeled neurons in individuals who were adult during nuclear bomb testing	Postmortem tissue (19-92yrs); many causes of death
	Boldrini et al., 2018	Dentate gyrus	Immunohistochemistry: immature neuronal marker DCX and PSA-NCAM	DCX+/PSA-NCAM+ cells in the dentate gyrus	Postmortem tissue (14-79yrs); many causes of death
	Moreno-Jiménez et al. 2019	Dentate gyrus, CA1 & CA3 hippocampal subfields, entorhinal cortex	Immunohistochemistry: immature neuronal marker DCX, combined with neuronal markers NeuN, calretinin	DCX+ cells in the dentate gyrus, only	Postmortem tissue (43-87yrs) from neurologically healthy adults
Negative	Dennis et al., 2016	Dentate gyrus, SVZ	Immunohistochemistry: immature neuronal marker DCX	Absent or sparse DCX+ labeling in adults	Postmortem tissue (infant-59yrs)
	Sorrells et al., 2019	Dentate gyrus, SVZ	Immunohistochemistry: immature neuronal marker DCX and PSA-NCAM	No DCX+/PSA-NCAM+ cells in the dentate gyrus after age 13yrs	Postmortem tissue (fetal-79yrs); many causes of death

Table 1.1 Published studies investigating evidence for adult neurogenesis in the hippocampus of humans. Contradictory evidence exists on whether humans produce new neurons into adulthood despite substantial positive evidence in other mammalian species. This table lists both positive and negative evidence in the literature, comparing the subjects and techniques used, and specific evidence found. *BrdU*, 5-bromo-2'-deoxyuridine; *DCX*, doublecortin; *MRI*, magnetic resonance imaging; *NeuN,* neuronal marker; *NSE,* neuron-specific enolase; *PSA-NCAM,* polysialylated-neural cell adhesion molecule; *SVZ,* subventricular zone.

Stressful experience effects on adult neurogenesis

Many studies have investigated the influence of stressful experiences on adult neurogenesis in the hippocampus using a wide range of stressors, including social stress, physical pain and illness. Although there are some inconsistencies in the literature, the majority of studies suggest

that stress has a suppressive effect on adult neurogenesis. Depending on the stage of adult neurogenesis (i.e., cell proliferation, neuronal differentiation, cell death), stressful experiences differ in their impact. Although most stress manipulation studies on adult neurogenesis have been carried out in rodent species, there is evidence for stress-induced new neuron formation in other species, including birds, tree shrews, and marmosets (Gould et al., 1997, 1998; Robertson et al., 2017). Additionally, it is worth emphasizing that observations of low or absent levels of adult neurogenesis (i.e. bats, macaques, and humans) may be explained by stress experienced by the organism prior to death.

Both the type and duration of stressor impact adult neurogenesis at different stages (**Fig. 1.3**). Studies have shown that a single exposure to a stressful experience can result in a decrease in cell proliferation in the adult rat dentate gyrus. Exposure to electric footshock (Malberg and Duman, 2003), restraint (Bain et al., 2004; Pham et al., 2003), cold swim (Heine et al., 2004), and predator odor (Falconer and Galea, 2003; Hill et al., 2006; Tanapat et al., 2001) have been reported to suppress adult hippocampal neurogenesis by lowering the rate of cell proliferation. A study examining the effects of predator odor exposure on adult neurogenesis failed to find a decrease in cell proliferation. However, this lack of effect is most likely a result of the experimental design, in which the experiment used BrdU (5-bromo-2'-deoxyuridine) labeling, a technique used to identify proliferating cells, prior to predator odor exposure, hence making a direct test of effects on cell proliferation impossible (Thomas et al., 2006). Multiple studies show that single episodes of subordination stress in adult mice, tree shrews, and marmosets decrease cell proliferation in the dentate gyrus (Gould et al., 1997, 1998; Lagace et al., 2010). In rats, subordination stress did not significantly affect cell proliferation, but rather decreased neuron survival (Thomas et al., 2007). As is evident in these studies, it is important to consider timing, techniques, and species used in the experimental design to assess whether or not the design is adequate to test neurogenic changes at various stages. In contrast, acute sleep deprivation has been shown to increase cell proliferation (Grassi Zucconi et al., 2006), and acute restraint stress

does not appear to elicit any notable changes in cell proliferation (Pham et al., 2003; Rosenbrock et al., 2005).

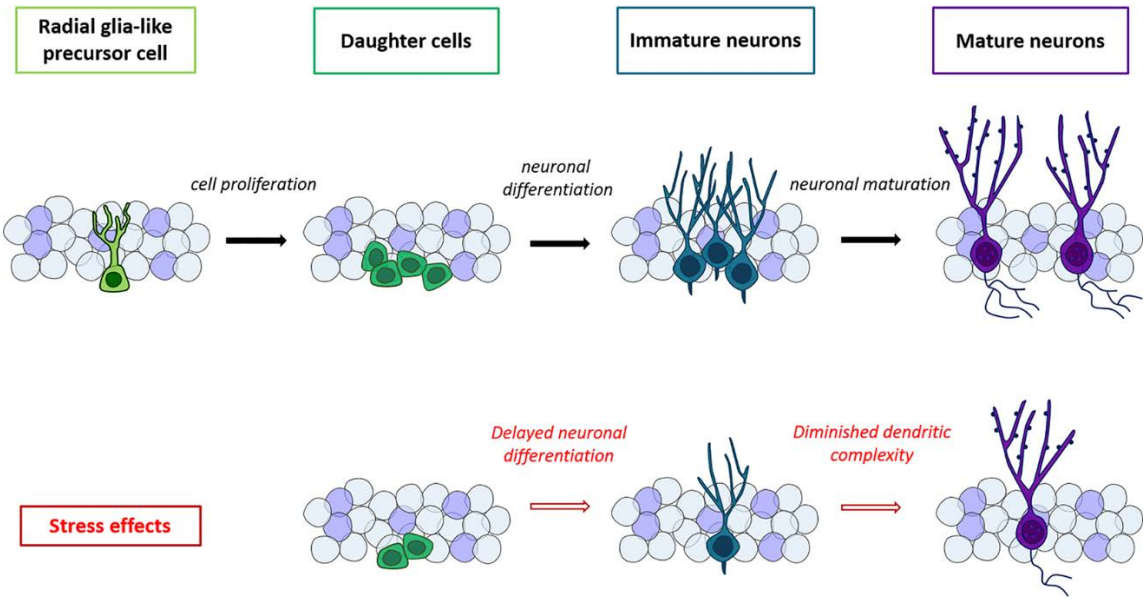


Figure 1.3 Stages of adult hippocampal neurogenesis and how stress can affect neurogenesis continuously or at different stages. This simplified schematic shows radial glia-like precursor cells proliferating and producing daughter cells, which then differentiate into immature neurons. A portion of these immature neurons will survive and become mature neurons, which have the potential to influence the hippocampal circuitry. Different stressors have been shown to affect adult neurogenesis by decreasing the number of proliferating cells, delaying neuronal differentiation, reducing the number of adult0born granule cells and diminishing their dendritic complexity.

These reported differences in effects of exposure to various stressful experiences on cell proliferation in the hippocampus raise the question of whether different stressors have similar effects on physiological stress systems. For instance, it is possible that certain stressors are more aversive than others. For example, restraint stress may not be particularly aversive to rodents with natural tendencies for burrowing behaviors, whereas predator odor exposure elicits an innate inhibitory behavioral response, and electric shock is likely to be especially aversive, because it is physically painful. These differences strongly suggest that there is not one specific effect of all stressful experiences on adult neurogenesis, but rather that different types of experiences are

likely to have varied influences on this process depending on how the stimulus is interpreted physiologically by the organism.

Studies involving repeated or chronic stress exposure to a variety of stressors, ranging from physical restraint to social stress, have shown decreases in both the proliferation and survival of immature granule cells in the adult dentate gyrus (Czéh et al., 2007; Ferragud et al., 2010; Hillerer et al., 2013; Pham et al., 2003; Simon et al., 2005; Van Bokhoven et al., 2011). Most of these studies are consistent with acute effects of the same stressors on these measures. By contrast, chronic sleep deprivation has been shown to exert the opposite effect on cell proliferation compared to the effect of short-term sleep deprivation. While the latter experience produced an increase in cell proliferation, long-term sleep deprivation, using forced locomotion, produced a reduction in cell proliferation (Guzmán-Marín Ruben et al., 2004; Mirescu et al., 2006; Sompol et al., 2011; Tung et al., 2005).

Chronic social stressors have been shown to decrease cell proliferation in tree shrews (Czéh et al., 2001; Simon et al., 2005) and rats (Czéh et al., 2007), as well as to slow differentiation of new neurons in mice (Ferragud et al., 2010). During a chronic social defeat stress paradigm, adult C57BL/6 subordinate mice were subjected to 10 consecutive days of social defeat interactions with an unfamiliar aggressor and subsequently housed in the same cage, with the aggressor, separated by a partition, for 24 h. Approximately, 30 days after the chronic social defeat stress paradigm, the morphology and electrophysiological properties of adult-born neurons, labeled post-stress using a retrovirus, were examined. The results showed a decrease in neuron survival and dendritic complexity, but no apparent change in new neuron firing properties (Chen et al., 2016). Contradictory evidence reported an increase in newborn granule cell survival after chronic social defeat stress in mice. However, these mice exhibited more social avoidance behaviors compared to their counterparts that did not show an increase in cell survival (Lagace et al., 2010). This study suggests that the interaction of sociability and stress may have more nuanced effects on adult neurogenesis than previously thought.

Although laboratory studies using the stress paradigms mentioned previously are informative in understanding stress effects on neurogenesis, it is often rare that animals in the wild have these experiences in nonsocial and unenriched contexts. Some studies have incorporated more complex environments into the experimental design to measure behavior in an ethologically relevant way using enriched caging, such as with the visible burrow system (VBS) (Blanchard et al., 1995; Kozorovitskiy and Gould, 2004; Opendak et al., 2016) or seminatural outdoor living enclosures (Cope et al., 2019). These studies have shown that the effects of stress on adult neurogenesis are dependent on the overall context in which the stressor is applied. A good example of the complexity of such responses can be observed with dominance hierarchy studies on adult neurogenesis using a VBS apparatus. When rats are housed in a VBS, they quickly form dominance hierarchies, where the dominant is defined as the most aggressive rat. Despite considerable fighting in the novel environment, neither dominants nor subordinates display decreases in adult neurogenesis measures (cell proliferation and overall new neuron number) once the hierarchy stabilizes. In fact, dominants exhibit more new neurons in the dentate gyrus compared with both subordinates and caged controls (Kozorovitskiy and Gould, 2004). These results are surprising at face value given the amount of fighting bouts dominants experience day to day, but analysis of the behaviors of dominants in conjunction with other studies suggests that this is due to a correlated increase in mating experiences (Kozorovitskiy and Gould, 2004; Leuner et al., 2010). A similar increase in the number of new neurons was observed in dominant baboons, although the link with sexual experience was not observed (Wu et al., 2014). In contrast with the effects of living in a stable hierarchy on adult neurogenesis, living in a disrupted hierarchy within the VBS with persistent fighting leads to reduced adult neurogenesis (cell proliferation and cell survival) in both dominants and subordinates (Opendak et al., 2016). These contrasting effects of stress in a stable versus disrupted hierarchy suggest that past history of animals and the context in which neurogenesis is assessed play important roles in determining the outcome of this measure of brain plasticity.

When stress is aversive enough and occurs in a context lacking other positive influences, it produces a suppressive effect on adult neurogenesis. It should be noted that similar negative effects on postnatal and adult neurogenesis have been observed when examining the effects of prenatal and postnatal stress (Fujioka et al., 2006; Lemaire et al., 2000; Oomen et al., 2010; Sliwowska et al., 2010) (but see studies by (Barha et al., 2011; Greisen et al., 2005), and adolescent stress on neurogenesis (Mouri et al., 2018).

A role for experience-dependent hormones in adult neurogenesis

Numerous studies have demonstrated that glucocorticoids, steroids that are released from the adrenal cortex in response to stress, exert inhibiting effects on a variety of tissues. Given the catabolic nature of these hormones, it is not surprising that increases in their levels reduce cell proliferation and the number of new neurons in the dentate gyrus, a region dense with mineralocorticoid and glucocorticoid receptors (De Kloet and Reul, 1987; De Kloet et al., 1998; McEwen et al., 1986). Administration of exogenous glucocorticoids has been shown to decrease adult hippocampal neurogenesis at the stages of cell proliferation and neuron survival (Brummelte and Galea, 2010; Cameron and Gould, 1994; Goshen et al., 2008; Workman et al., 2015). Moreover, adrenalectomy increased the number of newborn neurons (Cameron and Gould, 1994; Wong and Herbert, 2004, 2006). However, these effects were shown to be transient after 6 weeks (Lee et al., 2011). Stress-induced increases in glucocorticoids have been shown to participate in experience-driven decreases in adult neurogenesis. For example, clamping glucocorticoid levels with adrenalectomy and replacement with low dose corticosterone in the drinking water reversed the negative effects of stress on adult neurogenesis in studies of predator odor exposure, sleep deprivation, and postnatal stress (Mirescu et al., 2004, 2006; Tanapat et al., 2001). This suggests that activation of the hypothalamic pituitary adrenal (HPA) axis is at least one likely determining factor. However, it should be noted that studies have shown stress-induced decreases in neurogenesis in the absence of changes in CORT (Veenema et al., 2007) (**Fig. 1.4**).

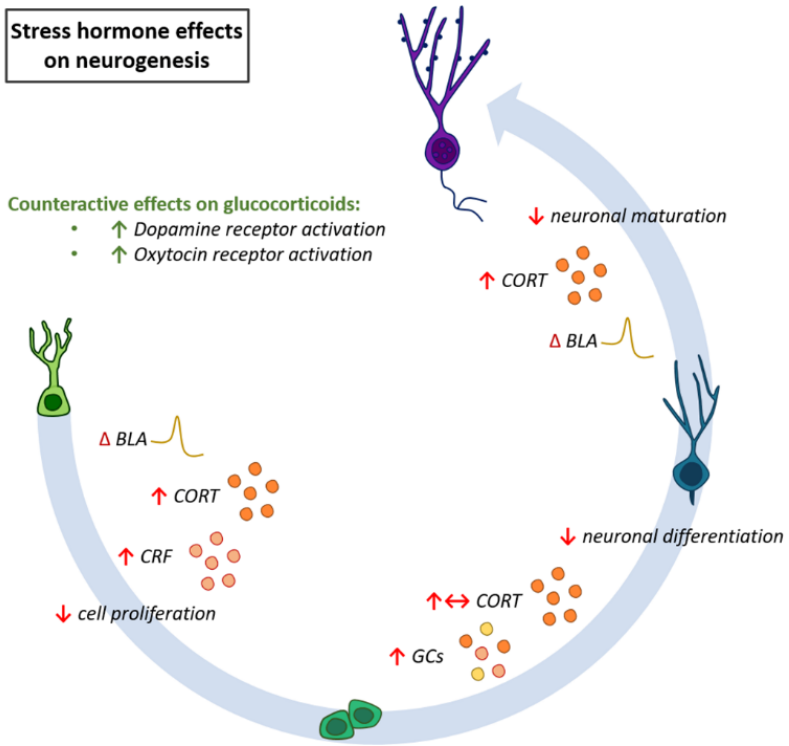


Figure 1.4 Hormonal and neural influences on the production of new neurons in the adult dentate gyrus at one or multiple stages of this process. Decreases in cell proliferation have been shown as a result of changes in basolateral amygdala activity and increases in CORT and CRF. Neuronal differentiation of daughter cells has been shown to decrease in the presence of increased levels of glucocorticoids. The number of adult-born new neurons is also decreased by changes in basolateral amygdala activity and increased levels of glucocorticoids. Evidence suggests that these effects can be counteracted by increases in both dopamine and oxytocin receptor activation. *BLA,* basolateral amygdala; *CORT,* corticosterone; *CRF,* corticotropin-releasing hormone; *GCs,* glucocorticoids.

It should also be emphasized, that numerous other studies have shown that experiences not typically thought of as “stressful”, but which activate the HPA axis robustly, such as sexual experience and physical exercise, stimulate the production of adult neurogenesis (Glasper et al., 2010; Leuner et al., 2010; Praag et al., 1999; Rhodes et al., 2003). It may be the case that experiences known to activate the HPA axis, but with a rewarding context, produce physiological changes that override the inhibiting effects of elevated glucocorticoids. For instance, voluntary

versus involuntary running increase and decrease neurogenesis, respectively (Praag et al., 1999; Rhodes et al., 2003; Stranahan et al., 2006). Physical exercise is also known to profoundly increase the rate of adult-born cell survival (Bednarczyk et al., 2011; van Praag et al., 1999; Wolf et al., 2011) and enhance the arborization of their dendrites (Vivar et al., 2016). Interestingly, single-housed access compared to group-housed access to a running wheel altered these positive effects on adult neurogenesis (Leasure and Decker, 2009; Stranahan et al., 2006), providing evidence linking a socially enriched environment to cell plasticity. Studies have investigated the influence of other positive experiences as well, such as learning and abundance of resources on adult neurogenesis. Hippocampal-dependent cognitive tasks (i.e., object memory, spatial learning, and associative learning) modify and enhance adult-born cell survival (Anderson et al., 2011; Gould et al., 1999c; Tronel et al., 2010), effects specific to the neurogenic niche of the dentate gyrus. Living in a stimulus-rich environment (e.g., group-housed, larger cage, toys, houses, running wheels) increases adult neurogenesis (Garthe et al., 2016; Kempermann et al., 1997; Monteiro et al., 2014; Nilsson et al., 1999; Sale et al., 2007). It is likely that learning and enrichment induces enhancement of structural plasticity of newborn neurons, allowing for easier integration into the preexisting circuitry and increased rates of survival. The enhancement of various stages of adult neurogenesis via these experiences play a functional role in hippocampal circuits important for learning and regulation of the HPA-axis.

Taken together with studies examining experiences in more enriched conditions, these findings highlight the complex effects of experientially elevated glucocorticoids on adult neurogenesis and raise questions about factors that might counteract negative effects. In this regard, oxytocin and dopamine receptor activation are interesting candidates because both show increased response to reward and stimulate adult neurogenesis in the hippocampus (Lin et al., 2017; Lloyd et al., 2010; Sánchez-Vidaña et al., 2016; Winner et al., 2009). Alternatively or in addition, increases in glucocorticoid levels may have suppressive effects on adult neurogenesis when they occur in conjunction with other aversive stimuli-induced neural effects, such as changes in amygdala activation (Kirby et al., 2012).

Function of experience-induced changes in adult neurogenesis

Notwithstanding contradictory evidence described previously, the overall picture that emerges with stress effects on adult neurogenesis in the male is one of inhibition. These findings raise the question about the functional significance of reduced adult neurogenesis in response to stress. Studies in unstressed rodents have provided evidence linking new neurons in the hippocampus to the learning and memory functions of this brain region (Aimone et al., 2006; Gould et al., 1999b; Nilsson et al., 1999; Sahay et al., 2011; Wiskott et al., 2006; see review, (Leuner et al., 2006). The majority of those studies suggest that new neurons play a positive role in cognition, which raises the possibility of whether stress-induced decreases in adult neurogenesis may impair learning and memory. On the surface, such a possibility seems potentially maladaptive, but given that new neurons have been linked to forgetting (Akers et al., 2014), reductions in their numbers may enable the persistence of memories that occur during stressful times. While this could lead to dysfunction, as with posttraumatic stress disorder, it could have beneficial effects if the mechanism is not exaggerated. New neurons have also been shown to participate in the feedback of the stress response, as well as in some of the stress-induced anxiety and depressive-like behaviors associated with the hippocampus (David et al., 2009). In these cases as well, it is easy to imagine how such a response might have deleterious consequences leading to dysfunctional anxiety and depression. However, it is important to keep in mind that such effects might be adaptive, particularly if aversive conditions continue. Increased anxiety and some withdrawal from exploration and reward seeking might protect organisms from harm. It would not necessarily impact them negatively, unless the response was so severe that it interfered with other behaviors associated with survival and reproduction. Additional evidence suggests stress effects may be cumulative; new neurons born during a period of chronic stress are more likely to exhibit an exaggerated response to subsequent stress in the future (De Miguel et al., 2018). Recent evidence suggests that stress-induced reductions in adult neurogenesis may also be important for social behavior (Opendak et al., 2016). These findings identify a role for experience-induced suppressed adult neurogenesis in a social preference for familiar conspecifics, which

may represent an adaptive response, by minimizing uncertain and potentially dangerous social situations.

Conclusions

Although adult-born neurons comprise only a small percentage of the total hippocampal neuronal population, many studies suggest that the production and survival of newborn neurons are responsive to environmental changes, and that changes in these cells may be functionally relevant. Chronic stress and activation of the HPA axis has been shown in numerous studies to reduce hippocampal neurogenesis, as well as alter several behaviors associated with the hippocampus. The previously mentioned examples have shown just how sensitive the rate of neurogenesis is to varying stressors, suggesting that hippocampal plasticity and circuit reorganization, prompted by changes in neurogenesis, may be an important coping mechanism in response to stress. However, the ability to cope effectively presumably lies on an inverted U-shaped curve, where neurogenic-induced change does not fall short of or exceed an “optimal” range. The extent to which combinations of stressors and stress hormone levels modulate new neuron production and their functional consequences remains to be further examined. Gaining a better understanding of how physical and psychosocial stress, in conjunction with hormone responsivity, affects the rate of adult neurogenesis and the incorporation of new neurons into the preexisting circuitry may allow us to better pinpoint therapeutic targets to treat stress-related disorders. Understanding how new neurons incorporate into the hippocampus, and what cell types they prefer as targets, can provide distinct examinable points where experience may be altering these processes.

Adult neurogenesis is just one example of structural plasticity within the hippocampus. Other forms of hippocampal plasticity include structural changes to dendrites and dendritic spines, and the modulation of synapses on mature neurons (see reviews: Gazzaley et al., 2002; Geinisman, 2000; Muller et al., 2000). Dendritic spines were first discovered by Cajal in the late 1800’s, hypothesized as a structural mechanism to connect axons and dendrites (Ramón y Cajal,

1891). This original assumption is now widely accepted in the field. Furthermore, dendritic spines in the hippocampus undergo experience dependent plasticity throughout the lifespan (Boyer et al., 1998; Harris and Stevens, 1989). Mature dentate gyrus granule cells receive excitatory input from entorhinal cortex onto their dendritic spines, forming new synapses or changing the size, shape, and location of preexisting spines, or both (Bonhoeffer and Yuste, 2002). Experiences such as learning and environmental enrichment have been shown to induce spine changes (Kozorovitskiy et al., 2005; Leuner et al., 2003), and coincidentally, these experiences are also known to increase adult neurogenesis (Gould et al., 1999c; Kempermann et al., 1997; Llorens-Martín et al., 2007). The purpose of experience-dependent enhancement in neuro- and spinogenesis, compensatory mechanisms that accompany these processes, and their effects on behavior remain to be fully understood. Nuanced experience-dependent effects on adult neurogenesis highlight the importance of better understanding structural plasticity and circuit reorganization in healthy and diseased brains. These next three chapters will highlight three separate research studies I have conducted over the course of my graduate work, encompassing the theme of structural and functional plasticity in the hippocampus and striatum.

CHAPTER 2: PLASTICITY IN THE DORSAL STRIATUM

Adapted from Briones BA, Tang VD, Haye AE, Gould E. (2018) Response learning stimulates dendritic spine growth on dorsal striatal medium spiny neurons. Neurobiology of Learning and Memory. 155: 50-59.

Chapter Introduction

In this chapter, I introduce my foundational graduate research project investigating striatal-dependent learning and its potential effects on the structure of inhibitory neurons. The striatum is a heterogeneous brain region that acts as an information hub important for a wide array of behaviors including behavioral flexibility, associative learning, reward processing, and initiating and inhibiting motor responses. Given this repertoire of behaviors, it is likely that the cells within this region undergo structural and functional changes throughout the lifespan, but few studies have explored this possibility. However, the work in the previous chapter revealed a very low rate of adult neurogenesis in the striatum, suggesting that this is not a dominant form of plasticity in this region. As a result, I sought to determine whether another form of experience-dependent plasticity exists in this region. Interestingly, the striatum is one of the few regions in the mammalian brain that comprise almost entirely inhibitory neurons; this feature makes the striatum a model region to further explore the connections between inhibitory neurons and PNNs, as is detailed in Chapter 4. Understanding striatal neurons within healthy brains and how they respond to experience may offer additional insight into how brains with pathologies, specifically those with learning and behavioral dysfunction, might differ.

Introduction

A large body of literature has linked several types of learning and memory to changes in dendritic spines, primary sites of excitatory synapses (reviewed in Bailey et al., 2015; Gipson and Olive, 2017; Murakoshi and Yasuda, 2012; Yuste, 2011). Synaptic plasticity at the level of the dendritic spine is generally accepted as an important mechanism underlying learning (reviewed in Feldman, 2009; Segal, 2001). Learning and synaptic plasticity have also been associated with structural changes in dendritic spines. Increases in the number of dendritic spines have been

reported in the hippocampus in response to spatial navigation learning (Mahmmoud et al., 2015; Moser et al., 1994) and trace or contextual classical conditioning (Leuner et al., 2003; Restivo et al., 2009) in the motor cortex and cerebellum in response to acrobatic training and motor learning (Fu et al., 2012; González-Tapia et al., 2017; Ma et al., 2016; Nishiyama and Yasuda, 2015), and in the somatosensory cortex in response to sensory learning (Jasinska et al., 2016; Kuhlman et al., 2014). In some cases, studies have also demonstrated that synaptic plasticity (LTP) induces dendritic spine increases in size and number (Park et al., 2006, Yuste and Bonhoeffer, 2001). Additionally, dendritic spine elimination has been shown to promote learning in the hippocampus during contextual fear conditioning (Sanders, Cowansage, Baumgärtel, & Mayford, 2012) and prelimbic cortex during action-outcome learning (Swanson, DePoy, & Gourley, 2017). Taken together, these findings suggest that learning induces change in dendritic spines in almost all systems examined. Evidence has further suggested that the increase in dendritic spine number may be causally linked to task acquisition (Liston et al., 2013) and memory consolidation (Vetere et al., 2003), suggesting that this growth may be an essential aspect of the cellular processes underlying the establishment and potentially, the maintenance of internal representations.

Habit, or response, learning has been linked to the dorsal striatum (Packard & Knowlton, 2002). The only study thus far to examine the influence of response learning on structural plasticity in the dorsal striatum reported no change in dendritic spine density or spine size on medium spiny neurons (MSNs) (Hawes et al., 2015). MSNs receive specific excitatory inputs from extra-striatal regions, including the neocortex and the ventral tegmental area, onto dendritic spines (Kötter, 1994). The lack of learning-induced change in spine density on MSNs raises the possibility that these excitatory synapses are less structurally plastic than those in other brain regions and/or that they utilize other cellular processes to acquire response learning associations. It is also worth noting that the striatum is an unusual brain region in that the overwhelming majority of its neurons are inhibitory. Studies have indicated that approximately 99% of neurons in the striatum are inhibitory, with 95% comprising MSNs and the remainder inhibitory interneurons (Chang et al., 1982, Lim et al., 2014). By contrast, only 10–15% of neurons in the hippocampus

and 20–30% in the neocortex are inhibitory (Markram et al., 2004, Pelkey et al., 2017), while an even smaller percentage of neurons in the cerebellar cortex, where excitatory granule cells vastly outnumber the other neuron types, are inhibitory (Llinas & Sotelo, 1992). The dramatic difference in the ratio of inhibitory to excitatory neurons in the striatum compared to hippocampus, neocortex, and cerebellar cortex raises the possibility that learning and behavior exert a fundamentally different influence on the striatum in contrast to these other brain regions.

Although MSNs are so named because of their morphological features, not all of these cells receive the same inputs nor are they functionally homogeneous. Thus, we reinvestigated the question of whether MSNs undergo dendritic spine growth and/or morphological changes by identifying subpopulations of these neurons based on expression or lack thereof of the protein products of immediate early gene zif 268, an indirect marker of neuronal activation, following early intensive training on a response learning paradigm. Using DiOlistic (DiI) labeling of MSNs, here we show an increase in dendritic spine density, more specifically an increase in spines with mushroom morphologies, in the dorsolateral striatum-dependent maze-trained group, an effect that appears to be specific to the dorsolateral striatum, but not to zif 268 labeled neurons.

Materials and methods

Animals and food deprivation

All animal procedures were performed in accordance with the Princeton University Institutional Animal Care and Use Committee regulations and conformed to the National Research Council Guide for the Care and Use of Laboratory Animals (2011). Adult male Sprague-Dawley rats (8–10 weeks-old, Taconic Farms, Inc.) were pair-housed in standard cages under a reverse 12-hour light–dark schedule (lights off at 0700). Rats were habituated to experimenter handling by passive holding once a day for 7 days, during which time they began food restriction. To motivate food reinforcement seeking, rats were food-restricted 5 days prior to behavioral training to maintain 85% body weight and given Kellogg Froot-Loop halves in their home cage in order to habituate to the novel food prior to training.

Response learning paradigm

To assess the effects of early training acquisition on a response training task, we used a plus maze paradigm (adapted from Chang & Gold, 2003) which requires a specific motor response (right or left-hand turn) while traversing a maze for food reinforcement. This task involved 3 days of maze exposure (see **Fig 2.1a**). We used this paradigm to capture early response acquisition within single sessions of training and testing.

The maze was enclosed in opaque curtains to minimize reliance on extra-maze visual cues and all maze exposure was conducted in the dark under red light illumination. Maze habituation, training, and testing were video recorded by a ceiling-mounted camera centered over the maze. Identical food cups were placed at the ends of all open arms. During habituation, Plexiglas barricades were used to block entry to 4 of 8 arms on an 8-arm radial maze to construct a plus-maze. During training, barricades were used to block entry to 5 of 8 arms on the maze to construct a T-maze. During testing, barricades were used to block entry to 4 of 8 arms on the maze (differing from the arms during habituation) to construct a plus-maze (see **Fig 2.1a**).

Controls and experimental design

Maze-enriched controls, which we will proceed to refer to as maze controls, used the same maze configurations as described above with a variable reinforcement contingency to promote non-strategic navigating, but with the same amount of exposure to the maze as their response trained counterparts, which we will proceed to refer to as response learners. We conducted this experiment twice. In the first experiment, we searched for evidence of dendritic spine density differences on dorsomedial and dorsolateral striatum medium spiny neurons between response learners and maze controls. In the second experiment, we examined spine density, morphology, and size on medium spiny neurons while considering brain side, lateralized to the trained response, and training-induced expression of the protein products of the immediate early gene zif 268 in response learners and maze controls. Behavioral manipulations were identical for both experiments.

Habituation – Both response learners and maze controls were given 4 trials to explore the plus maze for 180s per trial. Start arm for each trial was randomized and non-repeating. After the completion of a trial, rats were placed in their home cage behind the start arm for a 30s intertrial interval (ITI). Trained response (left or right-turn for reinforcement) was determined based on the initial turn, e.g., if on the first trial a rat turned right, then the assigned reinforced response for training and testing would be a left-turn response.

Training – Response learners were given a maximum of 70 trials on training day to reach criterion with a maximum time of 120s per trial. Start arm for each trial was pseudo-randomized, where arms were randomized within blocks of 4 trials. A trial was complete once reinforcement was retrieved (made a correct arm entry), made an incorrect arm entry, or timed out. If an incorrect arm entry was made during the first 4 trials, rats were allowed to trace back to the correct arm. After the completion of a trial, rats were placed in their home cage behind the start arm for a 30s ITI. Arms of the maze were rotated 90° counterclockwise after 3 correct choices in a row. Response learners were required to make the correct response 6 times in a row to reach criterion. Maze controls were yoked to the average number of response training trials and given a maximum of 120s per trial. Start arm for each trial was pseudo-randomized, where arms were randomized within blocks of 4 trials. Reinforcement schedule and distribution was randomized to prevent any strategy acquisition.

Testing – Response learners were given a maximum of 70 trials on testing day to reach criterion with a maximum time of 120s per trial. Start arm for each trial was pseudo-randomized, where arms were randomized within blocks of 4 trials. Trials were complete once reinforcement was retrieved (made a correct arm entry), not retrieved (made an incorrect arm entry), or timed out. After the completion of a trial, rats were placed in their home cage behind the start arm for a 30 s ITI. Arms of the maze were rotated 90° counterclockwise after 3 correct choices in a row. Response learners were required to make the correct response 9 out of 10 times to reach criterion. Maze controls were yoked to the average number of response testing trials and given 120 s for the first half of trials and 60 s for the last half of trials. Start arm for each trial was

pseudo-randomized, where arms were randomized in blocks of 4 trials. Reinforcement schedule and distribution were randomized to prevent any strategy acquisition.

Vicarious trial and error measurement and performance analysis

In the second experiment, vicarious trial and error (VTE) behavior was scored using BIOBSERVE tracking software, where a movement of the head from the direction of one arm to another at a choice point (in most cases the center hub of the maze) was counted as one instance of VTE (Hu & Amsel, 1995). If multiple entries through a choice point were made during a single trial, an average VTE score per entry was calculated for that trial. In both the first and second experiment, response preference was determined manually. For each trial, the initial response made out of the start arm, a right or left-hand turn during training, or the added option to go straight during testing, was recorded. For response learners, preference for the rewarded response was analyzed. For maze controls, preference for a right-hand turn response was analyzed.

Perfusion

Approximately 1 h after testing, all rats were deeply anesthetized with Euthasol and transcardially perfused with 1.5% paraformaldehyde (PFA) in phosphate buffered saline (PBS), pH 7.5. The brains were dissected and postfixed in 1.5% PFA for 72 h before processing. The post-training perfusion time point was selected to examine dendritic spines shortly after training and for the second experiment involving identification of zif 268 protein-expressing medium spiny neurons, at a post-neuronal activation time point when detection of immediate early gene protein products has been verified (Gill et al., 2007, Rogue and Vincendon, 1992).

DiI labeling and DiI co-labeling with zif 268 immunolabeling

To assess potential changes in dorsal striatum medium spiny neuron dendritic spines, 80 µm coronal sections (1:6) were cut from half brains into a bath of 0.1 M PBS, pH 7.5 using a Vibratome. Individual sections were shot with lipophilic DiI coated Tungsten particles using the BioRad Helios Gene Gun system (BioRad) and incubated for 24 h at 4 °C. Sections were then postfixed in 4% PFA for 1 h at room temperature, washed, and mounted onto suprafrost slides

and coverslipped using Vectashield. To assess potential changes in dendritic spines of medium spiny neurons which expressed protein products of the immediate early gene zif 268, tissue was collected as described above. Individual sections were shot with DiI as described above, free-floating sections were rinsed in 0.1 M PBS, pH 7.5, and incubated with 10% normal donkey serum, 0.1 M PBS with 0.01% Triton X-100, and rabbit anti-zif 268 (1:500; Santa Cruz Biotechnology, Cat# sc-189, RRID:AB_2231020), and stored at 4 °C for 24 h. After incubation in primary antisera sections were washed and incubated with Alexa Fluor 488 (1:200; Invitrogen) in the dark for 2 h at room temperature. Sections were then postfixed in 4% PFA for 1 h at room temperature; washed, mounted, and coverslipped as described above. Slides were coded until completion of analysis.

Both hemispheres were examined in response learners due to previous reports of hemispheric differences in neuronal activation as a result of learned motor responding (Cui et al., 2013, Kravitz et al., 2010). Hemispheres were categorized as either contralateral or ipsilateral to the learned motor response (e.g., a right-turn learned motor response = left hemisphere as contralateral and right hemisphere as ipsilateral to the turning response). Maze control hemispheres were neither, and thus were characterized as non-lateral.

Confocal microscopy

Images from dorsal striatum were taken using a Zeiss confocal microscope (LSM 700; lasers, argon 458/488; HeNe 568). Distinctions between dorsomedial and dorsolateral were based on region depictions by Devan, McDonald, & White, 1999 (medial to bregma, 1.5–2.5 mm; lateral to bregma, 3.0–4.0 mm). Density measurements of cell bodies labeled with mouse monoclonal antibody against NeuN, clone A60 (1:500, Millipore-Sigma Cat# MAB377) co-labeled with zif 268 immunolabeling were acquired using a 20 × 0.75 NA objective from 20 µm image stacks using ImageJ (NIH), where NeuN positive labeled cells and NeuN positive zif 268-positive co-labeled cells were counted exhaustively to obtain the density of neurons that expressed the protein product of zif 268. DiI labeled medium spiny neurons were visualized by using a 63 × 1.40 NA oil objective. Dendritic segments were obtained by imaging representative secondary or tertiary

dendritic branches, without overlapping dendrites from other labeled neurons, from 5 different cell bodies, for each brain region from each rat. Double-labeled DiI–zif 268 sections were visualized in the same manner as described for DiI. Because previous studies have shown neuronal activity changes related to brain side in tasks that involve repetitive left or right motor responses (Cui et al., 2013, Kravitz et al., 2010), we performed our analysis on both sides of the brain, separately, for response learners. For maze controls, we counterbalanced left and right hemispheres for analysis. Dendritic segments were obtained by imaging representative secondary and tertiary dendritic branches from a total of 10 medium spiny neurons in the dorsolateral striatum per hemisphere: 5 different cell bodies expressing zif 268 protein and 5 different cell bodies not expressing zif 268 protein, which we will from now on refer to as zif 268-positive and zif 268-negative, respectively. Dendritic segment measurements totaled 50 μm per neuron.

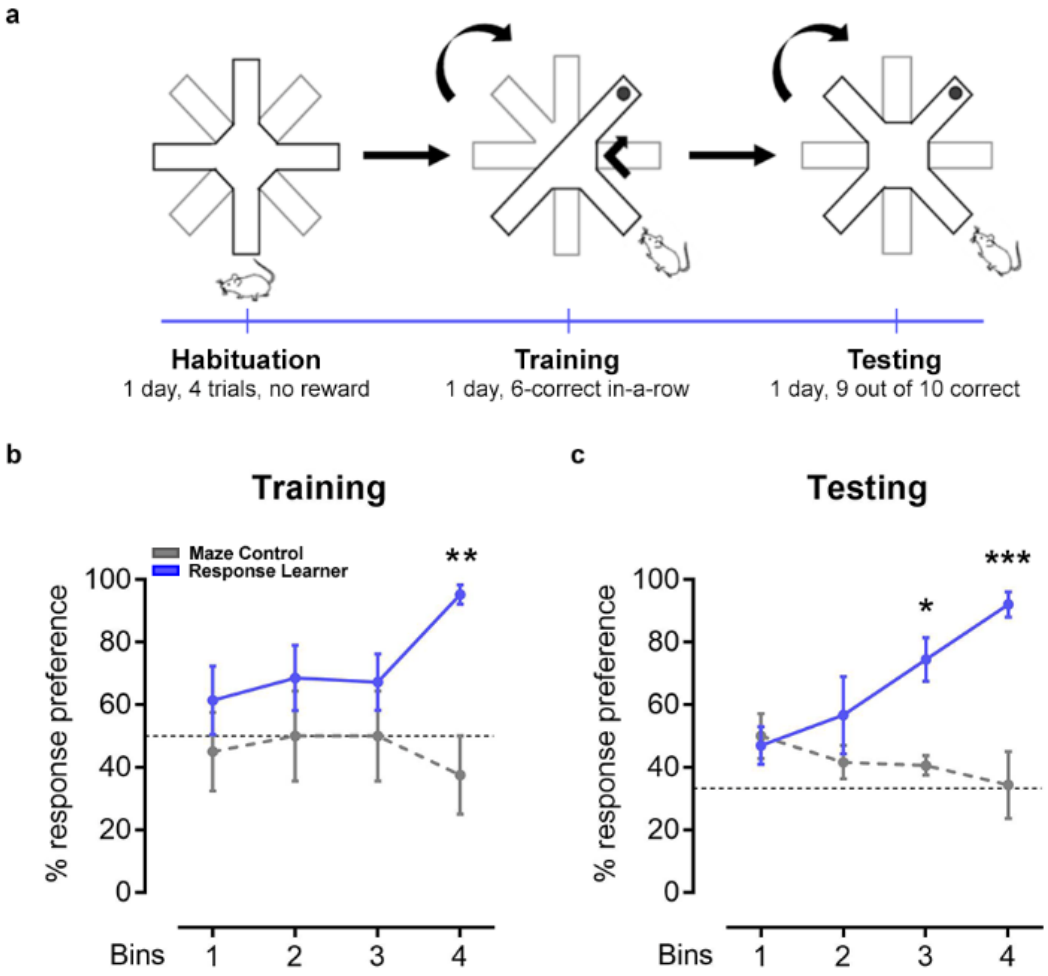
Spines were defined as obvious protrusions from the dendritic shaft with a length greater than 0.2 μm and spine neck width no greater than the dendritic shaft. Spine measurements (length, spine head width, morphology) were analyzed and traced by hand from 5–25 μm image stacks using ImageJ (NIH). Spine morphologies were determined based on previously published characterizations (Lee et al., 2006, Peters and Kaiserman-Abramof, 1970, Yuste and Bonhoeffer, 2004). Spines were classified as: (1) stubby if the length was less than 1.0 μm and had no difference in width between the spine head and shaft; (2) mushroom if the length was greater than 0.5 μm and did show a difference in spine head and shaft, where the spine head was much larger (on average >0.5 μm) than the shaft; (3) thin if the length was less than 2.0 μm and had a small head (on average ≤ 0.5 μm), where the spine head was larger than the shaft; and (4) filopodia if the length was greater than 2.0 μm, width less than 1.0 μm, and lacking an obvious head (see examples in **Fig 2.6**).

Statistics

Percent response preference data and VTE measures were analyzed using a repeated measures two-way ANOVA (within-subjects) with Sidak post hoc comparisons. Histology data collection and analyses were performed by an experimenter unaware of the animal group. Independent

variables for dendritic spine data included: region (dorsolateral or dorsomedial striatum), maze group (maze control or response learner), and hemisphere (non-lateralized, contralateral, or ipsilateral), for DiI-labeled and DiI-double labeled activation (zif 268-positive or zif 268-negative). Both DiI-labeled and DiI-double labeled dendritic spine data were analyzed using a linear mixed effects (lme) model, using the lme4 package (Bates et al., 2014), for comparing maze controls to response learner contralateral and ipsilateral (combined and separately) spine data, within one region. Population design weighted lme modeling was used for DiI-double labeled medium spiny neuron populations, where both zif 268-positive and zif 268-negative medium spiny neuron populations were combined, respective of percent neurons that were zif 268-positive per hemisphere per animal. The lme model was used in place of standard parametric tests because it avoids over-averaging errors in big data sets, weights unequal sample sizes accordingly, is a better statistical model for analyzing between (in our study maze control versus response learners) and within (hemisphere) subject comparisons, and models individual variances. It should be noted that, after computing the entire data set, the LME compares density per rat, not per number of dendritic segments. Unpaired Student's t-test were used for comparisons between two groups. Data sets were tested for outliers using a Grubbs' test with alpha = 0.01. GraphPad Prism 7.0 (GraphPad Software) and RStudio (RStudio Team, 2016) were used for statistical analyses.

Figure 2.1 Short-term training paradigm entrains a response learning strategy and increases response preference above chance levels.



(**a**) Timeline and depiction of early training paradigm for response learners. Black circles depict location of food reinforcer. (**b**) Line graph of percent response preference during training showing greater preference in response learners (blue) compared to maze controls (grey) during bin 4. Dotted black line depicts chance levels for preference (50%, two-response options). (**c**) Line graph of percent response preference during testing showing greater preference in response learners (blue) compared to maze controls (grey) during bin 3 and 4. Dotted black line depicts chance levels for preference (33.3%, three-arm options), ($n = 4–7$) *$p < 0.05$; **$p < 0.01$; ***$p < 0.001$.

Results

Response training results in increased response preference with the emergence of stereotyped behavior

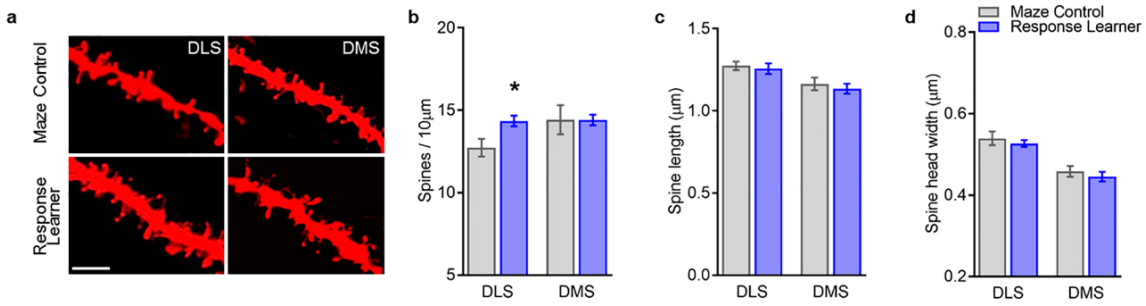
Rats were trained on a T-maze to reinforce a response navigation strategy (response learners) (**Fig 2.1a**), and as a control, a separate group of rats were allowed to traverse the maze for random reward (maze controls). Maze navigation preference for the 'response' arm was recorded and analyzed during training and testing. On average, the training paradigm took 17 trials for response learners to reach criterion and 34 trials to reach testing criterion. Repeated measures two-way ANOVA of percent response preference across binned trials showed a significant difference in navigation strategy preference between response learners and maze controls during training ($F(1, 9) = 5.806$, $p = 0.0393$) (**Fig 2.1b**). Post hoc analysis showed a significantly greater response preference in response learners ($95.23 \pm 3.08\%$), greater than chance levels, compared to maze controls ($37.5 \pm 12.5\%$), by the end of training (Bin 4: $p = 0.0028$) (**Fig 2.1b**). During the testing phase, response learners showed a consistent increase in response navigating compared to maze controls ($F(1, 9) = 10.01$, $p = 0.0115$) (**Fig 2.1c**). Response preference in response learners ($92.046 \pm 3.99\%$) was greater compared to maze controls, exhibiting arm entry preference at chance levels ($34.38 \pm 10.67\%$), throughout the latter half of testing trials (Bin 3: M: $40.63 \pm 3.13\%$; R: $74.47 \pm 6.93\%$; $p = 0.0296$; Bin 4: $p = 0.0001$) (**Fig 2.1c**).

Response training increases the density of dendritic spines on medium spiny neurons of the dorsolateral, but not dorsomedial, striatum

Two days of exposure to the response learning task (one day of training, one day of testing) resulted in a significant increase in the density of dendritic spines on medium spiny neurons of the dorsolateral striatum (confocal images shown in **Fig 2.2a**) compared to maze controls (lme model: $\beta = 1.6293$, $SE = 0.6003$, $p = 0.00915$) (**Fig 2.2b**). By contrast, no significant difference was observed in the density of response learning and maze control dendritic spines on medium spiny neurons of the dorsomedial striatum (lme model: $\beta = -0.1821$, $SE = 1.2002$, $p = 0.883$) (**Fig 2.2b**). No differences were observed in spine size (length or head width) among medium spiny

neurons of either brain region (DLS, length: β = −0.01663, SE = 0.05930, p = 0.786; DMS, length: β = −0.01131, SE = 0.05823, p = 0.85; DLS, width: β = −0.009849, SE = 0.020821, p = 0.65; DMS, width: β = −0.01498, SE = 0.03471, p = 0.676) (**Fig 2.2c, d**). Because the spine density difference was observed only in the dorsolateral striatum, we confined our subsequent analyses to this brain region.

Figure 2.2 Response learning increases density of dendritic spines on medium spiny neurons in the dorsolateral striatum during early training.



(**a**) Representative images of medium spiny neuron dendritic segments (DiI, red) in the dorsolateral (left) and dorsomedial (right) striatum of maze control (top) and response learner (bottom) groups (n = 4–7). Scale bar equals 5 µm. (**b**) Spine density difference between maze controls (grey) and response learners (blue) observed in the dorsolateral striatum only. (**c**) Spine length does not change with response learning in either dorsolateral or dorsomedial striatum. (**d**) Spine width does not change with response learning in either dorsolateral or dorsomedial striatum. Box and whisker graphs are plotted from min to max. *p < 0.05; DLS, dorsolateral striatum; DMS, dorsomedial striatum.

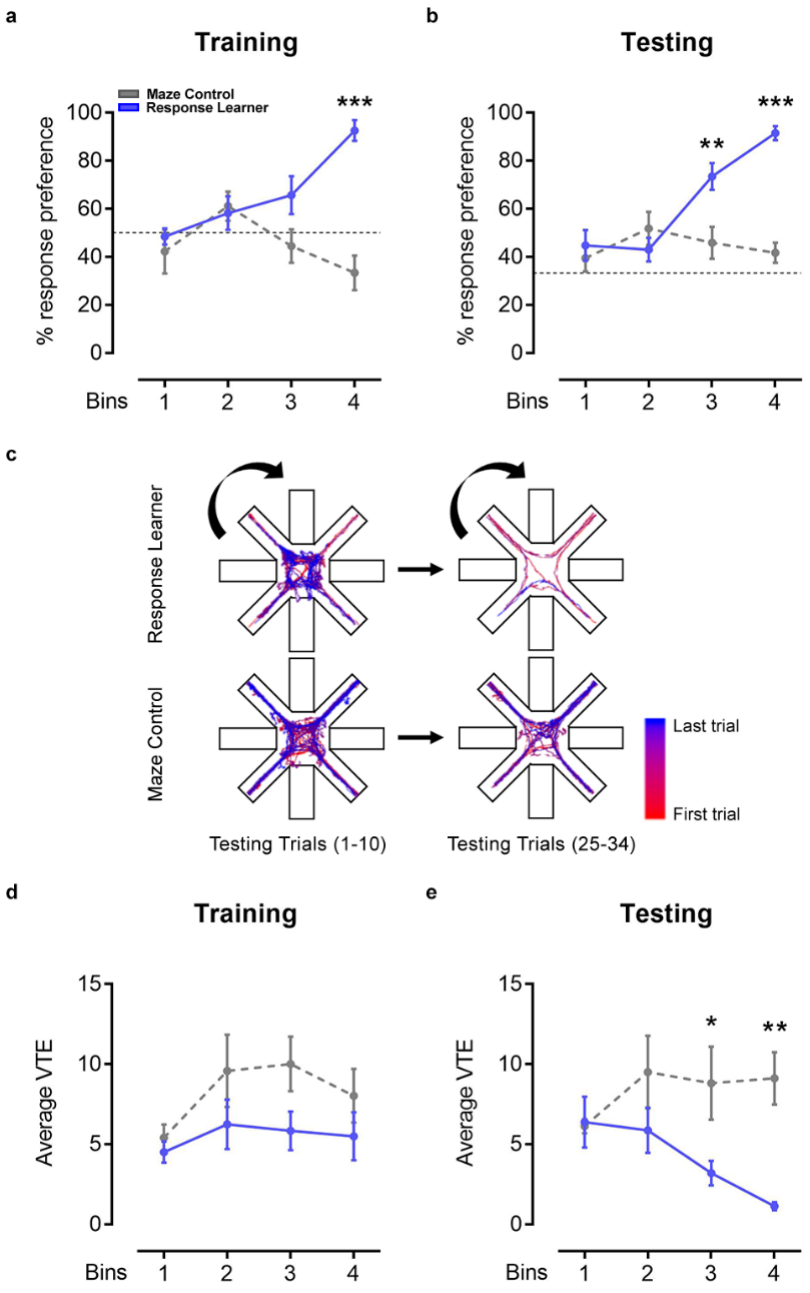
Response training results in reduced vicarious trial and error behavior coincident with the emergence of stereotyped behavior

To further investigate the effects from the first study, we tested a second cohort of rats on the response learning task. During training, repeated measures two-way ANOVA (within-subjects) of percent response preference across bins showed a significant main effect between response learners and maze controls (F(1, 17) = 18.81, p = 0.0004) and a significant interaction effect (F(3, 51) = 8.662, p < 0.0001), where post hoc analysis showed a significant increase in response

preference in response learners (92.57 ± 4.29%) compared to maze controls (33.33 ± 7.22%) at bin 4 ($p < 0.0001$) (**Fig 2.3a**). During testing, repeated measures two-way ANOVA (within-subjects) of percent response preference across bins again showed a significant main effect between response learners and maze controls ($F(1, 17) = 11.6$, $p = 0.0034$), a significant main effect across bins ($F(3, 51) = 12.15$, $p < 0.0001$), and a significant interaction effect ($F(3, 51) = 16.14$, $p < 0.0001$). Post hoc analysis showed a significant increase in response preference in response learners (91.5 ± 2.89%) compared to maze controls (41.67 ± 4.17%) in bin 4 ($p < 0.0001$), in addition to bin 3 ($p = 0.0027$) (**Fig 2.3b**). Coincident with a robust response preference by bin 4, response learners also qualitatively became more stereotyped in the path taken to the food reinforcer by the end of testing (**Fig 2.3c**).

We also analyzed vicarious trial and error (VTE) behavior exhibited in the center of the maze during the task. VTE behavior, which occurs mostly during the early stages of maze learning, has been used as a measure of deliberate processing (Muenzinger and Gentry, 1931, Muenzinger, 1938, Redish, 2016, Tolman, 1938, Tolman, 1939, van der Meer and Redish, 2010) where a decrease in VTE behavior coincides with response learning. VTE behavior was analyzed in 4 bins of trials for both training and testing for maze control and response learners. During training, repeated measures two-way ANOVA (within-subjects) analysis showed a significant main effect across bins ($F(3, 51) = 4.452$, $p = 0.0075$). In maze controls, VTE behavior increased between bin1 (5.41 ± 0.82) and bin 2 (9.58 ± 2.26) ($p = 0.0202$) and bin 1 and bin 3 (10.01 ± 1.7) ($p = 0.0081$) (**Fig 2.3d**). In response learners, VTE behavior did not significantly change across bins (**Fig 2.3d**). During testing, repeated measures two-way ANOVA (within-subjects) analysis revealed a significant main effect between response learners and maze controls ($F(1, 17) = 6.702$, $p = 0.0191$) and a significant interaction effect ($F(3, 51) = 5.386$, $p = 0.0027$) (**Fig 2.3e**). Post hoc analysis showed response learners exhibited significantly less VTE behavior compared to maze controls during bin 3 (M: 8.81 ± 2.27; R: 3.20 ± 0.76; $p = 0.0363$) and bin 4 (M: 9.11 ± 1.63; R: 1.13 ± 0.25; $p = 0.0012$) (**Fig 2.3e**).

Figure 2.3 Response training results in reduced vicarious trial and error behavior coincident with the emergence of stereotyped behavior.

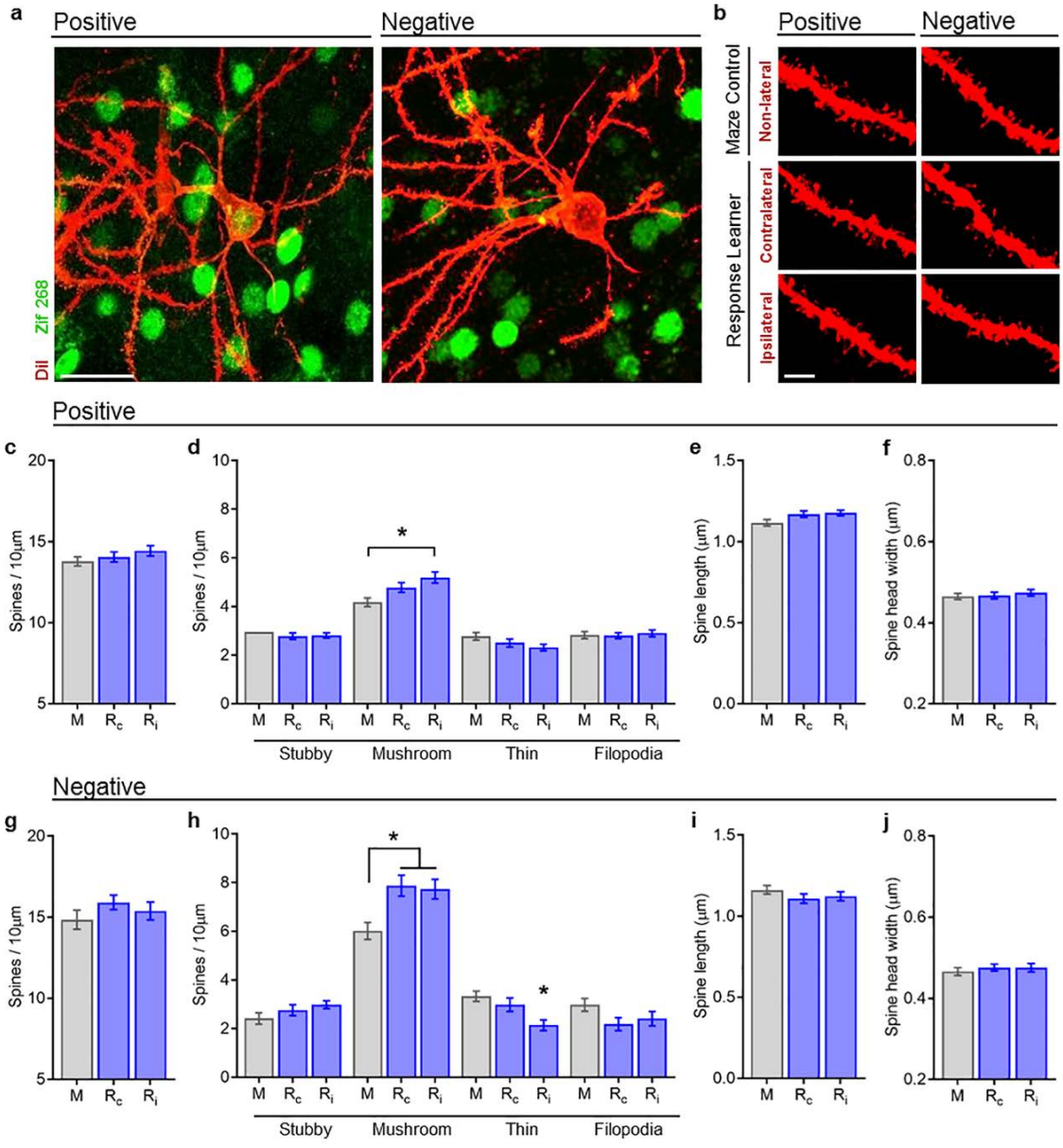


(**a**) Line graph of percent response preference during training showing greater preference in response learners (blue) compared to maze controls (grey) during bin 4. Dotted black line depicts chance levels for preference (50%, two-response options). (**b**) Line graph of percent response preference during testing showing greater preference in response learners (blue) compared to maze controls (grey) during bin 3 and 4. Dotted black line depicts chance levels for preference (33.3%, three-arm options) (n = 9–10). (**c**) Representative path traces of response learner (top) and maze control (bottom). Trials 1–10 during testing depicted on the left and trials 25–34 during testing depicted on the right. Red to blue color scale corresponds to successive trials. (**d**) Average VTE behavior increases in maze controls (grey), only, during training. Average VTE behavior does not change across time in maze controls (grey), but decreases in response learners (blue) during testing. VTE, vicarious trial and error. Testing trial paths shown are taken from one response learner and one maze control. *p < 0.05; **p < 0.01; ***p < 0.0001.

Response training increases the density of dendritic spines on medium spiny neurons, but is not specific to the zif 268-positive population

To determine whether the increase in dendritic spine density seen in our first experiment examining early training was driven by medium spiny neurons that were activated during maze behavior, we carried out a DiI analysis in conjunction with immunolabeling for the protein product of the immediate early gene zif 268, an indirect marker of neuronal activation (confocal images shown in **Fig 2.4a**). We also investigated whether spine changes were predominantly on one side of the brain or the other during the response learning task (contralateral or ipsilateral to the turning side). First we confirmed that response learning increased the density of zif 268-posiitve NeuN-positive neurons in the dorsolateral striatum (maze control: 7700 ± 906.4 cells/mm3; response learners: 10,982 ± 926.8 cells/mm3; $p = 0.0222$), and not in the dorsomedial striatum (maze control: 9341 ± 1757 cells/mm3, response learners: 8849 ± 1243 cells/mm3; $p = 0.8222$). Then we analyzed dendritic spines on zif 268-positive and zif 268-negative medium spiny neurons in the dorsolateral striatum (confocal images shown in **Fig 2.4b**). Surprisingly, analyses of spine density on zif 268-positive and zif 268-negative medium spiny neurons, separately, did not reveal any significant spine density differences in either subpopulation (zif 268-positive: $\beta = 0.2708$, SE = 0.4292, $p = 0.529$; zif 268-negative: $\beta = 1.0746$, SE = 0.7639, $p = 0.165$), nor were differences detected on one side of the brain or the other in either subpopulation (zif 268-positive: $\beta = 0.3819$, SE = 0.4393, $p = 0.386$; zif 268-negative: $\beta = -0.5295$, SE = 0.7361, $p = 0.475$) (**Fig 2.4c, g**). Again, no differences were observed in spine size (length or head width) among medium spiny neurons of either zif 268-positive or zif-negative (zif 268-positive, length: $\beta = -0.0479$, SE = 0.03397, $p = 0.173$; zif 268-negative, length: $\beta = -0.05188$, SE = 0.04553, $p = 0.27$; zif 268-positive, width: $\beta = -0.001654$, SE = 0.015095, $p = 0.914$; zif 268-negative, width: $\beta = 0.0098196$, SE = 0.0138948, $p = 0.483$) (**Fig 2.4e-f, i-j**).

Figure 2.4 The dendritic spine density increase after early response learning is not specific to zif 268-positive and zif 268-negative medium spiny neurons.



(**a**) Representative images of DiI-labeled (red) medium spiny neurons, positive (left) or negative (right) for immediate early gene zif 268 (green). Scale bar equals 25 µm. (**b**) Representative DiI-labeled (red) dendritic segments of medium spiny neurons, positive (left) or negative (right) for zif 268 (not depicted in segment images), from non-lateralized hemisphere of maze control (top row), contralateral hemisphere of response learners (middle row) and ipsilateral hemisphere of response learners (bottom row). Scale bar equals 5 µm. c-f, Zif 268-positive spine measurement data for

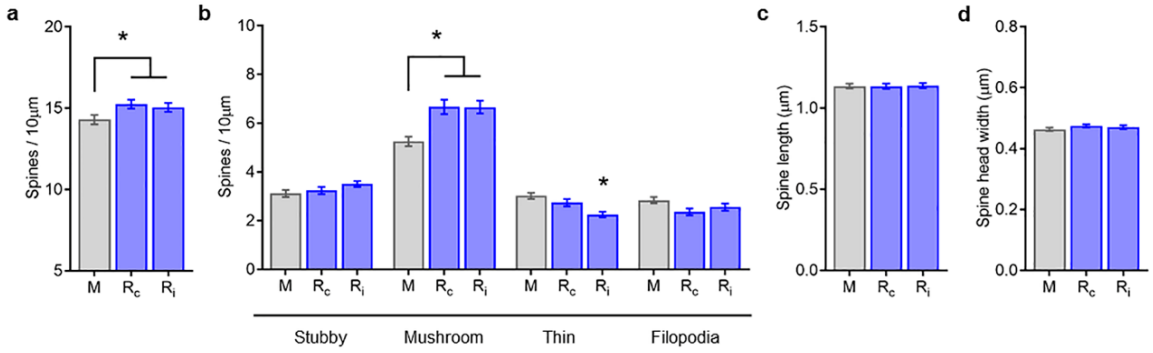
density per 10 μm (**c**), morphology density per 10 μm (**d**), length in μm (**e**), and head width in μm (**f**). Maze controls (grey) show significantly fewer mushroom spines than do response learners' ipsilateral hemisphere (blue). (**g–j**) Zif 268-negative spine measurement data for density per 10 μm (**g**), morphology density per 10 μm (**h**), length in μm (**i**), and head width in μm (**j**). Maze controls show significantly fewer mushroom spines than response learners. Response learner ipsilateral hemisphere shows significantly fewer thin spines than both maze controls and response learner contralateral hemisphere (**h**) (n = 9–10). *p < 0.05; M, maze control; Rc, response learner contralateral; Ri, response learner ipsilateral.

Despite the lack of significant differences in spine density within either of these two subpopulations, both the zif 268-positive and zif 268-negative medium spiny neurons showed significant differences in the density of spines with a mushroom morphology. Zif 268-positive medium spiny neurons showed a hemispheric difference, where the ipsilateral hemisphere of response learners had a greater mushroom spine density compared to maze controls non-lateralized hemisphere (β = 0.6069, SE = 0.2979, p = 0.0436; ipsilateral vs. non-lateral: p = 0.0109) (**Fig 2.4d**). Zif 268-negative medium spiny neurons showed an overall significant difference in mushroom spine density between response learners and maze controls (β = 1.9748, SE = 0.7079, p = 0.0147), where both contralateral and ipsilateral response learner hemispheres had a greater mushroom spine density compared to maze controls non-lateralized hemispheres. Additionally, there was an ipsilateral hemispheric decrease in the density of spines with a thin morphology compared to both response learner contralateral and maze control non-lateralized hemispheres (β = −0.8394, SE = 0.3359, p = 0.0153; ipsilateral vs. non-lateral: p = 0.001717, ipsilateral vs. contralateral: p = 0.02491) (**Fig 2.4h**).

We next investigated the proportion of neurons in the dorsolateral striatum that were zif 268-positive for each individual animal and used those data to analyze the two subpopulations combined (zif 268-positive and zif 268-negative). Spine density data from this experiment were analyzed using a population-specific weighted approach to better approximate the dorsolateral striatum medium spiny neuron population as a whole and to more accurately reflect the random

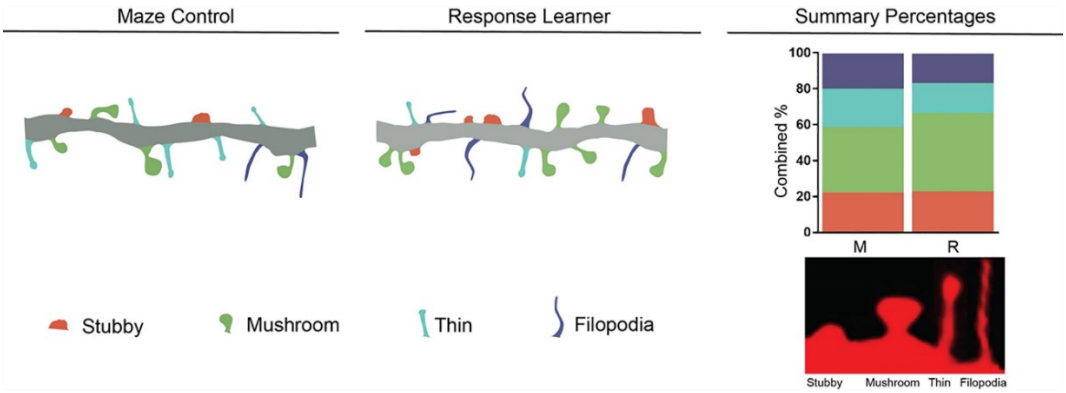
selection of medium spiny neurons from our first study. The weighted analysis replicated our previous finding of increased dendritic spine density on medium spiny neurons in response learners compared to maze controls (β = 0.8961, SE = 0.4263, p = 0.0455) (**Fig 2.5a**). We also found an increase in the density of spines with a mushroom morphology in response learners compared to controls (β = 1.24672, SE = 0.42426, p = 0.00771) and an ipsilateral hemispheric difference in thin spine density, where ipsilateral response learners had fewer thin spines (β = −0.4631, SE = 0.1816, p = 0.0115; ipsilateral vs. non-lateral: p = 0.001058, ipsilateral vs. contralateral: p = 0.021585) (**Fig 2.5b**). By contrast, no differences were observed in the density of spines between response learners and maze controls with stubby (β = 0.1061, SE = 0.1985, p = 0.598), filopodia (β = −0.4482, SE = 0.2768, p = 0.12) (**Fig 2.5b**), or double-headed morphologies (β = 0.01005, SE = 0.02332, p = 0.669) where the average density per 10 µm for double-headed morphologies in response learners was 0.061 ± 0.024 and 0.046 ± 0.02 for maze controls. Likewise, no differences were observed between groups in spine length or spine head width (**Fig 2.5c, d**). Taken together, the results of this study demonstrate overall significant differences in dendritic spine density and spine morphology of medium spiny neurons of response learners, effects which are not specific to brain side or to those cells that express the protein product of the immediate early gene zif 268 after training.

Figure 2.5 The zif 268-positive and zif 268-negative medium spiny neuron population combined replicates the dendritic spine density increase seen in early training.



(**a**) Overall spine density difference seen between maze controls and response learners in zif 268-positive and zif 268-negative combined spine measurement data for density per 10 µm. (**b**) Stubby, mushroom, thin, and filopodia spine morphology density per 10 µm. Maze controls show significantly fewer mushroom spines than response learners. Response learner ipsilateral hemisphere shows significantly fewer thin spines than both maze controls and response learner contralateral hemisphere (n = 9–10). (**c**) Dendritic spine length in µm, and (**d**) spine head width in µm. Bar graph error bars represent ± SEM. *$p < 0.05$; M, maze control; R_c, response learner contralateral; R_i, response learner ipsilateral.

Figure 2.6 Summary of response learning effects on number and morphology of medium spiny neuron dendritic spines.



Early trained response learners show increased overall spine density, with more mushroom spines, compared to maze controls. Combined percentages of spine morphologies are displayed in bar graphs on the right. Representative stubby, mushroom, thin, and filopodia spine types are shown in the confocal image on the bottom right. M, maze control; R, response learner.

Discussion

Our findings suggest that intensive, short-term training on a response learning maze task results in a small but significant increase in dendritic spine density of medium spiny neurons in the dorsolateral striatum of adult rats. These effects were not specific to medium spiny neurons that express the protein product of the immediate early gene zif 268 after training, nor were they specific to a side of the brain (ipsilateral or contralateral to the learned response). Instead, they appear to be general changes induced throughout this population of neurons within the dorsolateral, but not dorsomedial, striatum. In addition to overall increases in dendritic spine density with response learning, there was a more specific increase in the number of spines categorized as mushroom-shaped, along with a decrease in those categorized as thin-shaped, in response learners compared to maze controls.

Our findings on short-term training inducing increased dendritic spine density on medium spiny neurons are in direct contrast to those from a report indicating no such changes after response training on a similar maze (Hawes et al., 2015). There are many possible reasons for these differences; among them are the use of a different strain of rats (Long Evans versus Sprague Dawley) and a different method for labeling medium spiny neurons (biocytin versus DiI). Regarding this latter point, it may be relevant that our spine density values were more than double than those of the previous study (Hawes et al., 2015), raising the possibility of differential labeling between methods. It is also possible that differences in the duration of the training paradigm were important for the detection of a spine density difference in our study. Our response trained group received 2 days of response learning training and testing (in addition to a habituation day), with a total of approximately 51 response learning trials, while the previous study examined rats in an early training paradigm with 4–6 days of training, and on average 24 trials overall. Dendritic spine growth on medium spiny neurons may occur only very early on in training and it may require massed trials. In this regard, it may be relevant that our findings are consistent with a study examining inhibitory avoidance training using aversive stimuli, which showed that only pairings of stimuli with intensive shocks were sufficient to induce dendritic spine

growth (Bello-Medina, Flores, Quirarte, McGaugh, & Prado Alcalá, 2016). Nonetheless, our findings indicate that under certain circumstances, dorsolateral striatum medium spiny neurons undergo dendritic spine growth after intensive, short-term maze response training.

Our data suggest that the observed increase in overall dendritic spine density of medium spiny neurons in response learners with short-term intensive training reflects a learning-induced increase in both density and percentage of mushroom-shaped spines. Dendritic spine shapes have been studied extensively and appear to represent different stages of spine formation, as well as different functional states (Bosch and Hayashi, 2012, Bourne and Harris, 2007). Filopodia and thin spines are believed to be transient extensions that are sometimes, but not always, associated with synapses. These spine types are often described as indicators of plasticity, representing dendritic outgrowths that have the potential to develop into more mature spines with stable synapses in response to certain cues (Segal, 2001, Yoshihara et al., 2009). Mushroom, stubby, and double-headed spines, the last of which occur at very low frequency, are thought to represent more mature postsynaptic sites, with well-developed stable synapses (Bourne & Harris, 2007). The increase in mushroom spine density we observed in the response learners most likely represents a transition of immature spines to mature spines. Given our observation of a concomitant decrease in thin spine density, this appears to be a plausible scenario. However, given the overall small but significant increase in overall spine density, independent of spine morphology subtypes, it is likely that response learning also produced some spines de novo.

Previous studies indicate that the dorsolateral striatum is required for response learning whereas the dorsomedial striatum is required for place learning (Packard and Knowlton, 2002, Yin and Knowlton, 2006). At the outset of maze navigation training, it has been suggested that although the dorsomedial striatum is not critical for the acquisition of response learning (Packard & McGaugh, 1996), habits are formed through transitions from goal-directed behavior to routine responses (Furlong et al., 2014, Yin et al., 2004, Yin et al., 2006). Given the engagement of the dorsomedial striatum in early response learning maze training, we examined this brain region as well as the dorsolateral striatum. We did not observe any change in dendritic spine density in

response learners compared to maze controls for dorsomedial medium spiny neurons. This lack of an effect in the dorsomedial striatum may seem unexpected given the short training paradigm, however the task we used forced rats to use a non-spatial strategy from the outset, turning direction was predetermined before the training period, and there were no extra-maze cues. Thus, the stimulation of dendritic spine growth may require intensive engagement of neurons in a way that is critical for acquisition of the response.

A previous study examining the effects of enriched environment living compared to caged controls on medium spiny neuron dendritic spine density in the dorsolateral striatum did not reveal overall differences in spine density but observed an increase in double-headed spines (Comery, Stamoudis, Irwin, & Greenough, 1996), an effect we did not observe, likely due to the fact that our controls were also enriched, i.e., they were maze-exposed. Given that our controls were exposed to the maze in a time- and reinforcement-yoked manner, it is unlikely that the changes in dendritic spines we observed in the response learning group occurred as a result of general enrichment, as opposed to specific maze training. However, the lack of an increase in dendritic spine density specific to zif 268-positive cells or to brain side was unexpected and suggests generalized growth response to the learning task. Although studies have shown that activated neurons express zif 268 mRNA and protein (Håvik et al., 2003, Murphy et al., 1991) and that this transcription factor is associated with learning and memory (Hall, Thomas, & Everitt, 2001), it is possible that other immediate early genes will better label medium spiny neurons that are more specifically engaged in the response-learning task. It is also possible that the timing of perfusion relative to the activation of the relevant neuron types did not capture the neuronal subpopulation most engaged in the acquisition of the task. While we selected the one-hour post-testing time point to examine the zif 268-positive neuronal population at a time shortly after the rats had acquired the learned response, it remains possible that a different subpopulation of neurons was activated earlier in training which may have accounted for a greater degree of dendritic spine growth. Finally, it remains possible that different subsets of medium spiny neurons, such as those that express different dopamine receptors, will reveal subtype specific

dendritic spine effects. Our results, however, do not distinguish between these subtypes and suggest that the effect may be general to the entire population of medium spiny neurons in the dorsolateral striatum.

Some studies examining the effects of other types of learning on dendritic spine density and morphology in different brain regions, including the hippocampus and cerebellum, have revealed growth effects that are transient. That is, training initially stimulates dendritic spine growth and maturation, but these measures regress back to the control state even with continued training (Knafo et al., 2005, O'Malley et al., 2000). The majority of studies, however, have demonstrated that increases in spine growth and maturation with learning persist over time (González-Tapia et al., 2015, Íbias et al., 2015, Kuhlman et al., 2014, Lee et al., 2007, Ma et al., 2016, Moser et al., 1994, Uriarte et al., 2017). Regardless of the persistence of spine changes over time, several lines of evidence suggest that new dendritic spine growth and associated new synapses are substrates for learning and memory formation in other brain regions, including the hippocampus, neocortex, and cerebellum. First, training and synaptic plasticity have been associated with spine and synapse growth (González-Tapia et al., 2015, Hill and Zito, 2013, Kuhlman et al., 2014, Lee et al., 2007, Ma et al., 2016, Moser et al., 1994, Uriarte et al., 2017). Second, spine density has been shown to correlate positively with performance on spatial navigation and motor tasks (González-Tapia et al., 2015, Mahmmoud et al., 2015). Third, preventing the formation of new spines and synapses can block formation of some of these types of memories (Liston et al., 2013). Our results suggest a link may exist between new dendritic spine growth in the dorsolateral striatum and stereotyped response memories, as well. However, since these results are correlational, the extent to which new dendritic spines are required for response acquisition, habit formation, and the maintenance of these behaviors remains unknown.

Collectively, these results suggest that short-term, intensive training on a response-learning paradigm increases the density of dendritic spines on dorsolateral striatum medium spiny neurons, with the most robust changes occurring among those with a mushroom morphology, compared to maze controls. This effect appears to be general in that it is not dependent on zif

268 expression by the neuron or the side of the brain. The extent to which these structural changes underlie altered behavioral capabilities remains to be determined.

CHAPTER 3: ADULT-BORN GRANULE CELL MOSSY FIBERS PREFERENTIALLY TARGET PARVALBUMIN-POSITIVE INTERNEURONS SURROUNDED BY PERINEURONAL NETS

This work was presented in abbreviated form: Briones, BA, Pisano TJ, Haye AE, Diethorn EJ, Pitcher MN, Tawa EA, Lotito MJ, Cameron HA, Gould E. (2019) Mossy fibers from adult-generated neurons in the dentate gyrus are consistently associated with hilar interneurons surrounded by intense perineuronal nets. Society for Neuroscience, Poster 113.14.

Chapter Introduction

The study introduced in this chapter revisits the topic introduced in Chapter 1, hippocampal plasticity, and investigates adult-born neuron synaptic connections to inhibitory interneurons with PNNs. In the abstract and past two chapter introductions, I have briefly mentioned PNNs. First identified by Camillo Golgi in the 1890's, PNNs were described as non-neuronal "corset-like" structures that "impeded the spread of current from cell to cell" (Golgi, 1898). It was not until much later, with the advancement of cytochemistry, that PNNs were investigated in more detail, however, a similar notion remained that these extracellular matrix structures were important for the stabilization of the brain. This begs the question, do PNNs actively participate in mechanisms of plasticity or are they structural barriers to prevent plasticity, and if both are true, under what conditions are they true?

Introduction

A large body of evidence has shown that adult neurogenesis contributes to the function of the mammalian hippocampus. New neurons receive inputs from afferents and form connections with target cells, and participate in information processing and hippocampus-dependent behaviors, such as enhancement of learning, adaptability, and feedback of the stress response (van Praag et al., 1999; Laplagne et al., 2006; Sahay et al., 2011; Snyder et al., 2011; Akers et al., 2014). Adult neurogenesis is also susceptible to environmental influences (Sah et al., 2017; Vivar et al., 2016; Llorens-Martin et al., 2015; Schoenfeld et al., 2013, Opendak et al., 2016), suggesting that the microcircuitry of new neurons may serve as a substrate for experience-dependent change in hippocampal function.

Adult-born granule cells (abGCs) arise from progenitors located in the subgranular zone of the dentate gyrus. Shortly after their generation, new granule cells grow dendrites and axons.

Their dendrites extend toward the molecular layer where they receive extrahippocampal afferents from the entorhinal cortex, medial septum, and mammillary nuclei (Vivar et al., 2016), as well as from both excitatory and inhibitory neurons of the hippocampus (Sah et al., 2017). Their axons, or mossy fibers, extend into the hilus where they ramify and send processes to form synapses on several post-synaptic target cells. These cells are populations of excitatory neurons, including pyramidal cells of the CA2/CA3 regions and mossy cells of the hilus (Toni et al., 2008; Llorens-Martin et al., 2015); in addition to inhibitory interneurons of the CA2/CA3 regions and dentate gyrus (Toni et al., 2008).

Evidence suggests that parvalbumin-expressing (PV+) interneurons, the most abundant interneuron subtype in the hippocampus (Freund & Buzsaki, 1996), receive inputs from abGCs (Marin-Burgin et al., 2012; Song et al., 2013). PV+ cells reciprocally synapse onto abGCs, creating a feedforward inhibitory circuit, which has been shown to be important for modulating dentate gyrus excitability and pattern separation (Sahay et al., 2011; Ikrar et al., 2013). These studies, however, have treated PV+ interneurons as a relatively homogeneous group, despite the fact that some, but not all, of these cells are surrounded by perineuronal nets (PNNs) (Schüppel et al., 2002; Dityatev et al., 2007; Lensjø et al., 2017), specialized extracellular matrix structures known to modulate physiological and structural plasticity (Sorg et al., 2016; Favuzzi et al., 2017).

PNNs surrounding PV+ interneurons have been shown to reduce plasticity in the developing visual cortex by enabling the closure of the critical period for ocular dominance (Pizzorusso et al. 2002; Hou et al., 2017). Conversely, evidence has shown that PNNs facilitate functional and behavioral plasticity via enhancing feedback inhibition of PV+ interneurons in the hippocampus (Shi et al., 2019). Changes in PV+ protein expression in these cells correlate with changes in functional plasticity, where reduced expression correlates with a reduction in coordinated neuronal activity, gamma and theta-band oscillations, and NMDAR activity (Lodge et al., 2009; Amilhon et al., 2015; Behrens et al., 2007; Korotkova et al., 2010). Conversely, PV expression has been shown to increase with an increase in excitatory input (see review, McRae & Porter, 2012). These results suggest that PNNs surrounding PV+ interneurons play complex

roles, and may differ depending on region and developmental stage. In the dentate gyrus, PNNs surround approximately 40% of PV+ cells (Lensjo et al., 2017), the majority of which are likely to be basket cells (Yamada et al., 2015; Jansen et al., 2017), because PV+ bistratified interneurons also express somatostatin, which does not co-localize with PNNs (Murthy et al., 2019). Dentate gyrus PV+ interneurons are postsynaptic targets of abGCs, where their connections are known to play important roles in hippocampal plasticity. However, abGCs relationship to PNNs has not been previously explored. To investigate the potential relationship between abGCs and their PV+PNN+ target cells, we examined the proximity of mossy fibers of abGCs using GFP-retroviral labeling and endogenous microtubule protein 3R-Tau, which labels abGCs and their axons, to dentate gyrus PV+ interneurons with varying intensities of PNN components.

We found that retrovirus labeled and 3R-Tau+ abGC mossy fibers were more abundant surrounding dentate gyrus PV+PNN+ interneurons than PV+PNN- interneurons. Among the PV+PNN+ population, we also found that cells with more intense PNN labeling were more likely to have abGC mossy fibers nearby than those with weaker-labeled PNNs. This result raises the possibility that abGC connectivity influences PNN formation, and equally as possible that PNN components attract or stabilize abGC mossy fibers. To investigate whether the presence of new neurons in the dentate gyrus influences PNN formation, we investigated PNNs in three different comparisons of altered levels of adult neurogenesis in mice: 1) transgenic mice in which adult neurogenesis was almost completely inhibited, 2) age-related decline of adult neurogenesis, and 3) exercise-induced enhancement in adult neurogenesis. We found that, although changes in PNNs were detected, there was no clear linear relationship between the number of new neurons and PV+PNN+ interneurons across the three experiments. Together these results indicate that new neurons preferentially innervate PV+ interneurons surrounded by PNNs, but that new neuron innervation may not directly alter PNN formation, raising the possibility that PNNs may serve as a chemoattractant to new axons and provide an environment for sustained connectivity.

Materials and Methods

Animals and experimental manipulations

All animal procedures were conducted in accordance with the National Institutes of Health guidelines and approved by the Princeton University Institutional Animal Care and Use Committees (IACUC). All mice were housed five to a cage with enrichment, unless otherwise stated, under a reverse 12-hour light-dark schedule (lights off at 0700) with free access to food and water. Male C57BL/6J mice aged 5-7 weeks from The Jackson Laboratory (Bar Harbor, ME) (strain #000664) were used for retroviral labeling. Male C57BL/6J mice from The Jackson Laboratory were also used for 3R-Tau-labeling (aged 7-9 weeks) and the age-related decline study (5 weeks for young controls and 16 weeks for middle-aged adult mice). Transgenic mice, expressing HSV-TK under the GFAP promoter, and their wildtype CD1 littermates (NIMH, Bethesda, MD), were treated for 10.5 weeks with valganciclovir (vgcv, p.o., 227 mg/kg chow, 4 days/week) and perfused at age 19-20 weeks. Mice in the running study were male C57BL/6J bred in-house, where runners were housed for 4 weeks with *ad libitum* access to a wireless running wheel (Med Associates Inc., Fairfax, VT) beginning at 6 weeks, and controls with a locked wheel. Runner cages ran $\geq$10 km/day. At the conclusion of each experiment, mice were deeply anesthetized with 0.07 mL Euthasol (i.p. injection) and transcardially perfused with 4.0% paraformaldehyde (PFA) in phosphate buffered saline (PBS), pH 7.5. The brains were dissected and postfixed in 4.0% PFA for 48h before processing.

Production of viral vector

A VSV-G pseudotyped replication-deficient retroviral vector based on the Moloney murine leukemia virus and expressing GFP from the CAG promoter, was used to specifically transduce adult-born GCs as done previously (Zhao et al., 2006). Retroviral particles were produced and purified in the Princeton Viral Core at the Princeton Neuroscience Institute, as previously described (Sullivan and Wickersham, 2015). Briefly, a mix of three plasmids were co-transfected over HEK293T cells and viral particles were purified by a sucrose step gradient. Plasmid CAG-

GFP (Addgene #16664), was a gift from Fred Gage (Zhao et al., 2006). Plasmid pCI-VSVG (Addgene #1733), was a gift from Garry Nolan. Plasmid pUMVC (Addgene #8449), was a gift from Bob Weinberg (Stewart et al., 2003). Virus titer of $4x10^5$ transducing units/ml was determined after transduction of polybrene-treated murine fibroblasts and quantification of GFP-expressing cells.

Stereotaxic surgery for retroviral delivery

Mice 5-7 weeks of age at the time of surgery were anesthetized with 1-2% isoflurane and placed in a stereotaxic setup (Kopf, Tujunga, CA). A microsyringe was used to deliver retrovirus bilaterally to the dorsal dentate gyrus (1.0 µl per injection at 0.15 µl/min) using stereotaxic surgery coordinates according to Paxinos and Franklin's mouse brain atlas from bregma (mm): -2.0 anteroposterior, ±1.3 lateral, -2.0 dorsoventral (suprapyramidal blade); -2.0 anteroposterior, ±1.3 lateral -2.3 dorsoventral (infrapyramidal blade). Mice were perfused 3 or 6 weeks after surgery for histochemical labeling and confocal imaging.

Histology

All histochemistry was carried out on 50µm-thick free floating coronal brain sections. Sections were incubated in various combinations of primary antibodies against GFP, 3R-Tau, Synaptophysin, PSA-NCAM, and PV, and biotinylated lectin WFA, at 4°C for 48h in 0.1M PBS with 0.3% Triton X-100 and 3% normal donkey serum. After incubation in primary antisera, sections were washed and incubated in secondary antisera in 0.1M PBS with 0.3% Triton X-100 for 2h at room temperature. All labeled brain sections were counterstained with Hoechst 33342 or DAPI. For the list of antibodies used, **see Table 3.1**. For the GFAP-TK experiment, whole sections were imaged with a Hamamatsu NanoZoomer S60 (Japan), all other sections were imaged with a Zeiss confocal microscope LSM 700 (Oberkochen, Germany).

Table 3.1. Antibodies for histochemistry.

Name	Host Species	Dilution	Type	Company	Catalog #
Parvalbumin (PV)	Mouse	1:500	Primary	Sigma-Aldrich (St. Louis, MO)	P3088
Parvalbumin (PV)	Rabbit	1:2000	Primary	Abcam (Cambridge, UK)	ab11427
GFP	Rabbit	1:500	Primary	Molecular Probes (Eugene, OR)	G10362
Wisteria floribunda agglutinin (WFA) lectin	N/A	1:500	Primary	Sigma-Aldrich	L1516
3RTau	Mouse	1:500	Primary	Millipore (Burlington, MA)	05-803
Synaptophysin (SYP)	Mouse	1:200	Primary	Millipore	MAB329
PSA-NCAM	Rat	1:400	Primary	BD Pharmingen (San Diego, CA)	BDB556325
Donkey anti-mouse 568	Donkey	1:500	Secondary	Invitrogen (Carlsbad, CA)	A10037
Donkey anti-rat 488	Donkey	1:500	Secondary	Abcam	ab150153
Donkey anti-rabbit 488	Donkey	1:500	Secondary	Invitrogen	A21206
Donkey anti-rabbit 568	Donkey	1:500	Secondary	Invitrogen	A10042
anti-Streptavidin 647	N/A	1:500	Secondary	Molecular Probes	S32357
anti-Streptavidin 488	N/A	1:500	Secondary	Molecular Probes	S11223A

Confocal microscopy

Images were acquired using a Zeiss confocal microscope (LSM 700; four visible solid-state lasers: UV 405; argon 458/488; HeNe 555/568; far-red 639). For intensity and bouton analysis of mossy fibers (GFP or 3R-Tau), triple-labeled sections for mossy fibers, PV, and WFA were imaged. Images of labeled cells focused on single PV+ cell bodies and proximal dendrites; acquired (63x with 2x zoom; NA, 1.4; oil-immersion) taking z-stacks including the entirety of the cell body ±10µm, using 0.05µm z intervals (>300 optical slices per cell). Brain sections for comparison were stained together and all images were taken with identical confocal settings to allow for cross comparison of optical intensities. Only brain sections with visible GFP or 3R-Tau mossy fiber staining were scanned. From these sections, all PV+ cells in the hilus and sgz of the dentate gyrus were scanned. Approximate PV+ cell location was recorded separately on a dorsal hippocampus template to locate neighboring pairs (defined as ≤ 30µm distance apart) of PV+ with zero to low PNN expression (defined as WFA+ optical intensity < 400) and PV+ with high PNN expression (defined as WFA+ optical intensity > 400). For PSA-NCAM+, PV+WFA+, and WFA+ cell density analyses, images of the entire dorsal dentate gyrus were acquired (20x with 0.5x zoom; NA, 0.8) taking z-stacks at 3.0µm intervals (9–15 optical slices per cell). All slides were coded prior to analysis and the code was not revealed until the analysis was complete.

Mossy fiber intensity analysis

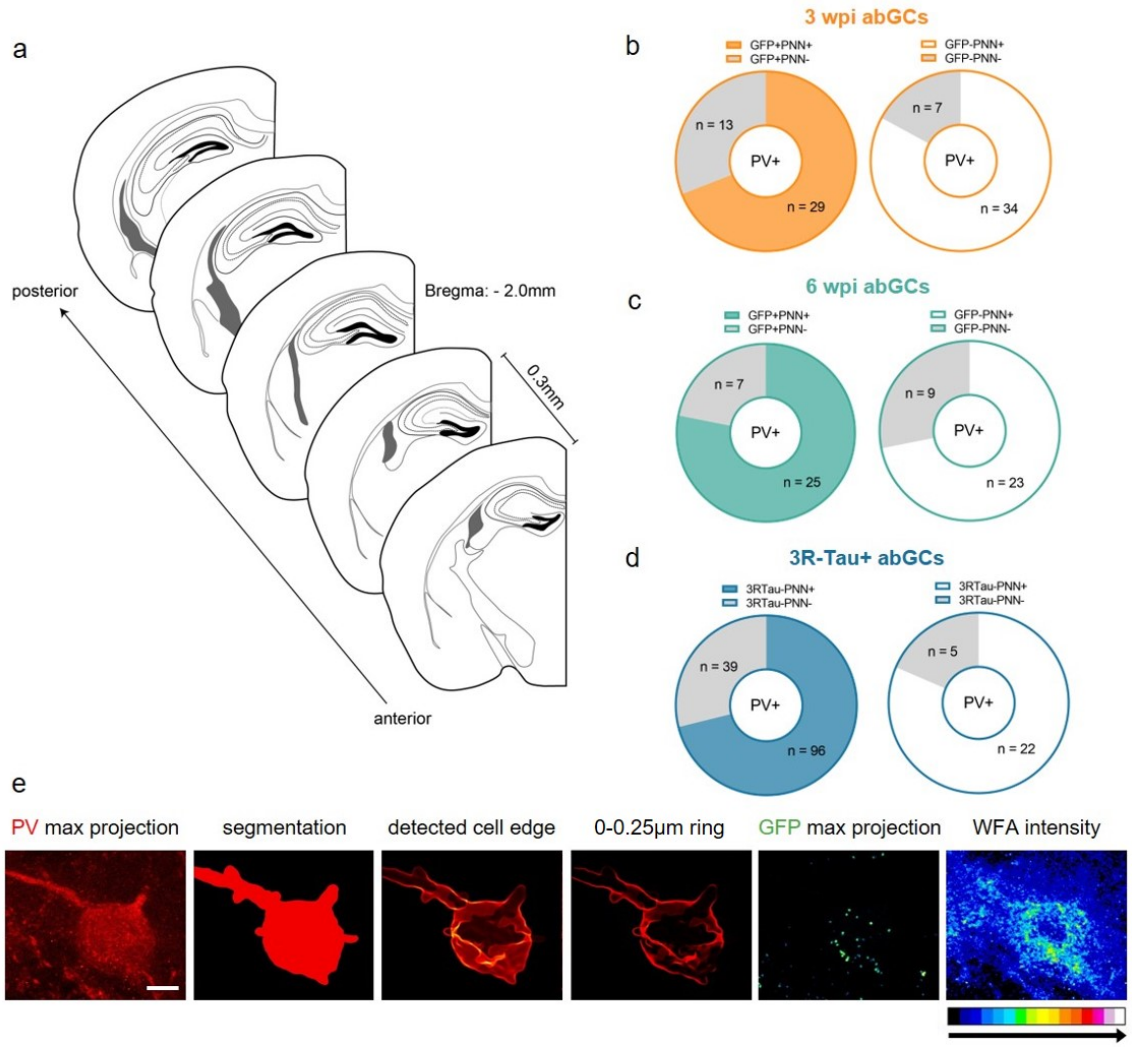
In order to detect mossy fiber labeling at various distances from the PV+ cell edge, we designed an analysis pipeline to preprocess the z-stack confocal images, segment fluorophore signal from markers for GFP, 3R-Tau, PV, or WFA, and analyze the optical intensity of the signal (**Fig S3.1b**). Analyses of mossy fibers and PNNs surrounding PV+ cells were conducted using custom Python software. Image loading was performed using Scikit-Image 0.13.11 (van der Walt et al., 2014) and SimpleITK 1.0.0 (Lowekamp et al., 2013). Statistical analyses were performed using SciPy 1.1.0 (Jones, Oliphant, & Peterson, 2001). Data manipulations were performed in Python 2.7 using Numpy 1.14.3 (Oliphant, 2006) and Pandas 0.23.0 (McKinney, 2010). Hard-coded preprocessing variables were determined empirically after several iterations, blinding to condition was maintained during this process.

Analysis pipeline.

PV+ cell segmentation: PV+ volumes were preprocessed by iteration (n = 3) through a series of Gaussian filtering (21 voxel kernel), eroding and dilating (9 voxel kernel each), and another Gaussian filtering. Voxels with intensities below 0.8 standard deviations from the mean were set to zero. Mossy fiber segmentation: Either GFP+ or 3R-Tau+ signal went through one iteration of Gaussian filtering (3 voxel kernel), eroding and dilating (3 voxel kernel each), and another Gaussian filtering. Threshold was set at 1.0 standard deviations above the mean. PNN segmentation: WFA+ signal went through two iterations of Gaussian filtering (25 voxel kernel), eroding and dilating (9 voxel kernel each), and another Gaussian filtering. Threshold was set at 0.8 standard deviations above the mean. This method of preprocessing was successful for a majority of cells, however, some segmentation was inadequate (GFP+: n = 5; 3R-Tau+: n = 9) and thus, cells that were identified as inadequate were removed from analysis. Cell edge detection and ring analysis: After preprocessing, voxel-wise distances from the PV+ cell edge were calculated (scipy.ndimage.morphology.distance_transform_edt). Quartile statistics were recorded for unprocessed mossy fiber and PNN voxels within each ring from the PV+ cell edge

(between 0 to 0.25, 0.25 to 0.5, 0.5 to 0.75µm). Mossy fiber intensity and corresponding PV+ and WFA+ PNN intensity values were plotted and Pearson's correlation coefficient (r) was computed to assess the relationship between mossy fiber intensity and the relevant PV+ cell.

Figure S3.1 Analysis pipeline for quantification of PV+ interneurons, abGCs, mossy fibers and boutons, and PNNs.



(**a**) Representative hippocampal coronal sections used for all analyses. (**b – d**) PV+ population ring charts showing proportion of cells scanned positive or negative for PNNs, and positive or negative for abGC mossy fibers (GFP or 3R-Tau-labeling). (**b**) GFP experiment: 3 wpi n = 83 total PV+ cells, n = 5 mice. (**c**) 6 wpi n = 64 total PV+ cells, n = 5 mice. (**d**) 3R-Tau: n = 162 total PV+ cells, n = 10 mice. (**e**) Representative maximum projection confocal image of sgz/hilar PV+ interneuron in red.

Left to right: *Segmentation* – custom Python software preprocessed the confocal image and detected positive labeling for PV+. *Detected cell edge* – the PV+ cell edge was determined from the segmentation. *0.25μm ring* (magenta) – was created from the cell surface as an ROI for mossy fiber intensity detection; example image is from a single z-plane. *GFP max projection* – GFP-retrovirus labeling (green-blue), proximal to the PV+ interneuron. For the bouton analysis, GFP+ puncta with a minimum Euclidean distance of 3μm from the PV+ cell surface with a volume between 8-50μm^3 was detected as a bouton. *WFA intensity* – heat map intensity-projection of a WFA-labeled PNN surrounding the PV+ interneuron. Arrow below color legend indicates increasing optical intensity. 3R-Tau+ labeled sections were analyzed identically. Scale bar = 10μm.

Mossy fiber bouton analysis

Mossy fiber intensity analysis assessed not only axon terminals, but also fibers in passing. To obtain a more specific measure of putative mossy fiber terminals, we carried out an additional analysis on the same z-stack confocal images using shape and volumetric criterion for mossy fiber boutons: spherical/puncta shape with a $3.0\mu m^3 \leq x \leq 50.0\mu m^3$ volume (Toni et al., 2008). We used a connected components analysis (scipy.ndimage.measurements.label) revealing grouped islands of non-zero voxels. Centers of mass (scipy.ndimage.measurements.center_of_mass) were then recorded for cell center and mossy fiber puncta. Individual voxel-wise Euclidean distances between edges of mossy fiber puncta and cell edge were calculated, where the voxel pair with the shortest distances were recorded. Post-processed mossy fiber puncta voxel intensity means and sums were also recorded. Only mossy fiber puncta values with the specified shape and volume criterion, described above, and a Euclidean distance ≤ 3.0μm from the PV+ cell were recorded. Mossy fiber bouton number and corresponding PV+WFA+ PNN intensity values were plotted and Pearson's correlation coefficient (r) was computed to assess the relationship between mossy fiber boutons and the relevant PV+ cell.

Cell density, intensity, and statistical analysis

Cell densities (PSA-NCAM; PV; WFA) were counted using FIJI (FIJI is just ImageJ, NIH), with the exception of the GFAP-TK experiment, which was counted using NDP2+ (Hamamatsu). Both were calculated by dividing the total number of positive-labeled cells within the dorsal hilus and

sgz of the dentate gryus over the traced volume. Volumes were traced from max projections in the DAPI channel by researchers unaware of the experimental groups. Percent colocalization of PV+ cells surrounded by PNNs was determined by calculating total number of PV+PNN+ cells over the total number of PV+ cells. Density and colocalization comparisons between groups were statistically analyzed using either linear mixed effects (lme) modeling using the lme4 package (Bates et al., 2014) in RStudio (RStudio Team, 2016), or unpaired t-tests (with or without corrections for unequal standard deviations). Data sets with multiple dependent variable values per animal were taken into account in lme models to prevent over-averaging errors. Statistics used throughout the manuscript include lme modeling, Pearson r correlations, simple linear regressions, and paired and unpaired t-tests, as described throughout the text, figure legends, and statistics tables. Unless otherwise stated, data are presented as mean ± SEM. Outliers were assessed using a robust regression and outlier removal (ROUT) method (Q = 0.2%) in GraphPad Prism 8.4.1 (GraphPad Software, San Diego, CA) for single-value dependent variables (see statistics tables). Outliers were assessed using the box plot statistics function, boxplot.stats, in RStudio for multiple-value dependent variables, where 5 brain section outliers were excluded in the aging study (see statistics tables). Non-normal or 'skewed' data sets were either log transformed or analyzed using nonparametric tests, as appropriate. Normality was assessed using Anderson-Darling test, Shapiro-Wilk test, D'Agostino & Pearson omnibus test, and Kolmogorov-Smirnov test, with a *p* value of 0.05.

Results

Mossy fibers and boutons from adult-born granule cells are more concentrated near PV+ neurons surrounded by PNNs

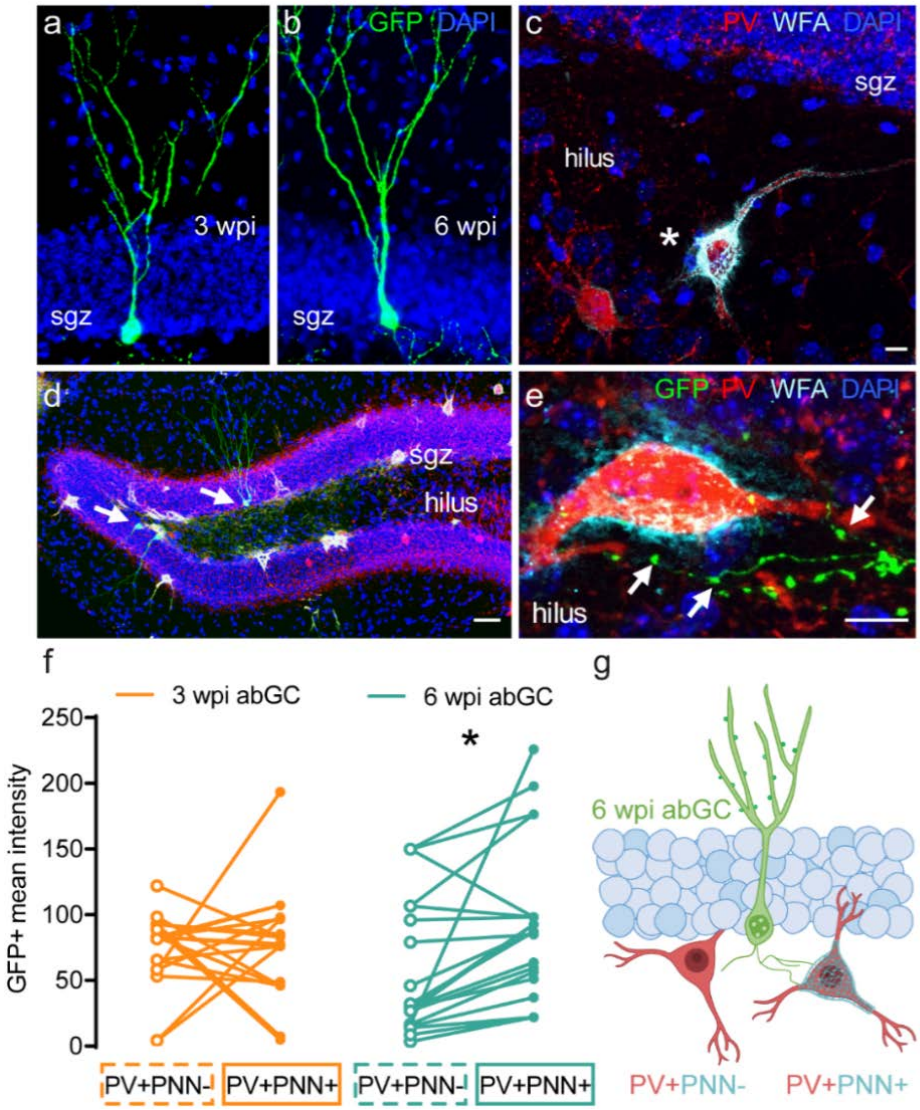
GFP-retrovirus injection in the dentate gyrus of adult mice at both 3 and 6 weeks post-infection (wpi) (**Fig 3.1a, b**) produced consistent labeling of cells with granule cell morphology in both the suprapyramidal and infrapyramidal blades of the granule cell layer (**Fig 3.1d**). GFP-labeled mossy fibers were observed emanating from GFP-labeled granule cells into the hilar region, and

had characteristic varicosities known to represent *en passant* synapses (Zhao et al., 2006; Toni et al., 2008). These GFP-labeled varicosities were often observed in close proximity to PV+ cells in the dentate gyrus (**Fig 3.1e**). In order to detect abGC mossy fiber labeling nearby PV+ interneurons, we created a 0.25μm ring surrounding the PV+ cell edge as our region of interest (ROI) for analysis. We designed an analysis pipeline to preprocess z-stack confocal images, segment fluorophore signal from markers for GFP, PV, and WFA, and analyze the optical intensity of the signals (**Fig S3.1e**). At both 3 and 6 wpi, we observed a large percentage of PV+ interneurons that had adult-born mossy fiber labeling within 0.25μm distance from the cell body surface (~50%), as well as a high percentage of PV+ interneurons labeled with *Wisteria Floribunda Agglutinin* (WFA) (~75%), a plant derived lectin that labels PNNs (**Fig S3.1b, c**).
In order to determine whether axons of new granule cells are more likely to be located near PV+ cells with or without PNNs, we compared mossy fiber intensity values between neighboring pairs of PV+PNN- and PV+PNN+ cells (see example, **Fig 3.1c**). At 3 wpi, GFP+ mossy fiber intensity appeared to be evenly distributed between PV+PNN- and PV+PNN+ pairs ($t_{18} = 0.2574$, $p = 0.7998$) (**Fig 3.1f**). Conversely, at 6 wpi, adult-born mossy fiber labeling was significantly greater near PV+PNN+ cells compared to PV+PNN- cells ($Z = -172.0$, $p = 0.0006$, Cohen's $d = 0.907$) (**Fig 3.1f**). This result suggests a greater likelihood of abGC connectivity with PV+ cells enwrapped in PNNs (see schematic, **Fig 3.1g**).

Previous experiments found that WFA binds primarily to aggrecan components of PNNs (Giamanco et al., 2010). Aggrecan is a chondroitin sulfate proteoglycan critical for the formation of PNNs, regulated by experience-dependent plasticity, where decreased excitatory input resulted in decreased PNN formation (McRae et al., 2007). Given this information, it is important to consider that not all PV+PNN+ interneurons are functionally homogeneous, nor do they share similar PNN profiles. When examining dentate gyrus PV+PNN+ interneurons from 3 and 6 wpi tissue, combined, we found varying levels of WFA intensity (representative images in **Fig 3.2a**), likely representing differing levels of activity-dependent PNN components. We found that with increasing WFA intensity, abGC mossy fiber intensity also increased ($r = 0.5238$, $p < 0.0001$) (**Fig**

S3.2a). In addition to looking at WFA intensity, we determined whether a relationship between PV and its surrounding PNN exists by analyzing cell body PV expression. We found that PV+ intensity was also positively associated with PNN intensity (r = 0.4065, $p < 0.0001$), where high-expressing PNNs were likely to surround high-expressing PV+ interneurons (**Fig S3.2b**).

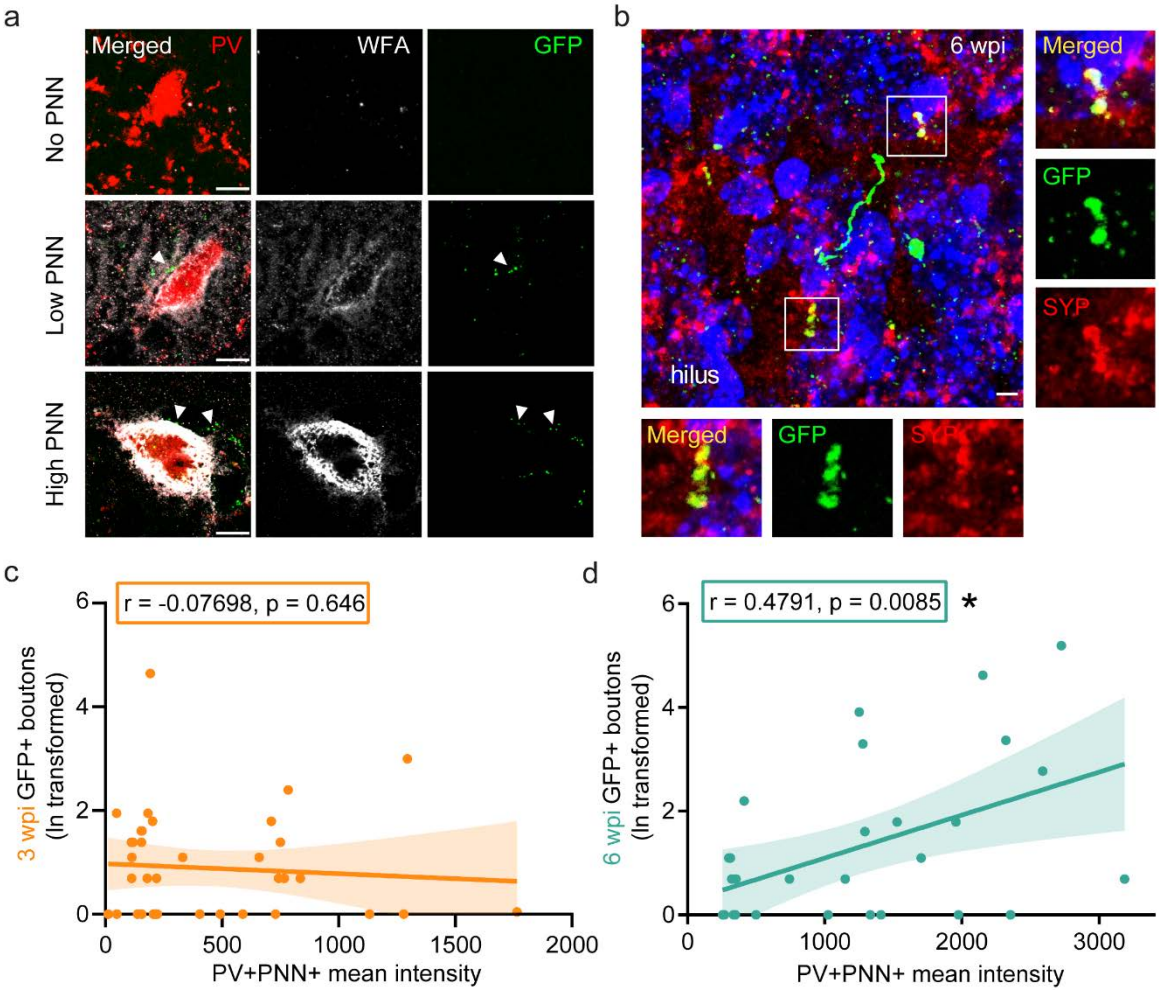
Figure 3.1 6 week old abGC mossy fibers are greater in intensity near PV+ interneurons enwrapped in PNNs compared to neighboring PV+PNN- interneurons.



(**a-b**) Adult mice (n = 10) were injected with retrovirus CAG-GFP (green) in the dDG. Representative high magnification images of a 3-week post-infection (wpi) abGC (**a**) and 6 wpi abGC (**b**). (**c**) Representative high magnification image of neighboring PV+ interneurons (red) in the hilus, where

one is enwrapped in WFA+ PNN (white-cyan; indicated with a white asterisk) and the other is not. Scale bar = 10μm. (**d**) Representative image of adult-born neurons infected with CAG-GFP (green; indicated by white arrows), PV+ interneurons (red), WFA+ PNNs (white-cyan), and DAPI (blue). Scale bar = 50μm. (**e**) Representative high magnification image of GFP+ abGC mossy fibers (green) proximal to a PV+PNN+ interneuron. Examples of GFP+ abGC boutons indicated by white arrows. Scale bar = 10μm. (**f**) Paired t-test comparison of abGC mossy fiber (GFP+) optical intensity within 0.25μm of the cell surface, between neighboring PV+ interneurons (PV+PNN- vs PV+PNN+) showed no difference at 3 wpi (t_{18} = 0.2574, p = 0.7998, n = 19 pairs), but showed greater intensity surrounding PV+PNN+ interneurons at 6 wpi (Z = -172.0, p = 0.0006, n = 20 pairs). (**g**) Conceptual schematic of an abGC sending more axon projections to a PV+PNN+ hilar interneuron at 6 wpi compared to the neighboring PV+PNN- interneuron.

Figure 3.2 Adult-born mossy fiber boutons are more abundant near PV+ interneurons surrounded by intensely labeled PNNs at 6 wpi.



(**a**) Representative high magnification images of PV+ interneurons (red) in the hilus with varied WFA-labeled PNNs (white), and proximal mossy fibers labeled with GFP (green). White arrows depict GFP+ mossy fiber boutons. Scale bars = 10μm. (**b**) Representative high magnification image of GFP+ adult-generated mossy fibers and boutons (green), presynaptic protein, synaptophysin (SYP; red), and counterstain (DAPI; blue) in the hilus at 6 wpi. Examples of co-labeled boutons are boxed. Merged images show co-labeled GFP and SYP boutons. Scale bar = 5μm. (**c**) No correlation between PV+ interneuron WFA optical intensity and number of proximal 3 wpi abGC boutons (r = -0.07698, *p* = 0.646). (**d**) Positive correlation between PV+ interneuron WFA optical intensity and number of proximal 6 wpi abGC boutons (r = 0.4791, *p* = 0.0085).

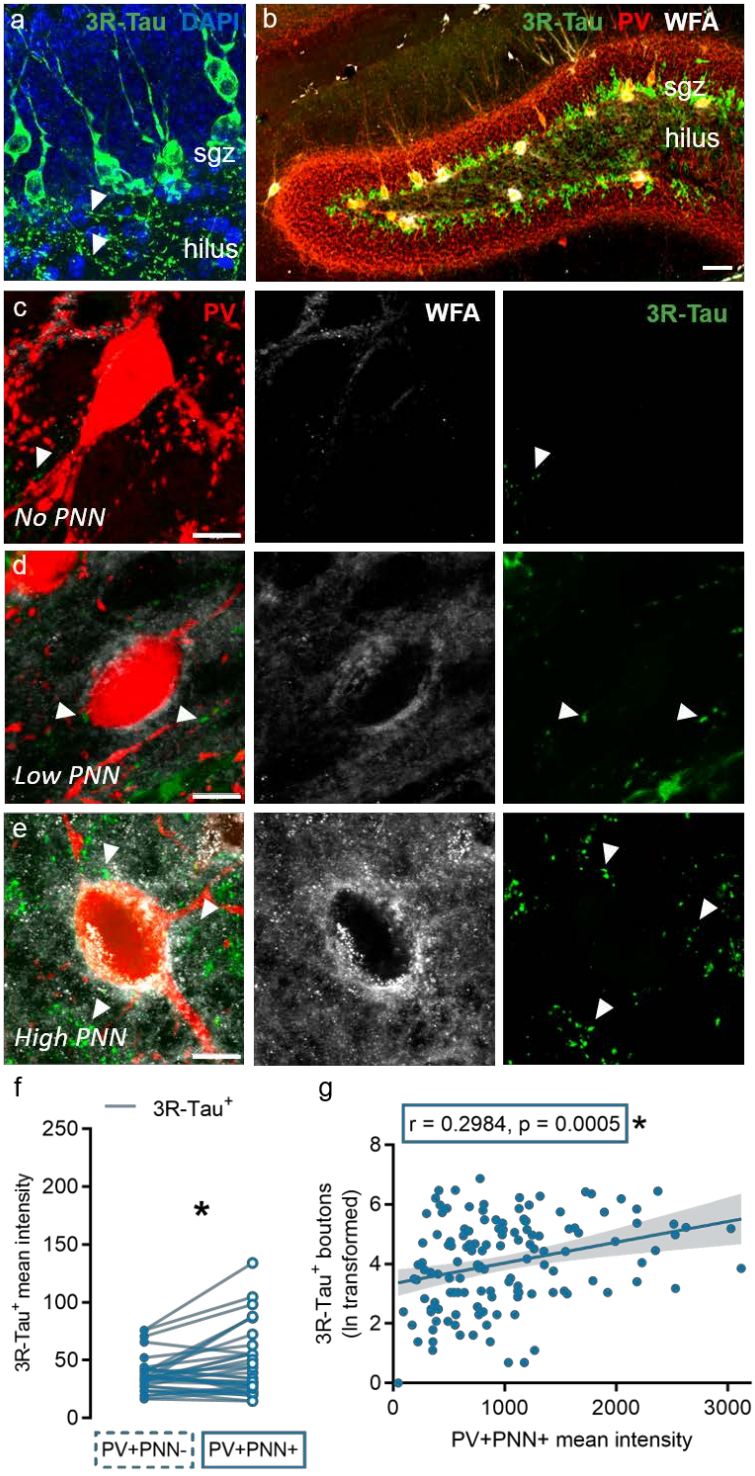
Considering that our GFP+ mossy fiber intensity values may represent axons passing by PV+ cells without forming synapses, we analyzed GFP-labeled bouton number, a more specific measure of putative mossy fiber terminals, using previously determined morphological criteria (Toni et al., 2008). We found a positive relationship between PV+ cell PNN intensity and nearby 6 wpi GFP+ bouton number ($r = 0.4791$, $p = 0.0085$) (**Fig 3.2d**), where greater abGC bouton number was more often located near PV+ cells with greater PNN intensities. This effect was not seen when analyzing 3 wpi GFP+ boutons ($r = -0.07698$, $p = 0.646$) (**Fig 3.2c**), suggesting that, as previously reported, 3 wpi abGCs exhibit immature connectivity compared to 6 wpi abGCs (Toni et al., 2008). We also verified whether these GFP+ boutons were likely sites of synaptic contact with presynaptic marker synaptophysin, and found positive evidence of co-labeling (**Fig 3.2b**).

To corroborate these findings using an endogenous marker of adult-born neurons, we analyzed 3-repeat Tau (3R-Tau) isoform labeling, a microtubule-associated protein found in immature neurons in the dentate gyrus of the adult mouse brain. 3R-Tau labels the cytoplasm of cell bodies, dendrites, and mossy fibers from abGCs at approximately 2-7 weeks after their generation (Llorens-Martin et al., 2012; Fuster-Matanzo et al., 2012). 3R-Tau labeling of the dentate gyrus of adult mice produced a large number of stained cells with the morphology and location consistent with adult-generated granule cells (**Fig 3.3a, b**). The number of these cells is consistent with those observed using two other commonly used markers of immature neurons in the mouse dentate gyrus: doublecortin and PSA-NCAM (Bullmann et al., 2007; Llorens-Martin et al., 2012). 3R-Tau labeled mossy fibers were observed emanating from labeled abGCs into the hilar region. Similar to what we observed with GFP-labeled mossy fibers, 3R-Tau labeled axons had characteristic varicosities and were often observed in proximity to PV+ cells in the dentate gyrus (**Fig 3.3c-e**). We observed a large percentage of PV+ interneurons with 3R-Tau abGC mossy fiber labeling within a 0.25μm distance from the soma (>80%), as well as a high percentage of PV+ interneurons enwrapped in PNNs (>70%) (**Fig S3.1e**). Comparison of the two approaches to label abGCs revealed similar staining patterns, with the exception that the GFP-

retrovirus labeled fewer abGCs than did 3R-Tau. Like our results with the GFP-retrovirus, we found that 3R-Tau mossy fiber intensity was greater surrounding PV+PNN+ interneurons compared to neighboring PV+PNN- interneurons (Z = -5.496, p = 0.0317, Cohen's d = 0.417) (**Fig 3.3f**). Similarly, we found a positive correlation between 3R-Tau mossy fibers and PV+ PNN intensity (r = 0.1923, p = 0.0266) (**Fig S3.2c**) and between PV+ intensity and its surrounding PNN intensity (r = 0.1776, p = 0.0238) (**Fig S3.2d**). Also as expected, 3R-Tau+ boutons were more often associated with PV+ interneurons with greater PNN intensities (r = 0.2984, p = 0.0005) (**Fig 3.3g**).

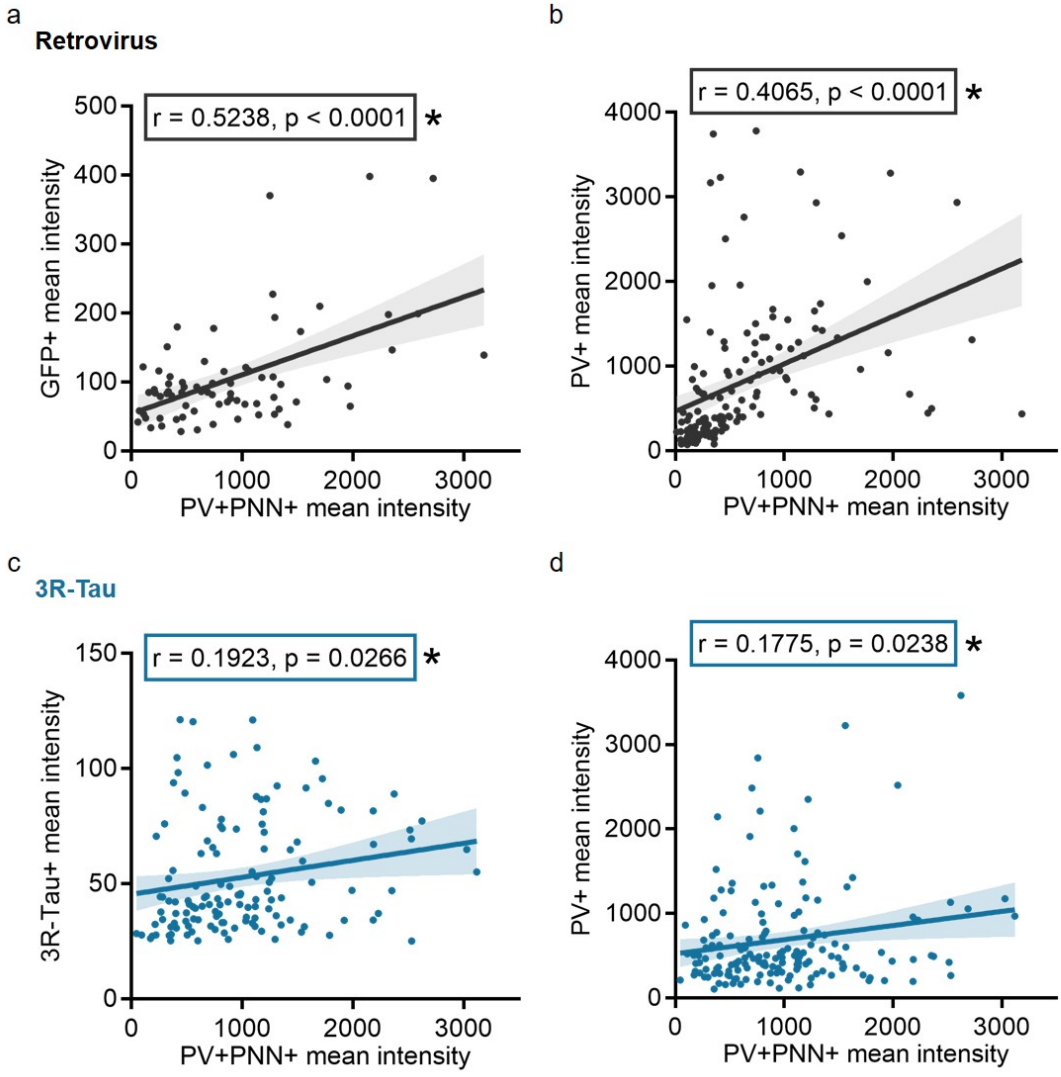
These results show that mossy fibers from abGCs, labeled with either GFP-retrovirus 6 weeks prior or the endogenous marker 3R-Tau, are more likely to be associated with PV+ cells surrounded by PNNs than those without PNNs, and that bouton number shares a positive linear relationship with PNN intensity. Additionally, we discovered that PV+ cells with greater PNN expression were more likely to have nearby immature mossy fibers compared to neighboring PV+ cells with less intensely stained or no PNN expression. These findings demonstrate that mossy fibers of abGCs are more likely to be found near PV+ interneurons with PNNs than those without. Additionally within the PV+PNN+ interneuron population, abGC mossy fibers are more likely to be found near those with more intense PNNs, which are also more likely to express PV at higher intensities.

Figure 3.3 3R-Tau labeled abGCs show the same affinity for PNN PV+ interneurons as GFP-retrovirus labeled abGCs.



(**a**) Adult mouse (n = 10) hippocampal sections were immunostained for microtubule-associated protein 3R-Tau (green) and counterstained with DAPI (blue). Representative high magnification image of abGCs and their mossy fibers, examples indicated by white arrows. (**b**) Representative image of adult-born neurons labeled with 3R-Tau (green), PV+ interneurons (red), and WFA+ PNNs (white). Scale bar = 50μm. (**c-e**) Representative high magnification images of PV+ interneurons (red) in the hilus with various WFA-labeled expressing PNNs (white), and proximal mossy fibers labeled with 3R-Tau (green). Increased number of 3R-Tau abGC boutons are associated with high expressing PNNs (**e**). White arrows indicate mossy fiber bouton examples. Scale bars = 10μm. (**f**) Within-subject comparison of neighboring PV+ interneurons (PV+PNN- vs PV+PNN+) showed greater abGC mossy fiber optical intensity near the PV+PNN+ interneurons ($Z = -261.0$, $p = 0.0317$, n = 35 pairs). (**g**) Positive correlation between PV+ interneuron PNN optical intensity and number of proximal 3R-Tau abGC boutons ($r = 0.2984$, $p = 0.0005$).

Figure S3.2 Adult-generated mossy fiber intensity near PV+ interneurons increases with increasing PNN intensity, where high-expressing PNNs are also associated with greater PV+ interneuron intensity.



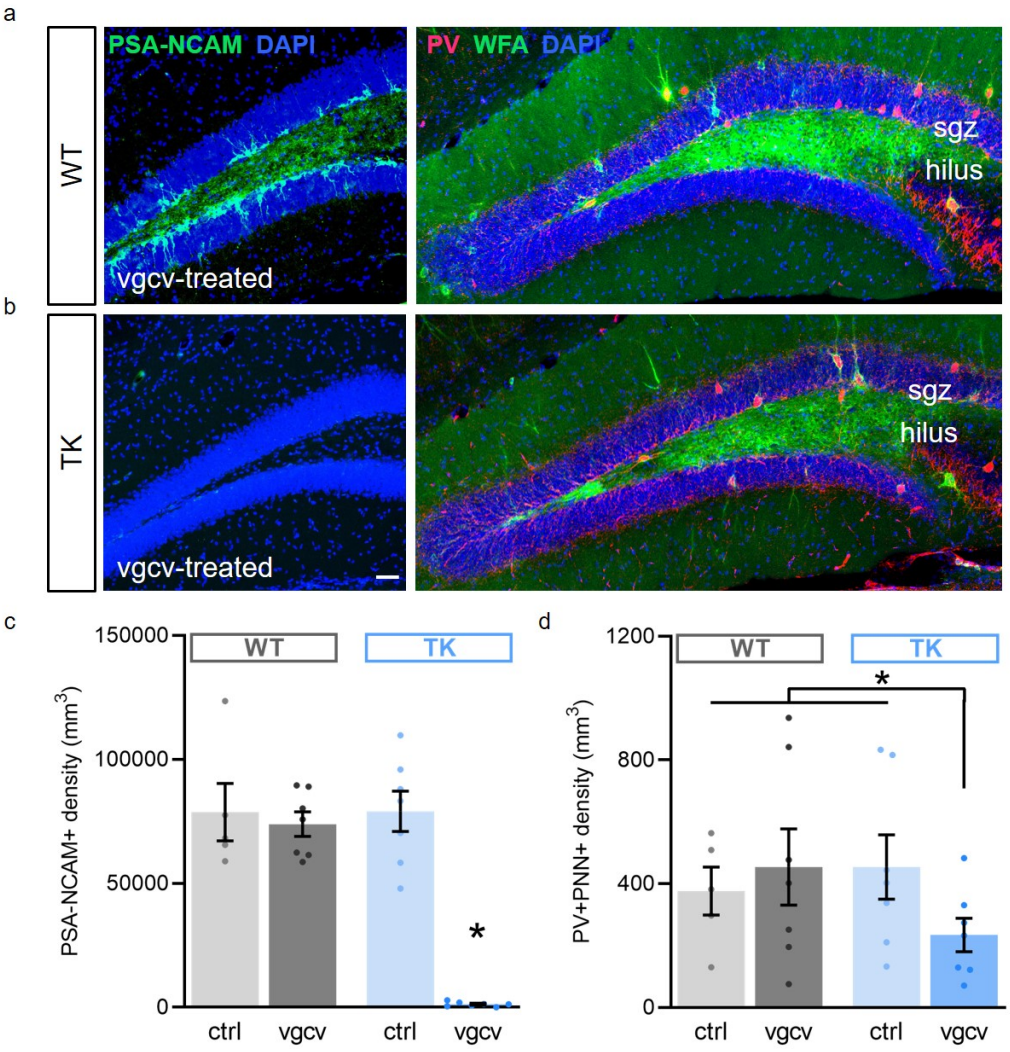
(**a**) Positive correlations between GFP-retrovirus labeled mossy fibers and corresponding PV+ target cell's PNN mean optical intensity (r = 0.5238, $p < 0.0001$) in 3 and 6 wpi sections, combined. (**b**) Positive correlation between PV+ interneuron optical intensity and its surrounding PNN mean optical intensity (r = 0.4065, $p < 0.0001$) in 3 and 6 wpi sections combined. (**c**) Positive correlation between 3R-Tau labeled mossy fibers and corresponding PV+ target cell's PNN mean optical intensity (r = 0.1923, $p = 0.0266$). (**d**) Positive correlation between PV+ interneuron optical intensity and its surrounding PNN mean optical intensity (r = 0.1775, $p = 0.0238$) in the 3R-Tau experiment.

Transgenic knockout of adult neurogenesis is associated with fewer PNN+ PV+ interneurons

To test whether the presence of axons from new neurons influences PNN expression around PV+ interneurons, we investigated the densities of PV+PNN+ interneurons in two instances of reduced adult neurogenesis using a transgenic knockout and differently aged mice. First, we confirmed new neurons were knocked out in GFAP-TK mice, a transgenic inducible-knockout of adult neurogenesis when treated with valganciclovir (vgcv), compared to controls (β = -78,261.46, SE = 9,375.88, $p < 0.0001$, Cohen's $d = 0.6878$) (**Fig 3.4c**). Once this difference was determined, we proceeded to compare the mice with ablated adult neurogenesis, TK-vgcv, to all three control groups combined. Next, we tested to see if new neuron densities corresponded with PV+PNN+ densities, and found that a reduction in new neuron numbers was coincident with a reduction in PV+PNN+ density ($t_{19.86} = 2.466$, $p = 0.0229$, Cohen's $d = 0.838$) (**Fig 3.4d**), and a reduction in the percent of total PV+ interneurons positive for PNNs (β = -16.20, SE = 6.39, $p = 0.0188$, Cohen's $d = 0.360$) (**Fig S3.3a**). We then examined whether blocking adult neurogenesis affected total PV and PNN density, separately, and found no changes (PV: β = -159.4, SE = 242.5, $p = 0.517$; PNN: β = 9.22, SE = 195.4, $p = 0.963$) (**Fig S3.3a**).

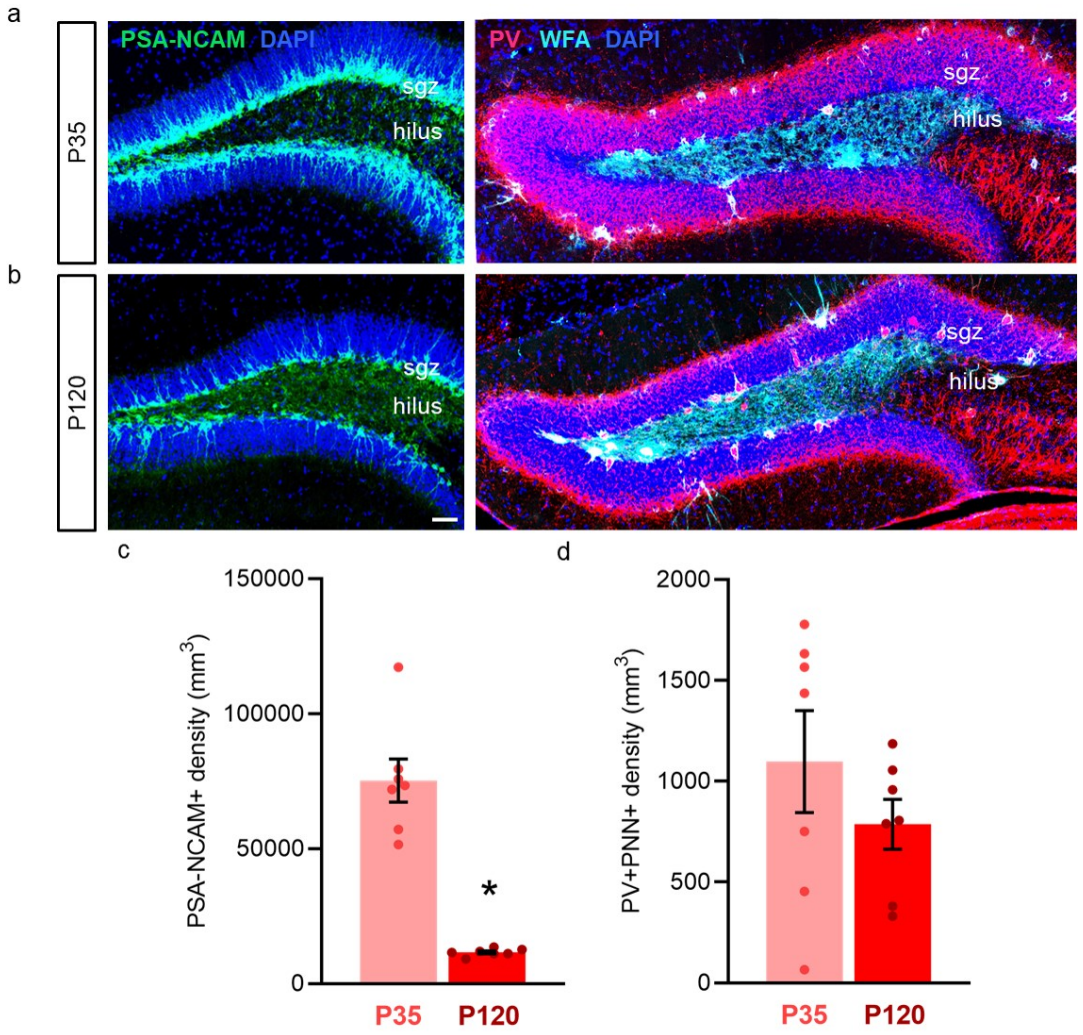
To follow up the results from the GFAP-TK experiment, we explored whether an age-related reduction in adult neurogenesis (P35 compared to P120 mice) was associated with changes in PNNs surrounding PV+ interneurons. As expected, we found that the density of PSA-NCAM labeled cells was significantly reduced in older mice ($U = 0.0$, $n_1 = n_2 = 7$, $p = 0.0006$) (**Fig 3.5c**), consistent with previous findings (Molofsky et al., 2006). Age-related decline of neurogenesis was not coincident with a significant reduction in the number of PV+PNN+ neurons (β = 283.93, SE = 282.66, $p = 0.335$) (**Fig 3.5d**). We did find that, in older mice, overall PNN+ cell density was decreased (β = 2,136.87, SE = 461.28, $p < 0.0005$, Cohen's $d = 0.478$), but the percent of total PV+ interneurons positive for PNNs (β = -0.1967, SE = 9.60, $p = 0.984$) and PV+ density (β = 310.58, SE = 354.35, $p = 0.398$) was unchanged (**Fig S3.3b**). While these findings suggest that reduced adult neurogenesis is associated with changes in PNNs, they do not suggest that abGC axons are necessary to maintain PNNs around PV+ interneurons.

Figure 3.4 Transgenic knockdown of adult neurogenesis is associated with reduced number of PV+PNN+ neurons in the dentate gyrus.



Adult GFAP-TK mice were given 10.5 weeks of vgcv (n = 7) before tissue collection and analysis, in addition to littermate controls (n = 7). Aged matched GFAP-TK mice (n = 7) and littermate controls (n = 5) without vgcv-treatment were also examined. (**a-b**) Representative images of PSA-NCAM+ labeled adult-born neurons (green) on the left, and PV+ interneurons (magenta), WFA+ PNNs (green), and DAPI (blue) labeled cells on the right. WT (**a**) and TK mice (**b**) treated with vgcv. Hilus and sgz = ROIs for cell counts. (**c**) TK mice treated with vgcv show a robust decrease in PSA-NCAM+ labeled new neurons in comparison to all control groups (β = -78261.463, SE = 9375.875, $p < 0.0001$). (**d**) TK mice treated with vgcv compared to all control groups combined, yields a significant decrease in PV+PNN+ density ($t_{19.86} = 2.466$, $p = 0.0229$). Data are presented as mean ± sem. Scale bar = 50μm.

Figure 3.5 Aging-induced reduction in new neurons is not associated with significant changes in PV+PNN+ interneuron number.



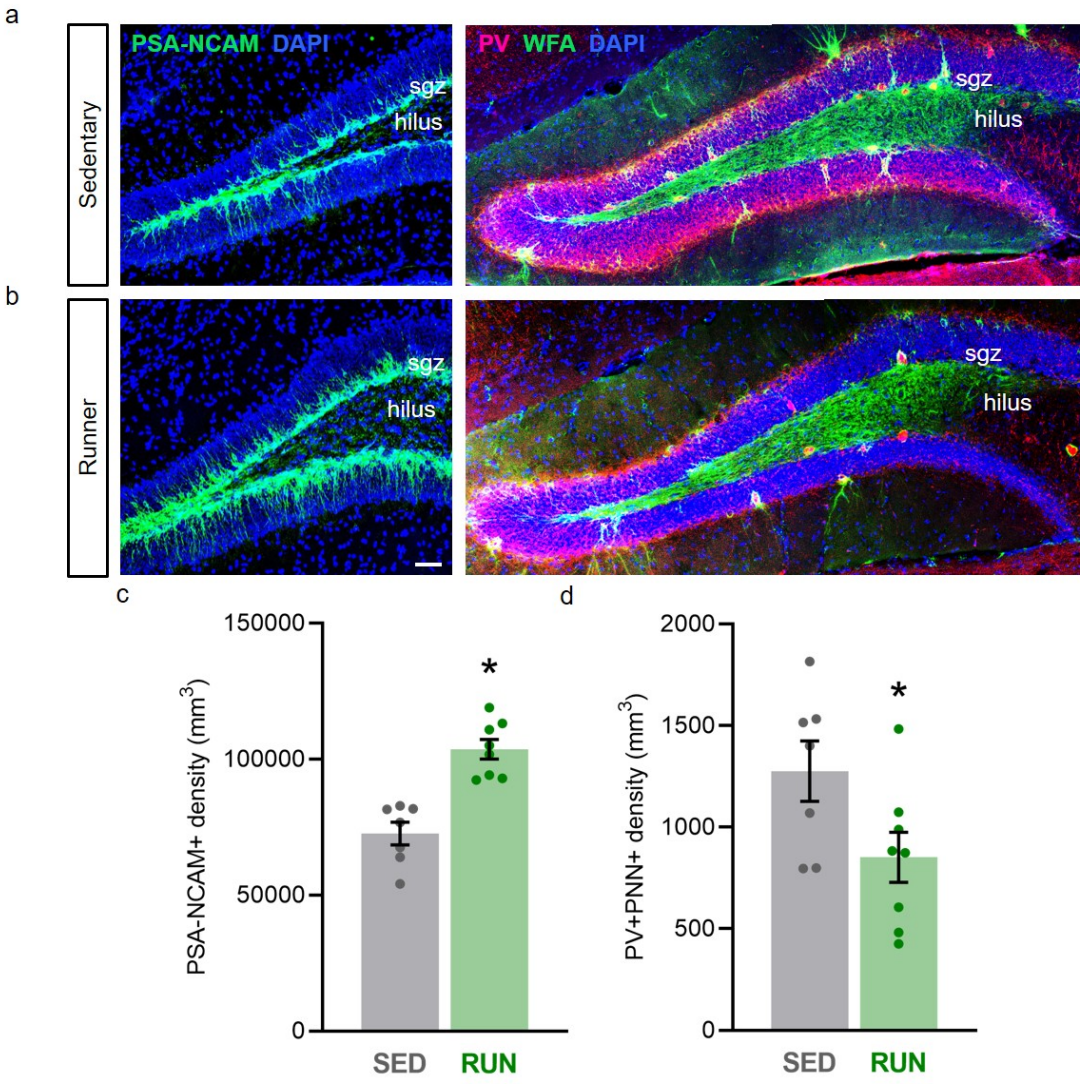
(**a-b**) Coronal sections from pubescent (P35, n = 7) (**a**) and mature adult (P120, n = 7) (**b**) mice were analyzed. Representative images of PSA-NCAM+ labeled adult-born neurons (green) depicted on the left, and PV+ interneurons (magenta), WFA+ PNNs (white-cyan), and DAPI (blue) labeled cells on the right. Hilus and sgz = ROIs for cell counts. (**c**) P120 mice show a robust decrease in PSA-NCAM+ labeled new neurons compared to P35 mice (Mann-Whitney $U = 0.0$, $n_1 = n_2 = 7$, $p = 0.0006$). The median for P35 = 73,493, and for P120 = 11,575. (**d**) No difference in PV+PNN+ density between P35 and P120 mice ($\beta = 283.93$, SE = 282.66, $p = 0.335$). Data in the bar graph are presented as mean ± sem. Scale bar = 50μm.

Running enhances adult neurogenesis and decreases PNNs

Next, we considered a condition where new neurons were increased in the dentate gyrus. Consistent with previous results (van Praag et al., 1999, 2005; Schoenfeld et al., 2013), we found an increase in adult neurogenesis in mice that had unlimited access to a running wheel compared to sedentary controls ($t_{11.35}$ = -5.774, p = 0.0001, Cohen's d = 0.404) (**Fig 3.6c**). However, the running-induced increase in adult neurogenesis was associated with a decrease in PV+PNN+ density, similar to the transgenic knockout study (β = -419.47, SE = 183.08, p = 0.0417, Cohen's d = 0.193) (**Fig 3.6d**). Surprisingly, running also decreased both the densities of PNN+ cells (β = 1120.9, SE = 446.9, p = 0.0144, Cohen's d = 0.478) and PV+ interneurons (β = -820.0, SE = 311.4, p = 0.0103, Cohen's d = 0.6484), separately (**Fig S3.3c**). However, this did not alter the percent of total PV+ interneurons positive for PNNs in runners compared to controls (β = 2.297, SE = 7.276, p = 0.758) (**Fig S3.3c**).

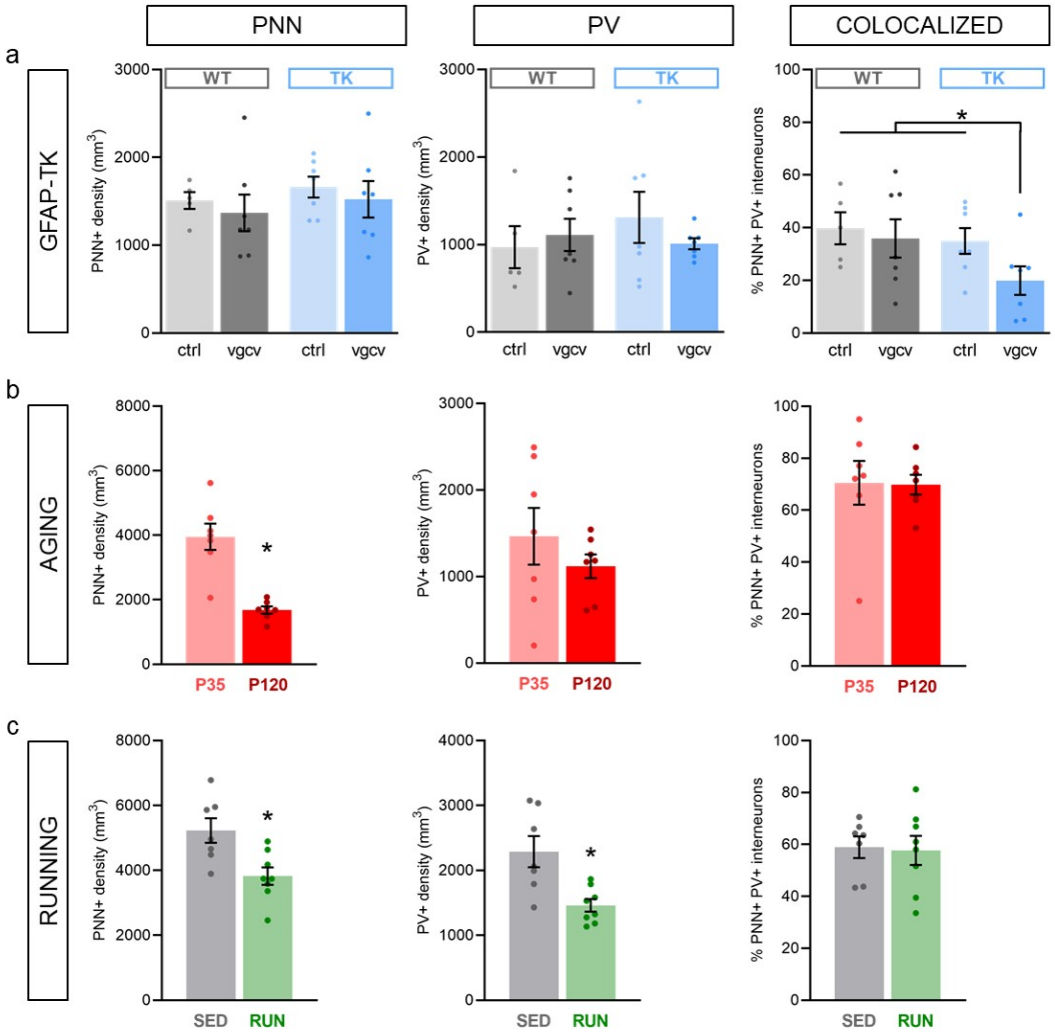
The results from these experimental manipulations do suggest that PV+ interneurons and PNNs often change in tandem. To test this assumption, we analyzed PV+ density and PNN+ density in all control groups (WT-ctrl & vgcv, TK-ctrl, P35, SED) and found a positive correlation between the two measures (r = 0.605, p = 0.00019). We did not find this to be true when analyzing a correlation between PSA-NCAM+ density and PV+PNN+ density (r = -0.022, p = 0.902). Collectively, these findings do not support the hypothesis that abGC axons stimulate PNN formation around PV+ interneurons, and instead suggest that aging and exercise likely induce widespread changes to the hippocampus, many of which are not directly related to abGCs.

Figure 3.6 Running-induced increases in new neuron number are associated with reduced numbers of PV+PNN+ neurons in the hippocampus.



(**a-b**) Coronal sections from sedentary (SED, n = 7) (**a**) and runner (RUN, n = 8) (**b**) mice were analyzed. Representative images of PSA-NCAM+ labeled adult-born neurons (green) depicted on the left, and PV+ interneurons (magenta), WFA+ PNNs (green), and DAPI (blue) labeled cells on the right. Hilus and sgz = ROIs for cell counts. (**c**) RUN mice (103,644 ± 3,570) show an increase in PSA-NCAM+ labeled new neurons compared to SED mice (72,654 ± 4,156) ($t_{11.35}$ = -5.774, p = 0.0001). (**d**) RUN mice also show a decrease in PV+PNN+ interneuron density compared to SED controls (β = -419.47, SE = 183.08, p = 0.0417). Data in the bar graph are presented as mean ± sem. Scale bar = 50μm.

Figure S3.3 Characterization of PNN+ density, PV+ interneuron density, and percent colocalization in the GFAP-TK (P140), aging (P35, P120), and running (P70) experiments.



(**a**) No differences were found when comparing TK-vgcv to all other groups for WFA-labeled PNN cell density (β = 9.224, SE = 195.42, p = 0.963) or PV+ interneuron density (β = -159.4, SE = 242.5, p = 0.517). Percent of PV+ interneurons that were PNN+ were significantly decreased in TK-vgcv mice (β = -16.196, SE = 6.39, p = 0.0188). (**b**) WFA-labeled PNN+ cell density was reduced in P120 mice (1,685 ± 111.5) compared to P35 mice (3,951 ± 407.3) (β = 2,136.87, SE = 461.28, p < 0.0005). No differences were found in PV+ density (β = 310.58, SE = 354.35, p = 0.398) or percent of PV+ interneurons positive for PNNs (β = -0.1967, SE = 9.60, p = 0.984). (**c**) Both PNN density and PV+ interneuron density were reduced in RUN mice (PNN: β = 1120.9, SE = 446.9, p = 0.0144; PV: β = -820.0, SE = 311.4, p = 0.0103). However, the PV+ percent population, that was positive for PNNs, was unaltered (β = 2.297, SE = 7.276, p = 0.758). Data in bar graphs are presented as mean ± sem.

Statistics Table 3.1. GFP-retrovirus experiment analyses.

GFP+ Retrovirus Experiment	Normality	Outliers	Statistical Test	Group(s)	N (data points)	N (animals)	Mean1	SEM	CI (95%)	Mean2	SEM	CI (95%)	p-value	Pearson's r	Cohen's d	R^2
3 wpi paired analysis	Passes	NA	Paired t-test	PV+PNN- vs PV+PNN+ cells	19 pairs	5 C57BL/6J	73.3	6.712	59.20; 87.40	76.58	9.438	56.75; 96.41	0.7998	-0.2203	--	0.003667
6 wpi paired analysis	Fail	NA	Wilcoxon matched-pairs rank test	PV+PNN- vs PV+PNN+ cells	20 pairs	5 C57BL/6J	57.84	11.44	33.89; 81.79	93.68	13.18	66.09; 121.3	**0.0006**	(Spearman) 0.7513	0.907	--
GFP/PNN intensity correlation	--	1	Correlation x-y paired	GFP+PV+ cells	73 pairs	5 C57BL/6J	GFP: 105.3	8.699	87.96; 122.6	PNN: 909.8	80.9	748.5; 1,071	**<0.0001**	0.5238	--	0.2744
GFP/PNN intensity linear regression	--		Simple linear regression				slope= 0.011	--	0.0347; 0.078	--	--	--		--	--	
PV/PNN intensity correlation	--	NA	Correlation x-y paired	All PV+ cells	147 pairs	5 C57BL/6J	PV: 811.8	67.18	679; 944.6	PNN: 618.0	48.59	522; 714.1	**<0.0001**	0.4065	--	0.1653
PV/PNN intensity linear regression	--		Simple linear regression				slope= 0.562	--	0.3547, 0.7694	--	--	--		--	--	
3 wpi bouton/PNN intensity correlation	log transform	4	Correlation x-y paired	GFP+PV+ cells	38 pairs	5 C57BL/6J	Bouton: 0.89	0.168	0.547; 1.228	PNN: 451.9	67.44	315.3; 588.6	0.646	-0.07698	--	0.005926
3 wpi bouton/PNN intensity linear regression	--		Simple linear regression				slope= $-1.9e^{-4}$	--	-0.001, 0.00065	--	--	--		--	--	
6 wpi bouton/PNN intensity correlation	log transform	3	Correlation x-y paired	GFP+PV+ cells	29 pairs	5 C57BL/6J	Bouton: 1.3	0.284	0.706; 1.868	PNN: 1,229	164	893.1; 1,565	**0.0085**	0.4791	--	0.2296
6 wpi bouton/PNN intensity linear regression	--		Simple linear regression				slope= 0.0008	--	$2.3e^{-4}$, $1.4e^{-3}$	--	--	--		--	--	

Statistics Table 3.2. 3R-Tau experiment analyses.

3R-Tau Experiment	Normality	Outliers	Statistical Test	Group(s)	N (data points)	N (animals)	Mean1	SEM	CI (95%)	Mean2	SEM	CI (95%)	p-value	Pearson's r	Cohen's d	R^2
3R-Tau intensity paired analysis	Fail	NA	Wilcoxon matched-pairs rank test	PV+PNN- vs PV+PNN+ cells	35 pairs	10 C57BL/6J	37.18	2.565	31.97, 42.39	46.69	4.933	36.67, 56.72	**0.0317**	(Spearman) 0.6338	0.417	--
3R-Tau/PNN intensity correlation	--	2	Correlation x-y paired	3RTau+PV+ cells	133 pairs	10 C57BL/6J	3R-Tau: 52.79	2.132	48.57; 57.01	PNN: 1,007	55.55	897.4; 1,117	**0.0266**	0.1923	--	0.037
3R-Tau/PNN intensity linear regression	--		Simple linear regression				slope= 0.0074	--	0.0008, 0.0139	--	--	--		--	--	
PV/PNN intensity correlation	--	NA	Correlation x-y paired	All PV+ cells	162 pairs	10 C57BL/6J	PV: 688.7	46.78	596.3; 781.1	PNN: 991.7	49.64	893.6; 1,090	**0.0238**	0.1776	--	0.0315
PV/PNN intensity linear regression	--		Simple linear regression				slope= 0.0733	--	0.0225, 0.3121	--	--	--		--	--	
3R-Tau bouton/PNN intensity correlation	log transform	2	Correlation x-y paired	3RTau+PV+ cells	133 pairs	10 C57BL/6J	Bouton: 4.04	0.131	3.782; 4.299	PNN: 1,011	56.08	899.6; 1,121	**0.0005**	0.2984	--	0.0891
3R-Tau bouton/PNN intensity linear regression	--		Simple linear regression				slope= $7.0e^{-4}$	--	$3.1e^{-4}$, $1.1e^{-3}$	--	--	--		--	--	

Statistics Table 3.3. Transgenic knockout experiment analyses.

GFAP-TK Experiment	Normality	Outliers	Statistical Test	Group(s)	N (animals)	Mean1	SEM	Mean2	SEM	β	SE	p-value	Cohen's d
PSA-NCAM density	Fail	NA	Linear mixed-effects model 2-way ANOVA	WT or GFAP-TK; vgcv or ctrl	7 mice/group* *WT-ctrl = 5	TK-vgcv: 1,316.55	305.4	WT-ctrl: 79,873.55	9,560.46	-78,261.46	9,375.88	**<0.0001**	0.6878
PV+PNN+ density	Fail	NA	Welch's t-test	TK-vgcv vs all ctrls	7 mice/group* *WT-ctrl = 5	TK-vgcv: 237.03	44.28	ctrls: 447.08	45.95	t = 2.466	--	**0.0229**	0.838
% PV+PNN+/PV+ cells	Pass	NA	Linear mixed-effects model	TK-vgcv vs all ctrls	7 mice/group* *WT-ctrl = 5	TK-vgcv: 20.39	3.91	ctrls: 36.3	2.90	-16.20	6.39	**0.0188**	0.36
PV+ density	Pass	NA	Linear mixed-effects model	TK-vgcv vs all ctrls	7 mice/group* *WT-ctrl = 5	TK-vgcv: 997.69	123.7	ctrls: 1,203.64	97.63	-159.4	242.5	0.517	--
PNN+ density	Pass	NA	Linear mixed-effects model	TK-vgcv vs all ctrls	7 mice/group* *WT-ctrl = 5	TK-vgcv: 1,550.78	133.5	ctrls: 1,540.01	64.13	9.22	195.4	0.963	--

**exception*

Statistics Table 3.4. Aging experiment analyses.

Aging Experiment	Normality	Outliers	Statistical Test	Group(s)	N (animals)	Mean P35	SEM	Mean P120	SEM	β	SE	p-value	Cohen's d
PSA-NCAM density	Fail	NA	Mann-Whitney t-test	P35 vs P120	7 mice/group	75,251	7,999	11,605	515.60	U = 0	--	**0.0006**	--
PV+PNN+ density	Fail	5	Linear mixed-effects model	P35 vs P120	7 mice/group	1,098	252.7	786.8	122.90	283.93	282.66	0.335	--
% PV+PNN+/PV+ cells	Pass	5	Linear mixed-effects model	P35 vs P120	7 mice/group	70.52	8.41	69.82	3.80	-0.1967	9.6	0.984	--
PV+ density	Fail	5	Linear mixed-effects model	P35 vs P120	7 mice/group	1,465	328.1	1,118	136.70	310.58	354.35	0.398	--
PNN+ density	Fail	5	Linear mixed-effects model	P35 vs P120	7 mice/group	3,951	407.3	1,685	111.50	2,136.87	461.28	**<0.0005**	0.478

Statistics Table 3.5. Running experiment analyses.

Running Experiment	Normality	Outliers	Statistical Test	Group(s)	N (animals)	Mean RUN	SEM	Mean SED	SEM	β	SE	p-value	Cohen's d
PSA-NCAM density	Pass	NA	Linear mixed-effects model t-test	RUN vs SED	RUN = 8; SED = 7	103,644	3,570	72,654	4,156	-29,296.44	5,074	**0.0001**	0.404
PV+PNN+ density	Pass	NA	Linear mixed-effects model	RUN vs SED	RUN = 8; SED = 7	852.3	123.00	1,276	148.6	-419.47	183.08	**0.0417**	0.193
% PV+PNN+/PV+ cells	Pass	NA	Linear mixed-effects model	RUN vs SED	RUN = 8; SED = 7	57.7	5.579	58.94	4.143	2.297	7.276	0.758	--
PV+ density	Pass	NA	Linear mixed-effects model	RUN vs SED	RUN = 8; SED = 7	1,460	97.12	2,290	240.2	-820	311.4	**0.0103**	0.6484
PNN+ density	Pass	NA	Linear mixed-effects model	RUN vs SED	RUN = 8; SED = 7	3,826	269.5	5,229	380.20	1,120.90	446.9	**0.0144**	0.4778

Discussion

Our findings suggest that axons of abGCs in the dentate gyrus preferentially target PV+ interneurons with PNNs compared to PV+ interneurons without PNNs. Within the PV+PNN+ interneuron population, abGC axons are more likely to be located near PV+ interneurons with intense PNNs compared to those with less intense PNNs. It is likely that these results suggest differences in synaptic contact rather than axons in passing, because the relationship was observed with the analysis of GFP+ synaptic boutons, axonal entities found to be colabeled with presynaptic protein synaptophysin. Recent findings have raised the concern that the use of viruses to label and manipulate neurons in the dentate gyrus may result in the death of abGCs (Johnston et al., 2020). However, our results using endogenous marker of abGCs, 3R-Tau, closely paralleled those from our retrovirus study, demonstrating that the relationship we observed between abGC axons and PNN+ interneurons is not the result of toxicity or plasticity mechanisms engaged through surgical interventions.

Considerable evidence suggests that PNNs play important roles as general plasticity inhibitors (Sorg et al., 2016; Pizzorusso et al. 2002; Hou et al., 2017; Faini et al., 2018). More specifically, PNNs have been shown to inhibit axonal growth (Wang et al., 2008) and limit receptor movement at hippocampal synapses (Frischknecht et al., 2009). This general view is consistent with recent evidence that PV+PNN+ interneurons in the dentate gyrus exhibit less experience-dependent dendritic plasticity than their PV+PNN- counterparts (Foggetti et al., 2019). Since adult neurogenesis is an important form of plasticity in the hippocampus, the increased propensity for abGC axons to contact PNN+ interneurons may function as a stability mechanism to enable the formation of new connections without maladaptively disrupting the underlying microcircuitry. However, recent findings suggest that PNNs also enhance LTP in the hippocampus (Shi et al., 2019), which may increase the impact of innervation by abGCs. Since abGCs have been shown to exhibit enhanced LTP, it is possible that at synapses, which involve postsynaptic PNNs, this effect is further augmented.

In the adult dentate gyrus, newly generated neurons receive inhibitory input and extend their axons into the hilus, where they primarily target GABAergic inhibitory interneurons (Toni et al., 2008; Restivo et al., 2015) and form a feedforward inhibitory circuit. Since PNN formation varies across the PV+ population, an important consideration is how PNNs influence the activity of the cell. Variation in PNN expression has been shown to be related to input where decreases in PNN expression have been associated with increases in inhibitory input, whereas increases in PNN expression have been associated with increases in excitatory input (Brückner et al., 1993). Recent work has shown that transient removal of PNNs in the anterior cingulate cortex and CA1 region of the hippocampus causes an increase in feedback inhibition onto PV+ interneurons, resulting in impaired theta oscillations. Conversely, increasing PNNs specifically around PV+ interneurons enhanced theta oscillations and improved memory-related behavior (Shi et al., 2019). Decreased GABAergic signaling was found to be coincident with the downregulation of PV protein expression (Lodge et al., 2009; Volman et al., 2011). In parallel, downregulation and upregulation of PV expression have been observed in conjunction with increases in inhibitory input and increases in excitatory input, respectively (Filice et al., 2016; Behrens et al., 2007; Kinney et al., 2006). One interpretation of these results suggests that increased PNN intensity would correlate with levels of PV positively, and we found this to be the case in both retrovirus and 3R-Tau-labeled tissue. Collectively, these results suggest that PV+ interneurons with weak or no PNNs receive and recruit more inhibitory input, potentially making these cells less likely to participate in excitatory synaptic plasticity.

One possible interpretation of our finding, that abGC axons are more often associated with PV+PNN+ cells, is that innervation by abGCs drives the formation of PNNs. To investigate this possibility, we examined PNNs in the dentate gyrus of three different conditions known to alter numbers of abGCs. First, we investigated a GFAP-TK transgenic mouse model of ablated adult neurogenesis and found that mice lacking new neurons in the dentate gyrus exhibited reduced density of PV+PNN+ cells. These findings are consistent with the hypothesis that abGC innervation may drive increased PNN formation in postsynaptic PV+ targets. Second, we

compared mice of two different ages, around the time of puberty and at 4 months of age, where the number of abGCs is known to drop precipitously between these time points. Although we did not detect a significant decrease in the density of PV+PNN+ cells in the older mice, the mean number of these cells was trending in the expected direction. Unlike the transgenic adult neurogenesis inhibition model, the observed decrease in new neurons in the older mice was not a complete reduction and comparatively presented more variation, which may explain the less definitive result in this latter study. Aging likely involves other major changes in the hippocampus in addition to decreases in the number of abGCs. In this regard, it is worth noting that, although older mice did not show a convincing reduction in PV+PNN+ cells, they exhibited a reduction in overall numbers of PNN+ cells, an effect we did not observe in the transgenic mouse model. Furthermore, our study shows a slight, but not statistically significant, reduction in PV+ cells, which has been shown to reduce with advanced age (Ueno et al., 2017). Third, we examined whether an experiential condition associated with increased numbers of abGCs, voluntary running, would have an effect on PV+PNN+ cells. Surprisingly, given our previous results, we found a decrease in numbers of PV+PNN+ neurons with this comparison, despite substantial increases in the number of abGCs. We also observed a decrease in the number of PNN+ cells in the dentate gyrus of runners, similar to what we observed in the older compared to younger mice. When considering all 3 experiments together, no clear relationship emerged between the number of abGCs and PV+PNN+ cells in the dentate gyrus.

The interneuron subtypes of PV-negative cells surrounded by PNNs remain elusive, as little to no calretinin+ or somatostatin+ interneurons have been found to be colocalized with PNNs in the hippocampus (Murthy et al., 2019). Thus, the consequences of reduced PV- PNN+ cells on hippocampal function in this study remain unknown. It is possible that the manipulations analyzed in this study induce downregulation of PV expression in cells enwrapped in PNNs, such that they are no longer detectable as PV+, but future studies are needed to test this. Of course, it is important to consider that both aging and running alter a number of cellular processes, e.g., dendritic complexity, synaptic plasticity, and glial cell numbers, many of which are unlikely to be

directly linked to abGCs. It remains the case, however, that the most specific alteration in abGCs, the transgenic model we examined, exhibited reduced PV+PNN+ cells in conjunction with reduced abGCs. Thus, we cannot rule out the hypothesis that abGC innervation onto PV+ interneurons may drive the cell to produce more molecules associated with PNNs. The lack of this effect in the other conditions may be due to the engagement of compensatory or unrelated processes during aging and running.

An alternative, but not mutually exclusive, hypothesis is that PNNs surrounding PV+ interneurons may have chemoattractive properties that guide more abGC axons to grow toward them. Although this hypothesis has not been directly tested, some molecules associated with PNNs, such as semaphorin 3A, a regulator of synaptic inputs (Dick et al., 2013; Vo et al., 2013), or neuronal pentraxin-2, known to regulate and recruit AMPA receptors on PV+ cells (Pelkey et al., 2015), are potential candidates to play this role. Brevican, neurocan, and tenascin PNN components have been shown to be necessary for both excitatory and inhibitory activity (Geissler et al., 2013) and maintenance of synaptic strength in the dentate gyrus (Jansen et al., 2017), bolstering the claim that PNNs are regulators, not just inhibitors, of plasticity. It could also be the case that PNNs stabilize inputs from abGCs, creating a more preferable environment for maintaining and supporting new synaptic connections.

In conclusion, this study reveals that axons and boutons of abGCs are more likely to be associated with PV+ cells surrounded by PNNs, and that a positive relationship exists between abGC axons and PNN intensity in the dentate gyrus. Here, we showed that blocking adult neurogenesis was sufficient to decrease PV+PNN+ cell density and colocalization, but that a moderate reduction with aging was not, nor was the converse observed with an increase in new neuron numbers with running. Together, our results suggest that PNNs surrounding PV+ interneurons within the dentate gyrus are the preferred targets of abGCs, but the extent to which this relationship is driven primarily by abGCs, their PNN+ targets, or both, remains undetermined.

CHAPTER 4: INVESTIGATING THE ROLE OF PERINEURONAL NETS AND STRIATAL PLASTICITY IN MOUSE MODELS WITH EXCESSIVE REPETITIVE BEHAVIORS

This work was presented in abbreviated form: Briones BA, Pitcher MN, Fleming WT*, Parel GT, Diethorn EJ, Haye AE, MacDowell CJ, Tawa EA, Zych AD, Buschman TJ, Gould E. (2019) Investigating the role of perineuronal nets and striatal plasticity in repetitive behaviors in mouse models of autism spectrum disorder. Gordon Research Conference on Modulation of Neural Circuits and Behavior, Poster 15.*

Briones BA, Pitcher MN, Fleming WT, Diethorn EJ, Zych AD, Haye AE, Murthy S, Gould E. (2018) Perineuronal nets are increased on parvalbumin+ interneurons of the dorsomedial striatum in three mouse models of autism spectrum disorder. Society for Neuroscience, Poster 639.07.

Chapter Introduction

In Chapter 2, I demonstrated that dorsal striatum inhibitory neurons, specifically MSNs, undergo experience-dependent plasticity in the healthy rodent brain. However, it is unknown how this phenomenon might be altered in pathologies concomitant with striatum-dependent deficits. In this chapter, I explore inhibitory neurons and PNNs in the dorsal striatum of mouse models exhibiting excessive repetitive behaviors to better understand the role of PNNs in inhibitory signaling and related behaviors. Considering the results from the hippocampus in Chapter 3, it is unclear what role PNNs play in the striatum and furthermore, whether PNNs participate in mechanisms of striatum-dependent plasticity. To get at this question, I first sought to identify whether PNNs in the dorsal striatum of mouse models exhibiting excessive repetitive behaviors differed from healthy controls and relatedly, if the structure and function of inhibitory neurons in the dorsal striatum also differs.

Introduction

Maladaptive repetitive and inflexible behaviors are a common core symptom associated with a multitude of disorders, including Autism spectrum disorder (ASD), obsessive-compulsive disorder (OCD), and other anxiety-related psychopathologies (National Institute of Mental Health (NIMH), 2017). These symptoms impair and disrupt everyday living throughout the lifespan, likely influencing the formation and increased severity of other associated symptoms, such as impaired

cognition and social deficits (Centers for Disease Control and Prevention (CDC), 2013; Hollander et al., 1996; Penadés et al., 2005; Shin et al., 2014). Within the human brain, numerous studies have linked repetitive and inflexible behaviors with corticostriatal circuits (Abbott et al., 2018; Langen et al., 2009, 2011), where an increase in severity may result from impairments in learning processes important for modulating sensorimotor cortex associations.

In nonhuman primates, tracing studies demonstrate that corticostriatal circuits are organized in feedforward “spiral” loop patterns which create interconnected, but functionally distinct subregions on a dorsal-ventral and medial-lateral axis (Haber et al., 2000). The rodent striatum is similarly subdivided, where the dorsomedial striatum (DMS) receives inputs from the prefrontal cortex, forming a circuit important for behavioral flexibility (i.e., action-outcome associations) (Packard and Knowlton, 2002). The dorsolateral striatum (DLS) receives inputs from sensorimotor cortex (Alexander et al., 1986; Haber et al., 2000; Selemon and Goldman-Rakic, 1985) and is necessary for the formation of stimulus-response associations and habitual behaviors (Devan et al., 2011; Yin et al., 2004; reviewed in: Yin & Knowlton, 2006). Similar to human studies, repetitive behaviors have been linked to the dorsal striatum of rodents (Ahmari et al., 2013; Burguière et al., 2013, 2015), and manifest as excessive digging, self-injurious over-grooming, and stereotyped movements that are resistant to changes in the environment..

The dorsal striatum is seemingly homogenous in its intrinsic cellular structure, where a striking 95% of its neurons are GABAergic medium spiny neurons (MSNs) (Bolam et al., 2000; Chang et al., 1982). The other 5% of striatal neurons are various interneuron subtypes (e.g., GABAergic, cholinergic). One of the larger subpopulations of GABAergic interneurons are parvalbumin-expressing (PV+) fast-spiking interneurons (FSIs) (Cowan et al., 1990; H. Kita et al., 1990; Kita, 1993). These interneurons, constituting but a small subset of the total number of neurons in the striatum, are thought to modulate excitatory input to MSNs, where inhibition from small populations of PV+ interneurons is sufficient to block action potentials in large populations of MSNs (Gittis et al., 2010; Lee et al., 2017).

A significant percentage of dorsal striatal PV+ interneurons are surrounded by specialized extracellular matrix structures called perineuronal nets (PNNs) (Lee et al., 2012). Studies have implicated PNNs in neuropsychiatric diseases including schizophrenia, Alzheimer's disease, and epilepsy (Pantazopoulos and Berretta, 2016; Rankin-Gee et al., 2015; Sorg et al., 2016; Yang et al., 2015). Mutations in extracellular matrix genes have also been identified in GWAS studies of humans with ASD (Carayol et al., 2011; Skaar et al., 2005), but even still, no studies have investigated whether extracellular matrix structures such as PNNs are abnormal in mouse models with behaviors commonly associated with repetitive behavior-related disorders. Despite the intriguing observations about the role of PV+ interneurons in dorsal striatal plasticity and behavior, it remains completely unexplored how PNNs around these neurons influence post-synaptic target cell physiology and behavioral output.

We examined the distribution of PNNs in the dorsal striatum of four mouse models known to exhibit excessive repetitive behaviors: BTBR, Cntnap2$^{-/-}$, Shank3$^{+/-\Delta C}$, and prenatal-toxin exposure to valproic acid (VPA). These four mouse models capture a wide breadth of etiologies, idiopathic (or unknown), genetic, and environmental causes. The BTBR mouse strain is an idiopathic mouse model used by many to study ASD-related pathologies including repetitive behaviors, and cognitive and social deficits (Ellegood and Crawley, 2015; Meyza and Blanchard, 2017; Sforazzini et al., 2016). Coincidentally, BTBRs have also been reported to have reduced adult neurogenesis in the hippocampus (Stephenson et al., 2011). Because a majority of psychopathologies present as idiopathic, the BTBR mouse is a potentially more representative system to study in further detail in comparison to transgenic models carrying single-gene mutations. Therefore, a majority of our study investigates PNNs in the DMS of BTBR mice. Cntnap2 and Shank3 are genes important for proteins involved in the maintenance and function of structural plasticity. Shank3 protein is highly expressed in the striatum and is a key regulator of postsynaptic densities on glutamatergic synapse (Peça et al., 2011). Mutations in the encoding of these proteins have been implicated in corticostriatal dysfunction and disorders associated with repetitive behavior phenotypes (Gdalyahu et al., 2015; Jiang and Ehlers, 2013; Kouser et al.,

2013; Peça et al., 2011; Peñagarikano et al., 2011). Prenatal exposure to toxins, infections, and drugs likely induce epigenetic changes that produce susceptibility to the development of psychopathologies. The VPA model in rodents, exposes pups in utero to VPA and produces aberrant behaviors, such as excessive grooming and digging, into adulthood (Nicolini and Fahnestock, 2018; Roullet et al., 2013). Although similar in behavioral abnormalities and striatal dysfunction, each mouse model, in addition to patients with excessive repetitive behaviors, presents an idiosyncratic combination of deficits, making the development of therapeutic targets near impossible.

To this end, we found consistent increases in the percent of PV+ interneurons enwrapped in PNNs in the DMS, but not DLS, across all four experimental mouse systems compared to healthy controls. This raises the possibility that excessive PNN formation in the DMS may restrict inhibitory plasticity, a subregion important for behavioral flexibility. To test this hypothesis, we transiently degraded DMS PNNs in BTBR mice, and found that the reduction of PNNs in the DMS was sufficient to diminish over-grooming and excessive digging behavior. These results suggest that an overabundance of PNNs around PV+ interneurons may exacerbate stereotyped behavior and rigidity in mouse models with excessive repetitive behaviors by disrupting inhibitory signaling in the DMS. We investigated DMS inhibitory transmission before and after PNN degradation by analyzing PV+ interneurons and their postsynaptic targets, MSNs, to gain better insight into the potential effects of PNNs on excessive repetitive behaviors in BTBR mice. We found no changes in immediate early gene neuronal activation in PV+ interneurons, however, putative MSNs showed decreased dendritic spines and ex vivo electrophysiology recordings of MSNs showed altered inhibitory transmission in mice with increased PNN expression. Together, these findings suggest that increased colocalization of PNNs enwrapping PV+ interneurons may prevent optimal synaptic plasticity in the DMS, contributing to maladaptive repetitive behaviors.

Materials and Methods

Animals and experimental manipulations

All animal procedures were conducted in accordance with the National Institutes of Health guidelines and approved by the NIMH and Princeton University Institutional Animal Care and Use Committees (IACUC). All mice were adults (between 10 – 24 weeks of age), and group housed with same-sex littermates and enrichment, under a reverse 12-hour light-dark schedule (lights off at 0700) with free access to food and water. Wildtype C57BL/6J mice (strain #000664) and inbred mouse strain BTBR T+Itpr3tf/J mice (strain #002282), from The Jackson Laboratory (Bar Harbor, ME), were used for behavior, histological, and physiological comparisons. Transgenic mice, Cntnap2$^{-/-}$ (strain #017482) and Shank3$^{+/-\Delta C}$ (strain #018398), were obtained from The Jackson Laboratory, subsequently bred at Princeton University, and used for histology experiments, only, and were additionally used for another study investigating glial cells in the hippocampus, medial prefrontal cortex, and dorsal striatum (Cope et al., 2016). VPA-treated mice were from genotype Thy1-GCaMP6f: C57BL/6J-Tg(Thy1-GCaMP6f)GP5.3Dkim/J, from The Jackson Laboratory (strain #028280). Both female (SAL = 4, VPA = 4) and male 9 (SAL = 4, VPA = 4) mice were used for histology, only, in this study, and were part of a larger study investigating the relationship between cortical dynamics and behavioral phenotypes (MacDowell and Buschman, 2020). The VPA model system was established and validated using previously reported methods (Gandal et al., 2010; Lauber et al., 2016; Moldrich et al., 2013; Yang et al., 2016). In brief, on embryonic day 12.5 pregnant dams received an injection of 600mg/Kg valproic acid dissolved in sterile water (controls received saline). During postnatal days (PND) 5 - 45, all pups underwent a series of various behavioral phenotyping tests and found an increase in self-grooming and marble burying, similar to previous reports (Kang and Kim, 2015; Wang et al., 2018). At the conclusion of each experiment, mice were deeply anesthetized with 0.07mL Euthasol (i.p. injection) and transcardially perfused with 4.0% paraformaldehyde (PFA) in phosphate buffered saline (PBS), pH 7.5. The brains were dissected and postfixed in 4.0% PFA for 48h before processing.

Chondroitinase ABC and penicillinase preparation

chABC (Sigma-Aldrich, St. Louis, MO) was prepared in sterile vehicle solution containing 1.0μL 0.1M PBS with 0.1% BSA and control enzyme pnase (Sigma-Aldrich) from *Bacillus cereus* was prepared in sterile 0.1M PBS vehicle solution. Both enzymes were prepared at a concentration of up to 50u/mL, based on previous publications (Cheng et al., 2015).

Stereotaxic surgery for chABC delivery

Mice 7 weeks of age at the time of surgery were anesthetized with 1-2% isoflurane and placed in a stereotaxic setup (Kopf, Tujunga, CA). A microsyringe and pump (World Precision Instruments, Sarasota, Fl) were used to deliver enzyme (chABC or pnase) to the DMS (0.3 μl per injection at 0.15 μl/min) using stereotaxic surgery coordinates according to Paxinos and Franklin's mouse brain atlas from bregma (mm): 1.3 anteroposterior, ±0.7 lateral, -3.0 dorsoventral (more anterior DMS); 0.0 anteroposterior, ±1.0 lateral -2.3 dorsoventral (posterior DMS). For the time course experiment, mice received chABC delivery into one hemisphere and pnase into the other, hemispheres were counterbalanced, and then perfused 4, 7, 14, or 21 days after surgery for histochemical labeling and confocal imaging. For the behavior experiment, mice received bilateral injections of either chABC or pnase. Grooming and digging behavior was observed 10 days post-surgery, and then perfused 2h after completion of behavior for histochemical labeling and confocal imaging.

Repetitive behavior testing

Wildtype and BTBR mice were scored for spontaneous grooming and digging as measures of repetitive behavior. Mice were placed in a dark open field apparatus enclosed inside an empty operant box (Med Associates, San Diego, CA) equipped with an overhead video camera, to limit anxiety-induced repetitive behaving. During grooming trials, mice were placed in a clean open field box where cumulative time spent grooming and number of grooming bouts were scored by experimenters blind to treatment, if any, and strain, even though coat color differences exist between strains, monochromatic video recordings eliminated this differentiation. Digging trials

were conducted and scored similarly, however, open field boxes were filled with a one-inch thick layer of home cage bedding to promote digging behavior. The day before testing, mice were habituated to the enclosed open field apparatus twice in one day for 5 mins at a time. Grooming and digging tests were 10mins each and order was counterbalanced.

Ex vivo electrophysiology

Mice were anesthetized with an i.p. injection of Euthasol (0.06ml/30g). Experimenters were blind to treatment, but could not be blinded to mouse strain because of strain differences in coat color. Mice were decapitated and the brain was extracted. After extraction, the brain was immersed in ice-cold NMDG ACSF (92mM NMDG, 2.5mM KCl, 1.25mM NaH_2PO_4, 30mM $NaHCO_3$, 20mM HEPES, 25mM glucose, 2mM thiourea, 5mM Na-ascorbate, 3mM Na-pyruvate, 0.5mM $CaCl_2 \cdot 4H_2O$, 10mM $MgSO_4 \cdot 7H_2O$, and 12mM N-Acetyl-L-cysteine; pH adjusted to 7.3-7.4) for 2 mins. Afterwards coronal slices (300μm) were sectioned using a VT1200s vibratome and then incubated in NMDG ACSF at 34 C for approximately 14 minutes. Slices were then transferred into a holding solution of HEPES ACSF (92mM NaCl, 2.5mM KCl, 1.25mM NaH_2PO_4, 30mM $NaHCO_3$, 20mM HEPES, 25mM glucose, 2mM thiourea, 5mM Na-ascorbate, 3mM Na-pyruvate, 2mM $CaCl_2 \cdot 4H_2O$, 2mM $MgSO_4 \cdot 7H_2O$ and 12mM N-Acetyl-l-cysteine, bubbled at room temperature with 95% O_2/ 5% CO_2).

Whole-cell recordings were performed using a Multiclamp 700B (Molecular Devices, Sunnyvale, CA), using pipettes with a resistance of 4-7 MOhm filled with an internal solution containing 100mM cesium chloride, 0.6mM EGTA, 10mM HEPES, 5mM NaCl, 20mM TEA, 4mM Mg- ATP, 0.3mM Na-GTP and 3mM QX 314 with the pH adjusted to 7.2 with CsOH and the osmolarity adjusted to around 289mmol kg^{-1} with sucrose. During recordings, slices were perfused with a recording ACSF solution (120mM NaCl, 3.5mM KCl, 1.25mM NaH_2PO_4, 26mM $NaHCO_3$, 1.3mM $MgCl_2$, 2mM $CaCl_2$ and 11mM D-(+)-glucose, and was continuously bubbled with 95% O_2/5% CO_2). Infrared differential interference contrast–enhanced visual guidance was used to select neurons that were 3–4 cell layers below the surface of the slices. The recording solution was delivered to slices via superfusion driven by peristaltic pump (flow rate of 4-5ml/min)

and was held at room temperature. The neurons were held at −70mV (voltage clamp), and the pipette series resistance was monitored throughout the experiments by hyperpolarizing steps of -1mV with each sweep. If the series resistance changed by >20 % during the recording, the data were discarded. Whole-cell currents were filtered at 1kHz and digitized and stored at 20 KHz (Clampex 9; MDS Analytical Technologies, Sunnyvale, CA). All experiments were completed within 4h after slices were made to maximize cell viability and consistency.

Miniature IPSCs (mIPSCs) were recorded in the presence of TTX (1μM), d-AP5 (50μM), and NBQX (20μM) in the recording ACSF solution. mIPSC data was analyzed with Stimfit (Guzman et al., 2014) using detection threshold of >7 pA, where detection results were visually verified. For each cell, a stretch of 250 mIPSCs were analyzed, with data collection beginning 5-10mins after patching onto each cell. For confirmation that currents were exclusively inhibitory, picrotoxin (100μM) was added to the bath after recordings.

Histology

All histochemistry was carried out on 50μm-thick free floating coronal brain sections. Sections were incubated in primary antibodies against PV and biotinylated lectin WFA at 4°C for 48h in 0.1M PBS with 0.3% Triton X-100 and 3% normal donkey serum. After incubation in primary antisera, sections were washed and incubated in secondary antisera in 0.1M PBS with 0.3% Triton X-100 and Alexa Fluors for 2h at room temperature. All labeled brain sections were counterstained with Hoechst 33342 or DAPI. For the list of antibodies used, **see Table 4.1**. For the behavior experiment, whole sections were imaged with a Hamamatsu NanoZoomer S60 (Japan), all other sections were imaged with a Zeiss confocal microscope LSM 700 (Oberkochen, Germany).

Table 4.1. Antibodies for histochemistry.

Name	Host Species	Dilution	Type	Company	Catalog #
Parvalbumin (PV)	Mouse	1:500	Primary	Sigma-Aldrich (St. Louis, MO)	P3088
Wisteria floribunda agglutinin (WFA) lectin	N/A	1:500	Primary	Sigma-Aldrich	L1516
cFos	Rabbit	1:500	Primary	Invitrogen (Carlsbad, CA)	PA1-830
Donkey anti-rabbit 488	N/A	1:500	Secondary	Invitrogen	A21206
Donkey anti-mouse 568	Donkey	1:500	Secondary	Invitrogen	A10037
anti-Streptavidin 488	N/A	1:500	Secondary	Molecular Probes	S11223A

Confocal microscopy

Images were acquired using a Zeiss confocal microscope (LSM 700; four visible solid-state lasers: UV 405; argon 458/488; HeNe 555/568; far-red 639). Brain sections for comparison were stained together, all images were taken with identical confocal settings, and equally sampled to allow for cross comparisons. Distinctions between DMS and DLS were based on previously reported region depictions (Devan et al., 2011) (medial to bregma, 1.5–2.5 mm; lateral to bregma, 3.0–4.0 mm). For PV+WFA+, PV+, and WFA+ cell density analyses, 4 to 6 sections (1:6 series) of the DMS were imaged (20x with 0.5x zoom; NA, 0.8) taking z-stacks at 3.0μm intervals (~16 optical slices per cell). All slides were coded prior to analysis and the code was not revealed until the analysis was complete.

Cell density, intensity, and statistical analysis

Cell densities (PV, WFA, cFos) were counted using FIJI (FIJI is just ImageJ, NIH), with the exception of the cFos experiment, which was counted using NDP2+ (Hamamatsu). Both were calculated by dividing the total number of positive-labeled cells within the DMS over the traced volume. Volumes were traced from max projections in the DAPI channel by researchers unaware of experimental groups. Percent colocalization of PV+ cells surrounded by PNNs was determined by calculating total number of PV+PNN+ cells over the total number of PV+ cells. Density and colocalization comparisons in BTBR and VPA experiments were statistically analyzed using unpaired t-tests, and the transgenic experiment was statistically analyzed using one-way ANOVAs with post-hoc Holm-Sidak multiple comparisons to compare Cntnap2 and Shank3 mice to C57BL/6 controls. Behavior was analyzed using two-way ANOVA and mixed three-way ANOVA, depending on the independent variables. Statistics used throughout the manuscript include lme modeling of ANOVAs, Pearson r correlations, simple linear regressions, and unpaired t-tests, as described throughout the text and figure legends. Unless otherwise stated, data are presented as mean ± SEM. Outliers were assessed using a robust regression and outlier removal (ROUT) method (Q = 0.2%) in GraphPad Prism 8.4.1 (GraphPad Software). (n = 1) BTBR mouse had zero PV+ expression in the DMS, and was removed from DMS histology comparisons in Fig

1. (n = 1) BTBR chABC-treated mouse was found to have missed targeting and was removed from behavioral and histological comparisons, but included in correlation analyses. (n = 1) C57BL/6 mouse was a grooming outlier at pre-treatment and was removed from all subsequent analyses related to grooming. (n = 1) BTBR mouse was a digging outlier at post-treatment and was removed from all analyses related to digging. Non-normal data sets were analyzed using nonparametric tests, as appropriate. Normality was assessed using Anderson-Darling test, Shapiro-Wilk test, D'Agostino & Pearson omnibus test, and Kolmogorov-Smirnov test, with a *p* value of 0.05.

Results

Multiple mouse models characterized as exhibiting excessive repetitive behaviors, show increased PNN expression around dorsomedial striatum PV+ interneurons.

Characterization of the DMS and DLS of adult mice with phenotypic excessive repetitive behaviors revealed consistent abnormal PNN distribution in the DMS, but not the DLS. Using fluorescent labeled *Wisteria floribunda agglutinin* (WFA) to label PNNs in fixed tissue, we observed PV+PNN+ interneurons throughout the striatum in 4 different mouse models (BTBR, Cntnap2$^{-/-}$, Shank3$^{+/-\Delta C}$, and VPA-treated) (see example images **Fig 4.1d**), all known to exhibit excessive repetitive behaviors (Cai et al., 2017; Meyza and Blanchard, 2017; Nicolini and Fahnestock, 2018; Peça et al., 2011; Peñagarikano et al., 2011; Roullet et al., 2013). In the DMS, a greater percentage of PV+ interneurons were colocalized with WFA-labeled PNNs for all 4 models compared to their respective age-matched controls (BTBR: $t_{13} = 2.229$, $p = 0.0204$, $\eta^2 = 0.277$; Cntnap2$^{-/-}$: $t_{19} = 2.552$, $p = 0.0195$, $\eta^2 = 0.42$; Shank3$^{+/-\Delta C}$: $t_{19} = 3.569$, $p = 0.0041$, $\eta^2 = 0.42$; VPA: $t_{14} = 2.21$, $p = 0.0445$, $\eta^2 = 0.258$) (**Fig 4.1a-c**). This consistent increase seen in the percent population of PV+ interneurons enwrapped in PNNs suggest that atypical distribution of PNNs in the DMS may be a common characteristic of aberrant repetitive behaviors. Despite these consistent changes in the DMS across these various mouse models, we found no PNN differences in the DLS (BTBR: $t_{14} = 1.089$, $p = 0.295$; Cntnap2$^{-/-}$ + Shank3$^{+/-\Delta C}$: $F(2,19) = 1.274$, $p = 0.3027$; VPA: $t_{14} = 0.255$, $p = 0.802$) (**Fig 4.1a-c**). The lack of difference seen here suggests

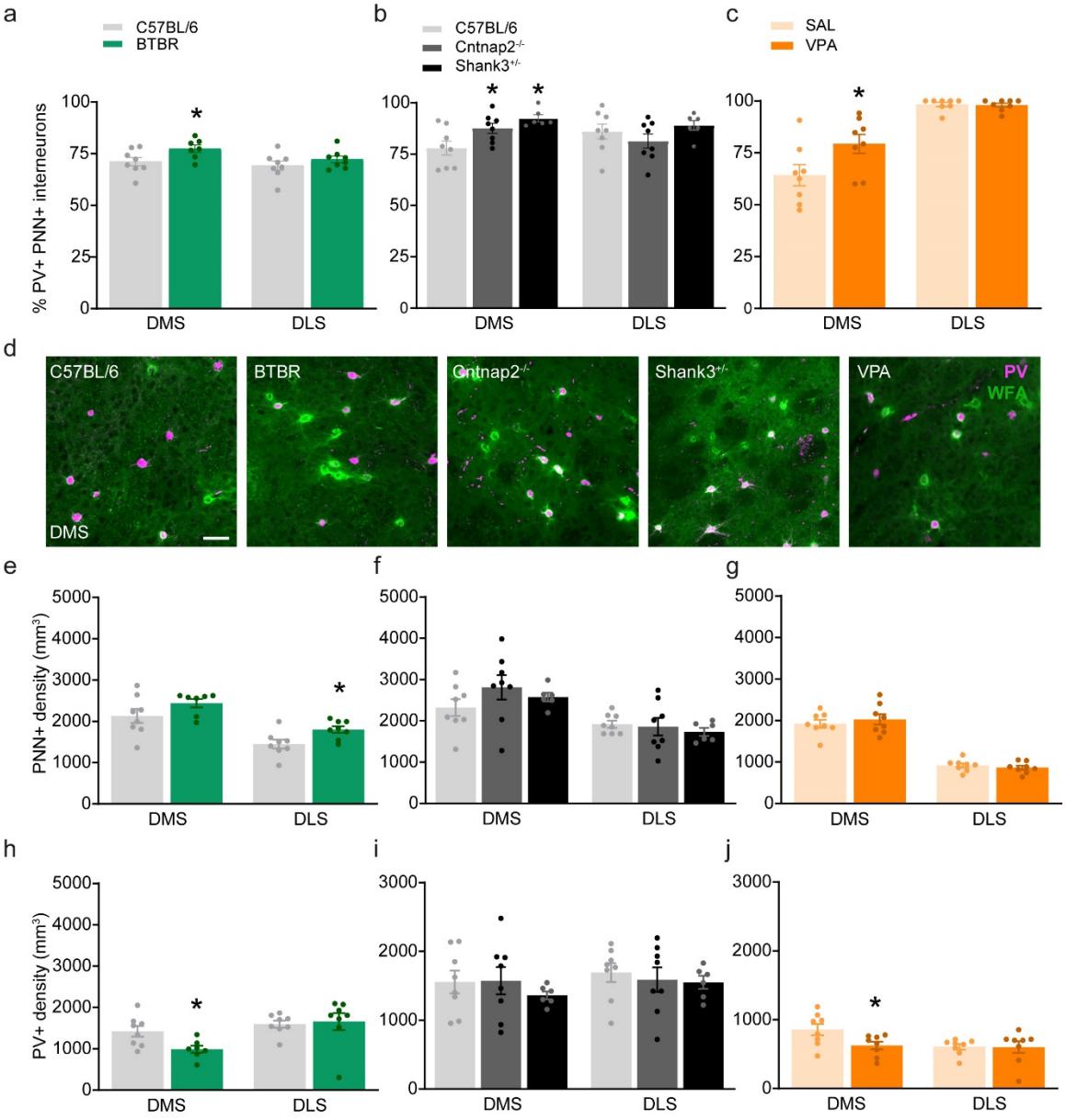
that PV-dependent inhibitory plasticity in the DLS, a region necessary for the formation of habitual behaviors, is unaltered by PNNs in mice with increased repetitive behaviors.

While we found differences, specific to the DMS, in the percent colocalization of PV+ interneurons positive for PNNs, we found no evidence of increased PNN+ cell density in the mouse models examined (**Fig 4.1e-g**). One exception was that BTBR mice had an increased number of PNN+ cells in the DLS compared to controls ($t_{14} = 2.66$, $p = 0.0186$, $\eta^2 = 0.336$) (**Fig 4.1e**). BTBR and VPA-treated mice showed a decrease in PV+ expressing interneurons in the DMS (BTBR: $t_{13} = 2.68$, $p = 0.0187$, $\eta^2 = 0.357$; VPA: $t_{14} = 2.66$, $p = 0.0186$, $\eta^2 = 0.336$) (**Fig 4.1h-j**). Tyramide amplification of PV+ protein expression in BTBR mice (data not shown here), resulted in a similar decrease, suggesting that BTBR, and potentially VPA-treated, mice have reduced PV+ interneuron densities. Additionally, little to no PNN+ expression was found surrounding other interneuron subtypes (calretinin+, somatostatin+, NPY+, ChAT+) in the dorsal striatum, as was the case in the PNN hippocampus study (Chapter 3). This phenomenon has also been observed in a previous study investigating PNNs in the striatum (Lee et al., 2012).

BTBR mice show robust over-grooming and excessive digging behavior.

To corroborate over-grooming behavior shown in previous studies (Amodeo et al., 2014; Kim et al., 2016; Wei et al., 2016), we characterized grooming behavior in BTBRs compared to C57BL/6 controls during 10 minute testing sessions. Unsurprisingly, BTBRs spent more time, in total, grooming ($t_{18} = 2.502$, $p = 0.0222$) and more time within a grooming bout ($U = 3.0$, $n_1 = n_2 = 10$, $p < 0.0001$) compared to controls (**Fig 4.2b**). Another measure used to characterize repetitive behaviors in mice is digging, so in addition to measuring grooming, we used a thick bedding model to promote mouse digging behavior (Deacon, 2006). BTBR mice also showed a robust increase in the total time spent ($t_{18} = 2.198$, $p = 0.0413$) and number of bouts digging ($t_{18} = 2.780$, $p = 0.0123$) compared to controls (**Fig 4.2c**). These robust behavioral differences lead us to further investigate the potential relationship between PNNs and repetitive behaviors in the BTBR mouse model.

Figure 4.1 Mouse models with excessive repetitive behaviors have a greater percent population of DMS PV+ interneurons enwrapped in PNNs.



(**a-c**) Histological analysis of WFA+ PNNs and PV+ interneurons revealed an increase in DMS percent colocalization in BTBRs (77.4 ± 1.79%, p = 0.0204) (**a**), transgenic mouse models (Cntnap2$^{-/-}$: 87.56 ± 2.42%, p = 0.0195; Shank3$^{+/-\Delta C}$: 92.46 ± 1.71%, p =0.0041) (**b**), and VPA-treated mice (79.3 ± 4.6%, p = 0.0445) (**c**). No differences were found in the DLS (BTBR: 72.19 ± 1.58%, p = 0.295 (**a**); Cntnap2: 81.33 ± 3.46%; Shank3: 88.98 ± 2.34%, p = 0.548 (**b**); VPA-treated: 97.99 ± 0.95%, p = 0.802 (**c**)). (**d**) Representative images of PV+ interneurons (magenta) and

WFA+ labeled PNNs (green) in the DMS. Scare bar = 50μm. (**e-g**) No differences were found in PNN+ density in DMS of BTBRs (p = 0.160) (**e**), transgenics (F(2, 19) = 0.2373, p = 0.791) (**f**), or VPA (p = 0.519) (**g**). DLS PNN+ density was increased in BTBRs (1,802 ± 78.47 cells/mm^3) compared to controls (1,451 ± 105.9 cells/mm^3) (p = 0.0186) (**e**), but not in transgenics (F(2, 19) = 0.3085, p = 0.7381) (**f**) or VPA (p = 0.445) (**g**). PV+ density was reduced in the DMS of BTBR (990.6 ± 85.32 cells/mm^3, p = 0.0187) and VPA-treated (627.2 ± 54.79 cells/mm^3, p = 0.0379) mice, but not transgenics (F(2, 19) = 0.4552, p = 0.641). (**h-j**) No differences were detected in the DLS (BTBR: p = 0.779 (**h**); Cntnap2$^{-/-}$ + Shank3$^{+/-\Delta C}$: F(2,19) = 0.2363, p = 0.7918 (**i**); VPA-treated: p = 0.968 (**j**)).

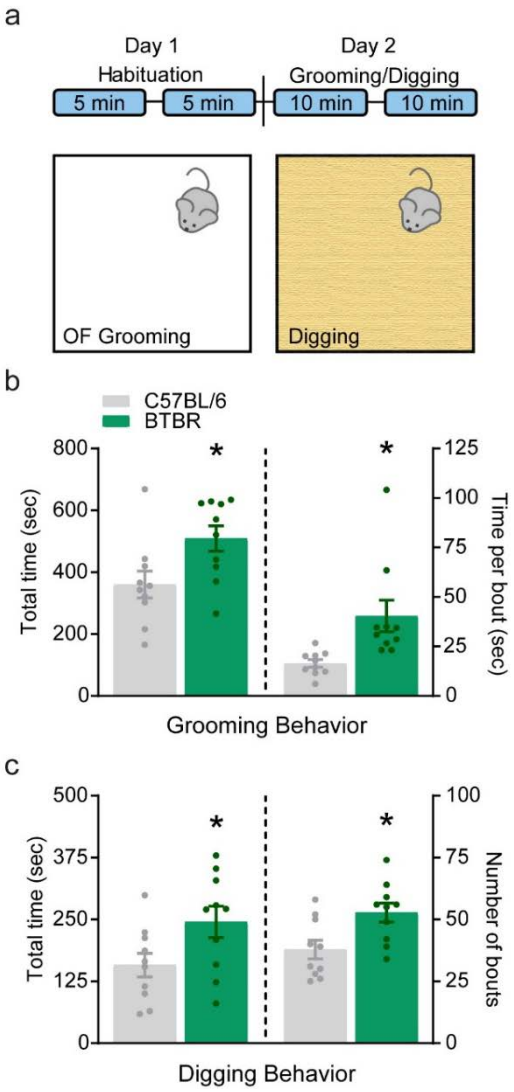


Figure 4.2 Grooming and digging behavior is increased in BTBRs compared to controls.

(a) All mice, a day prior to behavior testing, were habituated to an enclosed open field (OF) box twice for 5mins. The next day mice were tested in both OF grooming and thick bedding digging paradigm (counterbalanced). (**b**) BTBR mice showed elevated time spent grooming (509.4 ± 40.88 sec) compared to controls (360.3 ± 43.32 sec) (t_{18} = 2.502, p = 0.0222) and longer time spent grooming per bout (BTBR: 40.40 ± 7.96 sec, C57BL/6: 16.45 ± 1.89 sec; p < 0.0001). (**c**) BTBR mice showed greater time spent digging (245.2 ± 31.58 sec) compared to controls (158.1 ± 24.0 sec) (t_{18} = 2.198, p = 0.0413) and number of bouts (BTBR: 52.80 ± 3.82 sec, C57BL/6: 37.90 ± 3.758 sec; p = 0.0123).

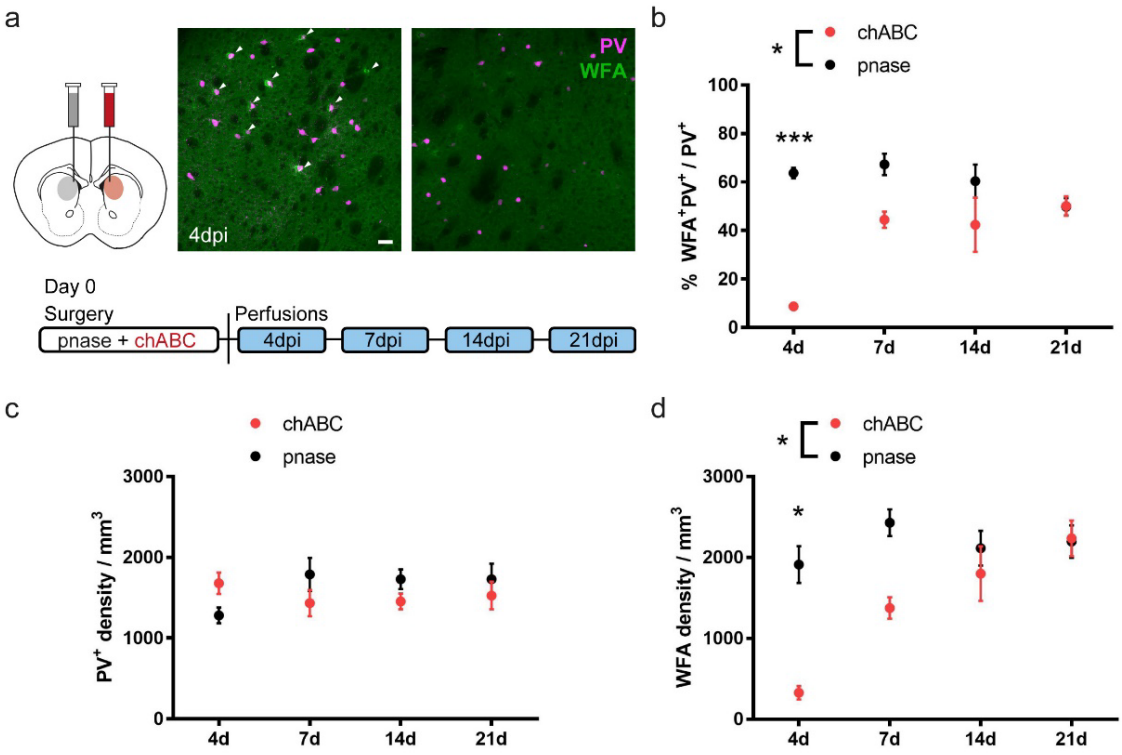
Chondroitinase ABC enzyme degradation of PNNs in the dorsomedial striatum is transient.

To test whether PNNs play a role in the manifestation of increased repetitive behaviors, we first characterized enzymatic digestion of PNNs in the DMS with unilateral stereotaxic infusion of chondroitinase ABC (chABC) in one hemisphere and control penicillinase (pnase) in the other (**Fig 4.3a**). Previous studies have used chABC successfully to degrade PNNs in specific brain regions in adult mice (Cabungcal et al., 2013; Yamada et al., 2015; Yang et al., 2015), where chABC degradation has been shown to have only transient effects on PNNs. Therefore, a time course study was necessary to asses when PNNs completely degraded, partially recovered, and fully recovered, specifically in the striatum. A time course study investigating chABC in the rat cortex found complete degradation at 3 dpi, partial recovery at 13 dpi, and complete recovery by 30 dpi (Slaker et al., 2015). We found a similar time course in the adult mouse striatum, an almost complete degradation at 4 dpi, approximately 60% regrowth at 7 dpi, and complete recovery by 21 dpi (**Fig 4.3b, d**), with no effect on PV+ interneurons (**Fig 4.3c**). This data was used to identify a time point to reduce PNNs to healthy control-like levels in BTBRs. Based on the growth curve from this experiment we chose a 10 dpi time point to explore the effects of reduced DMS PNNs on repetitive behaviors.

Chondroitinase ABC treatment in the dorsomedial striatum reduces excessive repetitive behaviors.

Analysis of initial grooming behavior before treatment showed, again, an increase in total time spent grooming ($t_{34} = 2.627$, $p = 0.0128$) and time spent grooming within a bout ($t_{34} = 4.098$, $p = 0.0002$) in BTBRs (**Fig S4.1a**). Digging behavior before treatment was comparable to behavior shown in Fig 4.2c, where BTBR mice spent significantly more time digging ($t_{35} = 5.855$, $p < 0.0001$) and initiated a greater number of digging bouts ($t_{35} = 2.480$, $p = 0.0181$) than controls (**FigS4.1b**). After recapitulating an excessive repetitive behavioral phenotype in this cohort of mice, we randomly assigned all mice to either stereotaxic chABC or control enzyme pnase treatment.

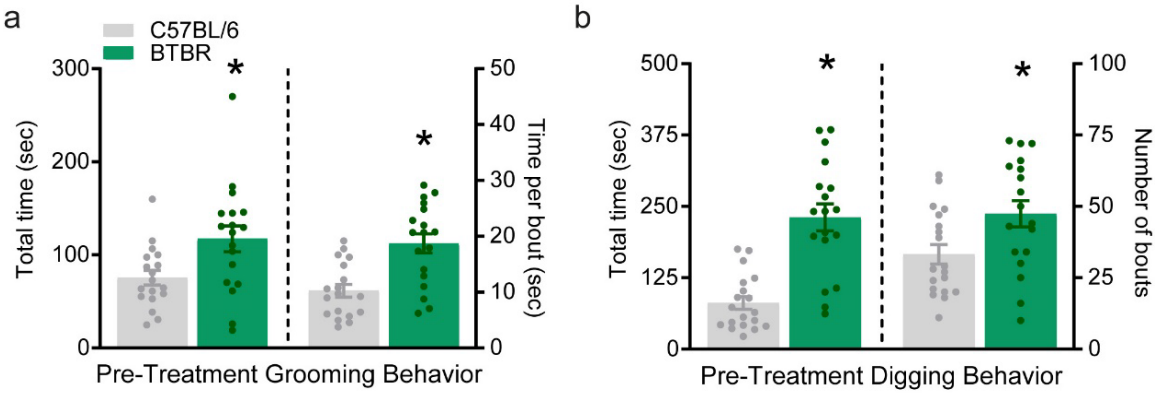
Figure 4.3 chABC transiently degrades DMS PNNs in C57BL/6 adult mice.



(**a**) Representative illustration of stereotaxic enzyme injection targeting of DMS, where pnase (grey-coloring) was injected into one hemisphere and chABC (red-coloring) in the other. Timeline shows the four days post-injection (dpi) analyzed of pnase and chABC treatment. Example histology images of PV (magenta) and WFA+ PNNs (green) at 4dpi with pnase-treatment on the left and chABC-treatment on the right. White arrows indicate colocalization of PV+ PNN+ cells. Scale bar = 50µm. (**b**) Percent PV+ interneurons positive for WFA+ PNNs reveals a significant treatment effect ($F(1, 4) = 14.1$, $p = 0.0199$). chABC treatment significantly reduces percent colocalization at 4dpi ($p = 0.0489$), but not at 7dpi ($p = 0.47$), 14dpi ($p = 0.6458$), or 21dpi ($p > 0.999$). (**c**) chABC and pnase treatment did not differ in PV+ interneuron density. (**d**) Similar to percent colocalization, WFA+ PNN density was significantly decreased 4dpi of chABC, but not 7, 14, or 21 dpi.

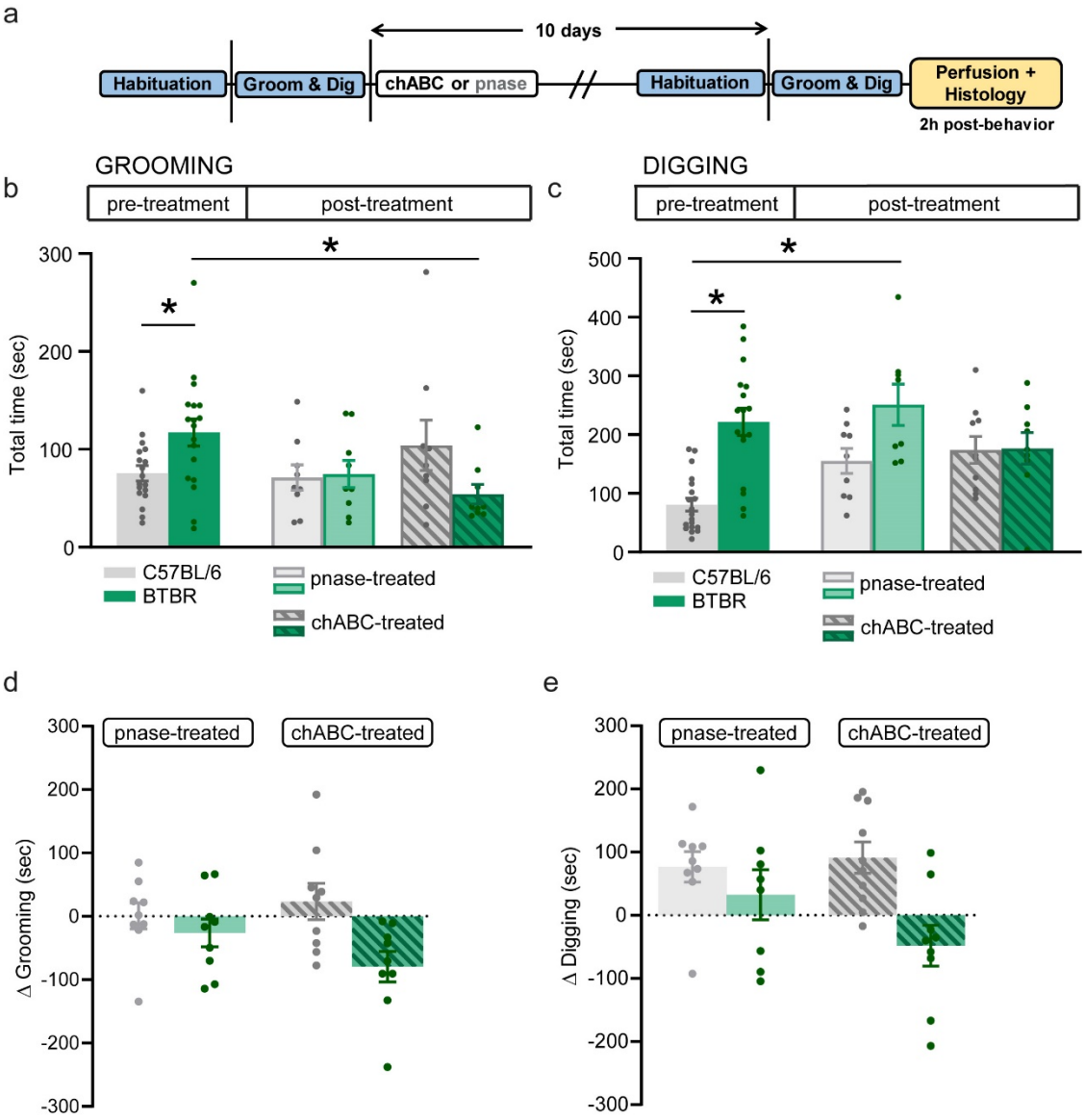
10 days after treatment, mice were tested for grooming and digging behaviors same as before. Mixed three-way ANOVA analysis of pre- and post-treatment grooming time yielded a significant interaction effect between strain and time ($F(1, 32) = 7.371$, $p = 0.0106$). Tukey post-hoc analysis showed that BTBRs treated with chABC were the only group to significantly reduce their grooming behavior after treatment (Δ-79.55 ± 24.05 sec, $t_{32} = 4.697$, $p = 0.0412$) (**Fig 4.4b, d**). Both pnase-treated groups' and chABC-treated C57BL/6 grooming behavior was unchanged from pre- to post-treatment (C57BL/6-pnase: $p > 0.999$, C57BL/6-chABC: $p = 0.9739$, BTBR-pnase: $p = 0.953$) (**Fig 4.4b, d**). These results suggest that chABC-treatment in BTBRs is sufficient to reduce over-grooming behaviors 10 days later.

Figure S4.1 BTBRs show an increase in repetitive behaviors before treatment, providing internal replication of an excessive repetitive behavior phenotype.



(**a**) Pre-treatment grooming behavior of C57BL/6 (n = 18) and BTBRs (n = 18) show greater time spent grooming (left y-axis) in BTBRs (117.3 ± 13.84 sec) compared to controls (75.52 ± 7.82 sec) ($t_{34} = 2.627$, $p = 0.0128$) and more time spent within a grooming bout (right y-axis, $t_{34} = 4.098$, $p = 0.0002$). (**b**) Pre-treatment digging behavior show BTBRs spend more time digging than C57BL/6 controls ($t_{35} = 5.855$, $p < 0.0001$), and initiate more digging bouts ($t_{35} = 2.480$, $p = 0.0181$).

Figure 4.4 chABC-treatment rescues excessive repetitive behaviors, reducing BTBR grooming and normalizing digging behavior.



(**a**) Experiment timeline of behavior pre-treatment, stereotaxic surgery, behavior post-treatment, and tissue collection for histology. (**b**) Grooming behavior was different between BTBR and C57BL/6 mice at pre-treatment (as depicted in **Fig S4.1**). chABC-treatment significantly reduced BTBR grooming, only (t_{32} = 4.697, p = 0.0412). (**c**) Digging behavior was increased in BTBR mice at pre-treatment (also depicted in **Fig S4.1**). chABC-treatment in BTBRs normalized digging behaviors (176.65 ± 26.9 sec) comparable to C57BL/6 mice (pnase-treated: 155.13 ± 21.3 sec; chABC-treated: 173.92 ± 22.78 sec), while pnase-treated BTBRs maintained high levels of digging (250.96 ± 35.27 sec). (d-e) Graphical representations of the change (Δ) in behavior from pre- to

post-treatment per mouse. Negative values depict a decrease in behavior, positive values depict an increase in behavior, and means near zero (dashed line) represent no significant change in behavior. chABC-treated BTBRs show decreases in grooming (Δ-79.55 ± 24.05 sec) and digging (Δ48.23 ± 30.07) behavior.

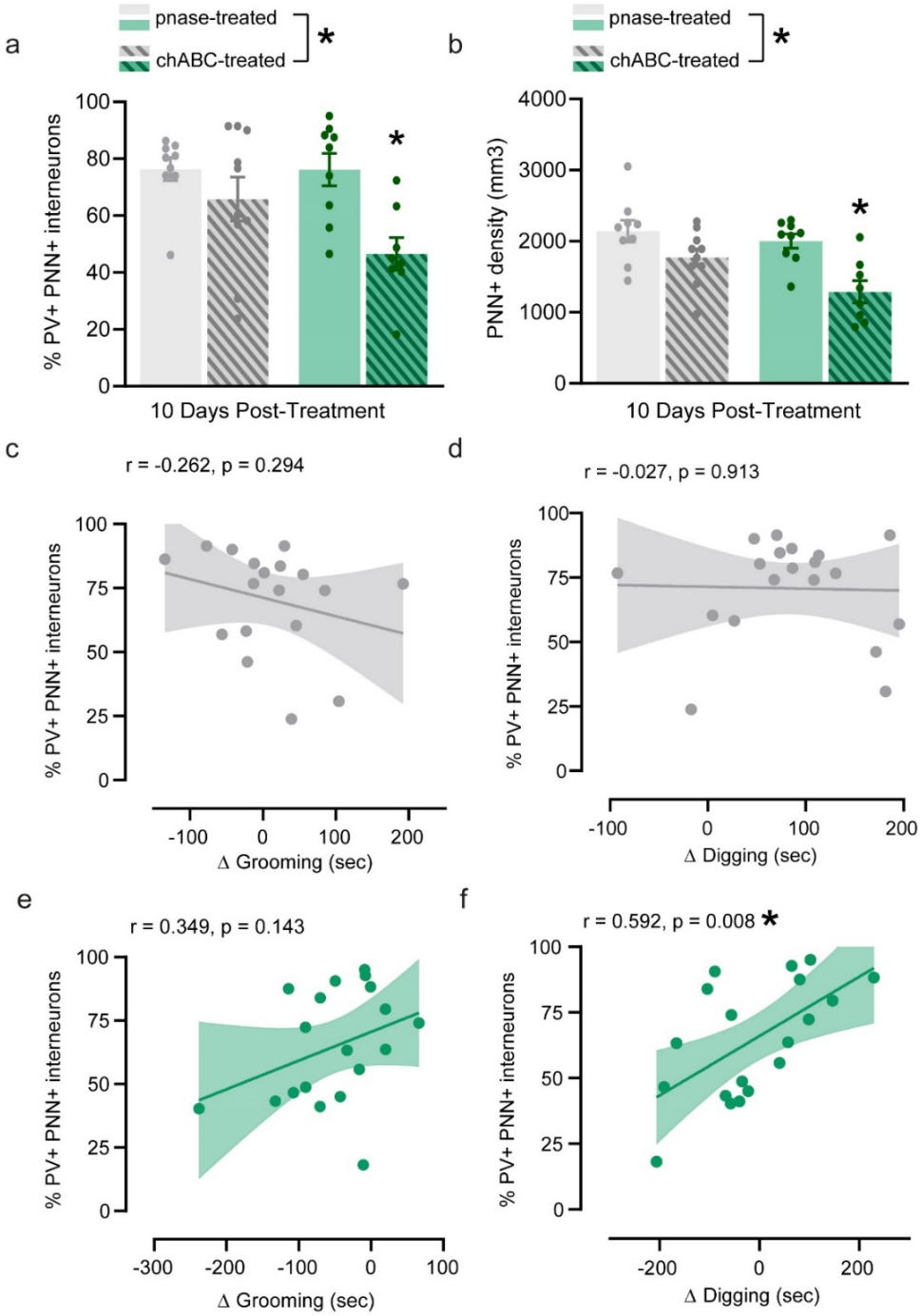
Mixed three-way ANOVA analysis of pre- and post-treatment digging time yielded a significant interaction effect between strain and time ($F(1, 32) = 9.267$, $p = 0.0046$), and a main effect of strain ($F(1, 32) = 20.03$, $p < 0.0001$), where the main effect of strain accounted for a substantial amount (25.28%) of the total variation. Tukey post-hoc analysis showed that time spent digging post-treatment in chABC-treated BTBRs (176.65 ± 26.93 sec) was unrecognizable from both C57BL/6 groups (C57BL/6-chABC: 173.92 ± 22.78 sec, $p > 0.999$, C57BL/6-pnase: 155.13 ± 21.3 sec, $p > 0.999$) (**Fig 4.4c**). chABC treatment in BTBRs produced a decrease in digging behavior, spending 48.23 ± 30.07 seconds less time digging than before chABC treatment, although within-subjects matching was not found to be significant ($t_{32} = 1.604$, $p = 0.9078$) (**Fig 4.4c, e**). As expected, BTBRs treated with pnase maintained an elevated amount of time spent digging across time (250.96 ± 35.27 sec, $t_{32} = 1.019$, $p > 0.999$). Surprisingly, C57BL/6 mice post-treatment showed, albeit not significant, an increase in time spent digging from pre-treatment (C57BL/6-pnase: Δ76.7 ± 24.1 sec, $p = 0.3586$; C57BL/6-chABC: Δ91.2 ± 24.79 sec, $p = 0.0837$) (**Fig 4.4c, e**). As is with repeated testing over time, it is important to consider that mice may acclimate to the testing apparatus, increasing the likelihood to behave with less restraint. Thus, mitigating the ability to detect differences from pre- and post-treatment. It is also important to note that excessive digging in BTBR groups (pre-treatment and pnase-treated) may exhibit digging levels near maximum, creating a ceiling effect. Overall, chABC treatment, on average, restored BTBR excessive digging behaviors to levels comparable to controls.

To assess chABC and pnase treatment, we analyzed the percent of PV+ interneurons positive for PNNs in the DMS 10 days after treatment and found a main effect of treatment ($F(1, 32) = 10.75$, $p = 0.0025$), with no strain differences ($F(1, 32) = 2.528$, $p = 0.122$) (**Fig 4.5a**). C57BL/6 mice showed no differences when comparing treatments at the 10 day time point ($t_{32} =$

1.249, p = 0.3926), as was expected given the time course study. However, chABC treatment in BTBRs produced a significant decrease in the % of PV+ interneurons enwrapped in PNNs compared to BTBRs treated with pnase (t_{32} = 3.332, p = 0.0044) (**Fig 4.5a**). The same effect was seen when analyzing PNN+ density (**Fig 4.5b**). To test whether changes in behavior relate to numbers of PNNs, we tested for relationships between behavior and histology measures. The Δ grooming from pre- to post-treatment did not significantly correlate with percent colocalization of PV+ PNN+ interneurons in BTBRs, although a positive slope exists (r = 0.349, p = 0.143) (**Fig 4.5e**). C57BL/6 mice also showed no relationship between the two measures (r = -0.262, p = 0.294) (**Fig 4.5c**). The Δ digging positively correlated with the percent of PV+ interneurons positive for PNNs in BTBRs (r = 0.592, p = 0.008) (**Fig 4.5f**), but, again, not in controls (r = -0.027, p = 0.913) (**Fig 4.5d**). This suggests that repetitive behaviors are likely to be modulated by DMS PNN expression associated with PV+ interneurons in cases when there is a pre-existing condition of increased PV+PNN+ colocalization.

To test whether PV+ activity was altered in BTBR mice treated with chABC, we analyzed immediate early gene, cFos, an indirect marker of neuronal activation. We found no difference in the percent activation of PV+ interneurons in chABC-treated BTBRs (3.38 ± 0.33%) compared to pnase-treated BTBRs (3.54 ± 0.5%) (t_{24} = 0.0774, p = 0.939). The same was true when comparing treatment in C57BL/6 mice (t_{24} = 1.139, p = 0.266). This result was unexpected given previous studies showing altered inhibitory activity after PNN degradation (Dityatev et al., 2007; Lensjø et al., 2017), comparatively we looked at chABC effects at a later time point after degradation – which may account for this discrepancy. In addition, considering that the striatum is 98% inhibitory, the role PV+PNN+ interneurons play in behavioral plasticity and within the striatal microcircuitry are likely to be complex and interdependent.

Figure 4.5 Percent of PV+PNN+ interneuron colocalization is significantly reduced in chABC-treated BTBRs, coincident with a positive relationship to behavior.



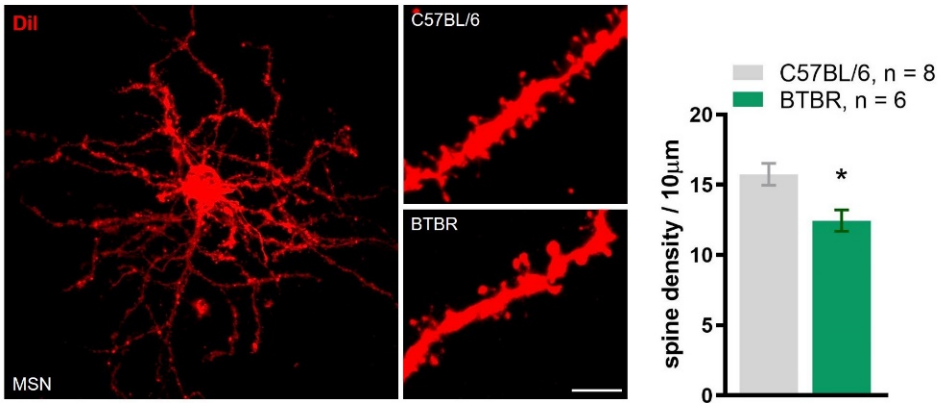
(**a**) Histological analysis of WFA+ labeled PNNs confirms reduction in the percent of PV+ interneurons positive for PNNs in chABC-treated BTBRs (46.53%) compared to pnase-treated BTBRs (76.15%) (p = 0.0112) and (**b**) reduction of PNN density (p = 0.0046). (**c-d**) Correlation of

percent colocalization of PV and PNNs compared to Δ grooming and Δ digging reveal no relationship in C57BL/6 mice. (**e-f**) Correlation of percent colocalization of PV and PNNs compared to Δ grooming in BTBRs shows no significant correlation, but a positive slope. Comparison of histology to Δ digging reveals a positive relationship in BTBRs.

Dorsomedial striatum MSNs show altered structure and physiology in BTBR mice.

PV+ cells provide a primary source of inhibition onto MSN cell bodies, so in order to understand how plasticity might be altered in the DMS, we investigated measures of structural and functional plasticity in MSNs. The DMS has been shown to integrate a heterogeneous set of inputs from prefrontal cortex, premotor cortex, and thalamus (Hunnicutt et al., 2016). MSNs receive specific excitatory inputs from these extra-striatal regions onto dendritic spines, sites of excitatory synapses (Kötter, 1994; Selemon and Goldman-Rakic, 1985). We examined dendritic spine density in BTBR mice and found a reduction in the number of spines on secondary and tertiary dendrites of MSNs in the DMS ($t_{42} = 2.978$, $p = 0.0048$) (**Fig 4.6b**). This evidence is suggestive of altered plasticity and information processing from excitatory input to MSNs.

Figure 4.6 BTBRs show decreased dorsomedial striatum MSN dendritic spines.



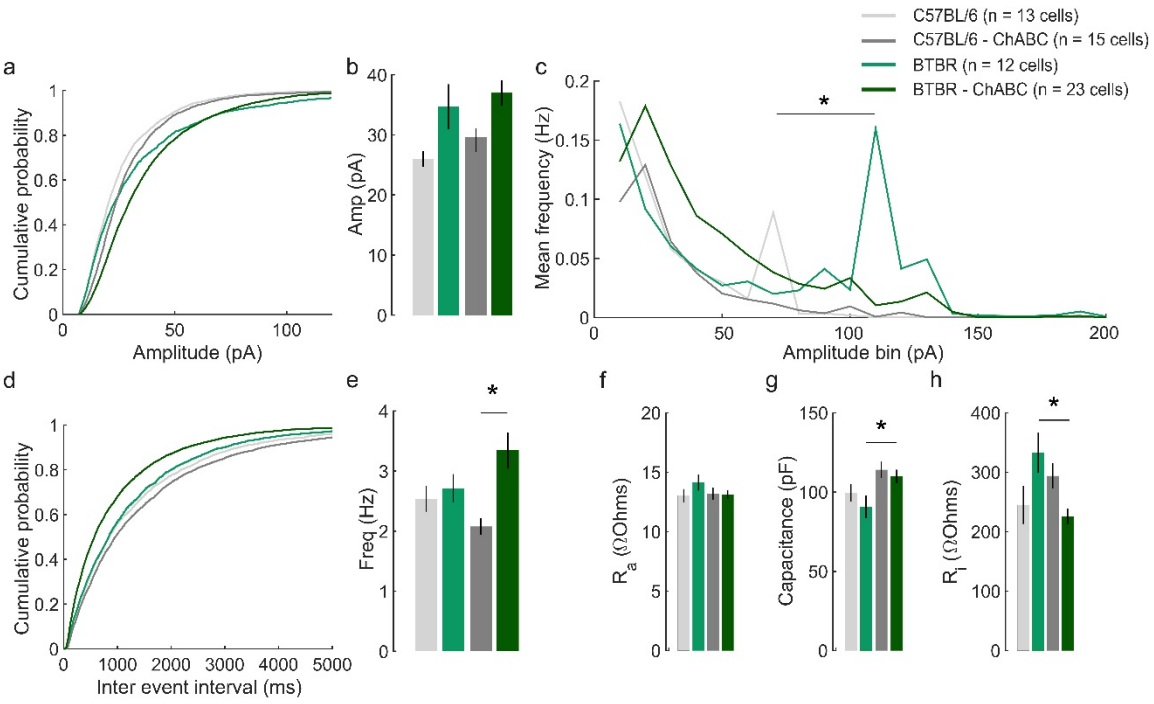
(**a**) Representative images of MSN cell (left) and dendritic segments (DiI, red) in the DMS of C57BL/6 (top) and BTBR (bottom). Scale bar equals 5 µm. (**b**) Spine density difference between controls were observed ($t_{42} = 2.978$, $p = 0.0048$).

Because of the observed diminished structural plasticity in BTBR MSNs, we compared mini inhibitory post-synaptic currents (mIPSCs) onto MSNs from BTBR and C57BL/6 mice. First we collected data at “baseline”, absent of manipulations or behavior, to determine whether differences existed in inhibitory synaptic input and strength. Comparison of overall mIPSC mean frequencies, a proxy for inhibitory presynaptic strength, yielded no difference ($p = 0.689$) (**Fig 4.7d, e**). Comparison of mIPSC mean amplitudes, a proxy for inhibitory post-synaptic strength, at baseline also produced no difference between groups ($p = 0.404$) (**Fig 4.7b**). However, cumulative probability curves of the mIPSC amplitude data suggested differences existed when comparing events with amplitudes > 80pA (**Fig 4.7a**). Higher amplitudes are thought to be representative of events proximal to the soma (Strüber et al., 2015), which is precisely where PV+ interneurons synapse onto MSNs (Gittis et al., 2010). We compared baseline BTBR and C57BL/6 mIPSC events at 80-100 pA and 100+ pA and found an increase in BTBR mean frequency (80-100pA: $p = 0.0118$; 100+pA: $p = 0.0047$) (**Fig 4.7c**). This increase in mIPSC events at higher amplitudes suggests increased inhibitory transmission in BTBR mice.

To understand how chABC treatment may affect inhibitory synaptic strength in BTBR and C57BL/6 mice, we hypothesized that chABC treatment would alter inhibitory synaptic strength at DMS MSNs. Additionally, the endogenous differences in levels of PV+ PNN+ cells between BTBR and C57BL/6 mice led us to hypothesize that chABC may have only an effect in BTBR mice. Mice were injected bilaterally with chABC into the DMS; then ten days later, brain slices were collected for mIPSC measurements at presumed MSNs. In analyzing mIPSC frequencies, there was a significant interaction between strain and treatment ($p = 0.029$, strain*treatment in an LME), and no general main effect of strain or treatment alone (strain: $p = 0.763$; treatment: $p = 0.238$) (**Fig 4.7d**). This effect was mediated by a chABC-driven decrease in mIPSC frequency in C57BL/6 mice, and increase in mIPSC frequency in BTBR mice. When comparing mIPSC amplitudes across all groups we found no differences (strain: $p = 0.322$; treatment: $p = 0.078$; interaction: $p = 0.461$, in an LME) (**Fig 4.7a**). Again, when analyzing amplitudes > 80pA there is a significant main effect of strain (80-100pA: $p = 0.0455$; 100+ pA: $p = 0.0008$), where BTBRs show

increased events at high amplitudes compared to C57BL/6 mice. However, there was no main effect of chABC treatment (80-100pA: p = 0.3787; 100+ pA: p = 0.467) and no interaction effect (80-100pA: p = 0.510; 100+ pA: p = 0.848).

Figure 4.7 chABC has bidirectional effects on inhibitory synaptic strength at DMS MSNs.



(**a-b**) mIPSC amplitude analysis of BTBR data at baseline (light green) and chABC-treatment (dark green), and C57BL/6 data at baseline (light grey) and chABC-treatment (dark grey), yield no differences in mean amplitudes. (**c**) Line graph of mean frequency by amplitude shows a significant difference between baseline BTBR and C57BL/6 mice at amplitudes > 80pA (80-100pA: p = 0.0118; 100+pA: p = 0.0047). (**d-e**) Significant interaction of strain and treatment for mIPSC frequency data (p = 0.029) shows how chABC treatment differentially effects BTBR and C57BL/6 mice (p = 0.00144). (**f-h**) Membrane tests show no difference in access resistance (**f**), but differences exist in capacitance (p = 0.0411) (**g**) and input resistance (p = 0.0264) (**h**) between BTBRs at baseline and after chABC treatment.

Discussion

The four mouse models we examined (BTBR, Cntnap2$^{-/-}$, Shank3, VPA) share a common link of increased repetitive behaviors, phenotypes typical to those seen in patients with ASD, OCD, trichotillomania, substance abuse, among other anxiety-related disorders (APA, 2013; Gittis et al., 2010; Langen et al., 2014; Lewis and Kim, 2009). The acquisition of habits are important in certain contexts for efficient information processing, but when this becomes restrictive, it interferes with other processes such as sociability, cognition, and anxiety regulation (D'Cruz et al., 2013; Miller et al., 2015; Rodgers et al., 2012). Striatal dysfunction has been implicated across these disorders, where excessive repetitive behaviors may reflect impairment in the transfer of information between striatal circuits (Langen et al., 2009, 2011). These disorders are multifaceted, and likely affected by a combination of factors. Strikingly, we found that BTBR, Cntnap2$^{-/-}$, Shank3, and VPA mice all show an increase in PNNs surrounding PV+ interneurons in the DMS, a brain region in the rodent important for maintaining flexible behaviors. Given the comorbid characterizations of high PV+ PNN+ colocalization in the DMS and excessive repetitive behaviors, we hypothesized that overexpression of DMS PNNs alters the organization of DMS information processes, resulting in behavioral dysfunction. This lack of behavioral flexibility likely results in increases in DLS-dependent repetitive behaviors, a region where PV+ PNNs were unaltered in the aforementioned mouse models.

This increase in PNNs throughout the DMS PV+ population of mice exhibiting restrictive behavior is consistent with the belief that PNNs modulate inhibitory plasticity. In the visual cortex, PNN formation and accumulation demarcates the onset and offset of the critical period, stabilizing the circuit once fully formed (Ye and Miao, 2013; Hou et al., 2017; Faini et al., 2018). Thus, it is plausible that excessive PNN accumulation in the DMS exacerbate repetitive behaviors, resultant of inhibitory dysfunction. It is unclear in the mouse models we examined which phenotype presents first – increased repetitive behaviors or increased PNNs around PV+ interneurons. Future studies examining the developmental stages in mouse models of excessive repetitive behaviors are needed to assess the time course of events.

BTBR mice exhibit corticostriatal dysfunction (Han et al., 2014) and robust repetitive behavioral phenotypes (Amodeo et al., 2017a; Ellegood and Crawley, 2015; Moy et al., 2007), a phenotype we successfully replicated in our study. The BTBR strain is a well-characterized inbred strain thought by some researchers to represent idiopathic ASD in humans (Crawley, 2012; Ellegood and Crawley, 2015; Kazdoba et al., 2016; Meyza and Blanchard, 2017). These mice exhibit neuroanatomical abnormalities, such as agenesis of the corpus callosum and a reduced hippocampal commissure (Fenlon et al., 2015; Sforazzini et al., 2016), exhibiting cognitive and social deficits (Amodeo et al., 2017b; Kim et al., 2016; Moy et al., 2007; Seese et al., 2014), features of idiopathic ASD. The robust differences in behavior between BTBR and control mice provide us with a good model to further assess the effects of PNN expression surrounding PV+ interneurons on behavior.

To test the hypothesis that reduction of PV+PNN+ expression in BTBRs would mitigate aberrant repetitive behaviors, we bilaterally injected chABC, an enzyme known to degrade primary components of PNNs and reinstate juvenile-like plasticity in the visual cortex (Faini et al., 2018; Sorg et al., 2016). These studies showed that chABC effects are transient, PNNs begin to form again over time. To identify the time scale of regrowth in the DMS when PNNs are completely abolished and, subsequently, fully recovered, we conducted a time course study to capture these points in time. Analysis at 4 days revealed very little to no PNNs in the DMS, and by 3 weeks PNN numbers were similar to levels seen in the contralateral control-treated hemisphere. Based on our time course study, we designed our behavior experiment to capture a point in time where PNNs would be partially recovered. Thus, we tested behavior before enzyme treatment and 10 days after. Subsequent to PNN degradation, repetitive behaviors were successfully reduced in BTBR mice, but not controls, supporting the hypothesis that atypically abundant PNNs surrounding PV+ cells impose barriers to inhibitory signaling that contribute to behavioral dysfunction.

PV+ FSIs, modulate excitatory input to MSNs, where inhibition from small populations of PV+ interneurons is sufficient to block action potentials in large populations of MSNs (Lee et al.,

2017). An overabundance of PNNs surrounding the DMS PV+ population of neurons could interfere with inhibitory modulation. As discussed in previous chapters, PNNs are known to regulate mechanisms of plasticity (Pantazopoulos and Berretta, 2016; Sorg et al., 2016), where PNNs in the mouse visual cortex prevent inhibitory cell recruitment and maintain feed-forward inhibition (Faini et al., 2018). PNNs have also been associated with neuronal oscillations in other brain regions (Lensjø et al., 2017; Steullet et al., 2014), suggesting they play a role in modulating coordinated network activity. PV+ interneurons in the striatum are known to fire in synchrony (Gittis et al., 2011; von Nicolai et al., 2014; Sharott et al., 2012), and some evidence suggests that neuronal synchrony in the striatum is important for healthy function of this brain region. For example, increases in inhibitory cell recruitment among striatal FSIs correlated with feedforward inhibition of MSNs during successful associative learning (Bakhurin et al., 2016). Furthermore, studies have shown that atypical neural activity in the dorsal striatum is associated with dysfunctional behavior in animal models of several neuropsychiatric diseases (Hong et al., 2012; Uhlhaas and Singer, 2012). Although less is known about how the link between neuronal synchrony and mental health translates to humans, abnormalities in neuronal oscillations have been reported in humans with ASD (Cornew et al., 2012; Larrain-Valenzuela et al., 2017; Sun et al., 2012; Turner et al., 2006; Wang et al., 2013).

Because chABC-treatment did not alter cFos expression in DMS PV+ interneurons, we examined whether PV+ PNNs may impact the plasticity of DMS MSNs, a primary postsynaptic target of PV+ interneurons. DMS MSNs are altered in BTBRs with a decrease in spine density and an increase in spontaneous GABA release, suggestive of dysfunction in striatal mechanisms of excitatory plasticity and stronger inhibitory output. E/I imbalance is hypothesized as a primary contributor to the development and maintenance of aberrant behaviors, especially in cases of ASD. Specifically, a NLGN1-knockout mouse resulting in decreased long-term synaptic plasticity in the CA1 and dorsal striatum caused cognitive deficits and increased repetitive behaviors (Bemben et al., 2014; Blundell et al., 2010). GABAergic interneuron-specific deletion of MECP2, transcriptional regulator important for inhibitory transmission, also resulted in increases in

repetitive behaviors (Chao et al., 2010). We propose that concomitant decreases in excitatory synapses and increases in inhibitory transmission on DMS MSNs in the BTBR mouse model, are driving their excessive grooming and digging behaviors.

To extend our understanding of how PNNs might affect DMS MSNs in BTBRs, mIPSCs were recorded ex vivo from BTBR and C57BL/6 mice at baseline and 10 days after chABC treatment. Given that chABC treatment reduces repetitive behaviors in BTBR mice with respect to C57BL/6 mice, we expected to find baseline differences between strains in mIPSC statistics that chABC treatment would normalize. Baseline data yielded results that suggested an increase in BTBR spontaneous GABA release onto putative MSN cell bodies, with no differences in overall mean frequency. However, once analyzed with chABC-treated mice, we found that chABC treatment generates both an increase in inhibitory synaptic strength at BTBR mice MSNs, and an opposing decrease in inhibitory synaptic strength at C57BL/6 mice MSNs. It should be noted that PV+ cells are not the exclusive source of inhibition onto MSNs; rather, MSNs also receive dendritic inhibition from neighboring MSNs. The changes we observe here likely resemble a complex reorganization of inhibitory circuit strength, perhaps influenced by other endogenous physiological differences between strains. While we cannot be certain if this directly reflects modulation from PV+ interneurons, there is a possibility that concomitant inhibitory signaling is altered in BTBRs and driven by the PNNs surrounding them. chABC treatment altered mIPSC frequency, capacitance, and input resistance in BTBR mice, all resulting in increases from baseline. These differences may underlie the behavioral changes seen. Assuming the MSNs sampled in this study are an equal distribution of direct and indirect pathway neurons, an increase in capacitance suggests an increase in MSN surface area (Gertler et al., 2008; Steiner and Tseng, 2010). Although we did not investigate dendritic spine density after chABC treatment, an increase in MSN surface area may suggest an increase in dendritic spines, thus restoring baseline deficits. We did not detect any changes in mIPSCs of C57BL/6 mice from chABC treatment. This result was expected, given no significant changes in grooming or digging behavior were observed.

These findings further suggest that an overabundance of PNNs surrounding PV+ interneurons in the DMS prevent adaptive disengagement from repetitive behaviors, potentially through abnormal inhibitory signaling between PV+ interneurons and MSNs. Additional work must be done to fill in the remaining gaps in our knowledge about inhibitory mechanisms associated with excessive repetitive behaviors. Moreover, understanding the various PNN components and their role in modulating plasticity may provide additional findings critical for identifying neurobiological mechanisms related to repetitive behavior.

Concluding Remarks

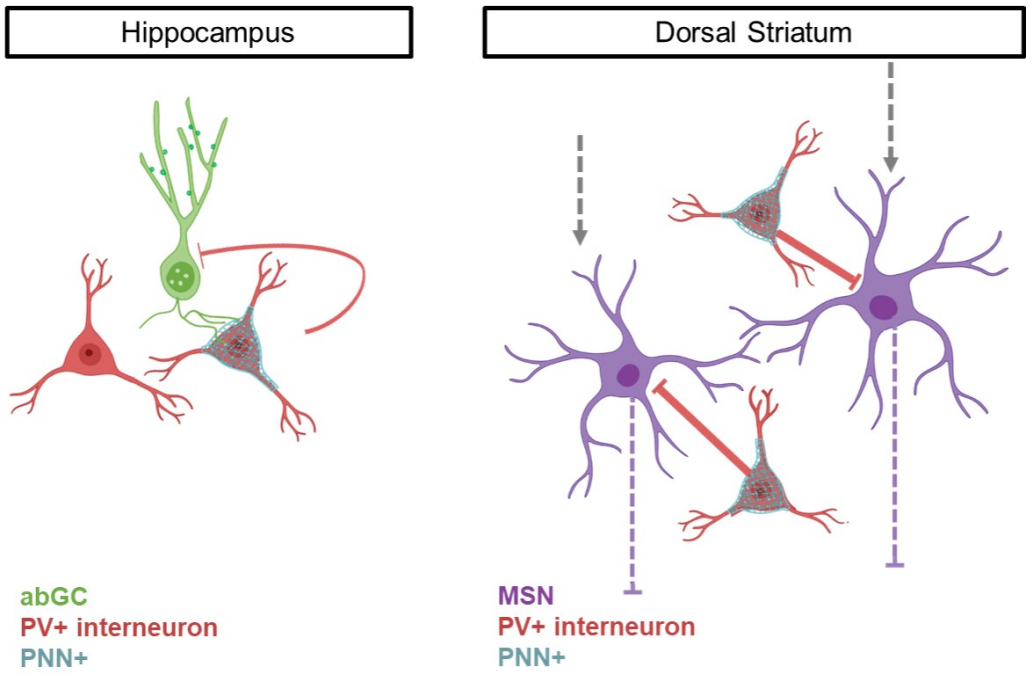
Our results in both the hippocampus and striatum suggest a more complex role of PNNs, dependent on brain region and the components of its microcircuitry. In the hippocampus, we discovered that adult-born granule cells preferentially target PV+PNN+ interneurons (see **Schematic 4.1**), an unexpected effect given previous findings. A majority of the PNN literature support the hypothesis that PNNs act as stabilizers and inhibitors of plasticity. However, the majority of this work has been conducted in the visual cortex, providing a restricted frame of reference into the roles of PNNs. Our study investigating PNNs in the dentate gyrus, suggests that PNNs do not exclusively inhibit plasticity, and conversely, play a role in excitatory plasticity. In the dorsomedial striatum, PNNs around PV+ interneurons were linked to increased grooming and digging behaviors in mouse models of excessive repetitive behaviors. Here, PNNs are not related to mechanisms of plasticity, but rather, increase rigidity and strengthening of inhibitory signaling (see **Schematic 4.1**).

In comparing the two studies, it begs the question why and through what signaling mechanisms can PNN structures play different roles. There is literature to suggest that specialized PNN components, i.e., tenascin-C and hyaluronic acid, have properties and functions important for modulating activity-dependent synaptic changes (reviewed in Dityatev et al., 2010), although the mechanism in which they regulate synaptic plasticity is still unclear. Throughout Chapters 3 and 4, PNNs were detected and analyzed using *Wisteria floribunda agglutinin* only, limiting our ability to detect specific PNN component differences across the two brain regions. PNNs are complex structures consisting of a large variety of CSPGs and core proteins, thus it is possible that PNNs in the dentate gyrus comprise more components important for plasticity compared to the dorsal striatum. Future studies should compare PNN components across brain regions to better understand PNNs role in plasticity throughout the brain.

Without the proper tools to manipulate these cells and circuits, we can only provide circumstantial evidence to support the role of PNNs in hippocampal-dependent structural plasticity and striatal-dependent behavioral and physiological plasticity. Given these studies together, it is

important that future studies consider how non-neuronal components in the brain, such as PNNs, contribute to mechanisms of plasticity and that the role(s) they play can vary region to region.

Schematic 4.1 Proposed models of hippocampal and striatal circuits involving perineuronal nets



References

Abbott, A.E., Linke, A.C., Nair, A., Jahedi, A., Alba, L.A., Keown, C.L., Fishman, I., and Müller, R.-A. (2018). Repetitive behaviors in autism are linked to imbalance of corticostriatal connectivity: a functional connectivity MRI study. Soc. Cogn. Affect. Neurosci. *13*, 32–42.

Ahmari, S.E., Spellman, T., Douglass, N.L., Kheirbek, M.A., Simpson, H.B., Deisseroth, K., Gordon, J.A., and Hen, R. (2013). Repeated Cortico-Striatal Stimulation Generates Persistent OCD-Like Behavior. Science *340*, 1234–1239.

Aimone, J.B., Wiles, J., and Gage, F.H. (2006). Potential role for adult neurogenesis in the encoding of time in new memories. Nat. Neurosci. *9*, 723–727.

Aimone, J.B., Deng, W., and Gage, F.H. (2010). Adult neurogenesis: integrating theories and separating functions. Trends Cogn. Sci. *14*, 325–337.

Akers, K.G., Martinez-Canabal, A., Restivo, L., Yiu, A.P., Cristofaro, A.D., Hsiang, H.-L. (Liz), Wheeler, A.L., Guskjolen, A., Niibori, Y., Shoji, H., et al. (2014). Hippocampal Neurogenesis Regulates Forgetting During Adulthood and Infancy. Science *344*, 598–602.

Alexander, G.E., DeLong, M.R., and Strick, P.L. (1986). Parallel organization of functionally segregated circuits linking basal ganglia and cortex. Annu. Rev. Neurosci. *9*, 357–381.

Altman, J., and Bayer, S.A. (1990). Migration and distribution of two populations of hippocampal granule cell precursors during the perinatal and postnatal periods. J. Comp. Neurol. *301*, 365–381.

Alvarez-Buylla, A., Theelen, M., and Nottebohm, F. (1988). Mapping of radial glia and of a new cell type in adult canary brain. J. Neurosci. Off. J. Soc. Neurosci. *8*, 2707–2712.

Amodeo, D.A., Jones, J.H., Sweeney, J.A., and Ragozzino, M.E. (2014). Risperidone and the 5-HT2A receptor antagonist M100907 improve probabilistic reversal learning in BTBR T + tf/J mice. Autism Res. Off. J. Int. Soc. Autism Res. *7*, 555–567.

Amodeo, D.A., Rivera, E., Cook, E.H., Sweeney, J.A., and Ragozzino, M.E. (2017a). 5HT2A receptor blockade in dorsomedial striatum reduces repetitive behaviors in BTBR mice. Genes Brain Behav. *16*, 342–351.

Amodeo, D.A., Grospe, G., Zang, H., Dwivedi, Y., and Ragozzino, M.E. (2017b). Cognitive flexibility impairment and reduced frontal cortex BDNF expression in the ouabain model of mania. Neuroscience *345*, 229–242.

Amrein, I., and Lipp, H.-P. (2009). Adult hippocampal neurogenesis of mammals: evolution and life history. Biol. Lett. *5*, 141–144.

Amrein, I., and Slomianka, L. (2010). A morphologically distinct granule cell type in the dentate gyrus of the red fox correlates with adult hippocampal neurogenesis. Brain Res. *1328*, 12–24.

Anderson, M.L., Sisti, H.M., Curlik, D.M., and Shors, T.J. (2011). Associative learning increases adult neurogenesis during a critical period. Eur. J. Neurosci. *33*, 175–181.

Association, A.P. (2013). Diagnostic and Statistical Manual of Mental Disorders (DSM-5®) (American Psychiatric Pub).

Bailey, C.H., Kandel, E.R., and Harris, K.M. (2015). Structural Components of Synaptic Plasticity and Memory Consolidation. Cold Spring Harb. Perspect. Biol. *7*.

Bain, M.J., Dwyer, S.M., and Rusak, B. (2004). Restraint stress affects hippocampal cell proliferation differently in rats and mice. Neurosci. Lett. *368*, 7–10.

Bakhurin, K.I., Mac, V., Golshani, P., and Masmanidis, S.C. (2016). Temporal correlations among functionally specialized striatal neural ensembles in reward-conditioned mice. J. Neurophysiol. *115*, 1521–1532.

Bannerman, D.M., Grubb, M., Deacon, R.M.J., Yee, B.K., Feldon, J., and Rawlins, J.N.P. (2003). Ventral hippocampal lesions affect anxiety but not spatial learning. Behav. Brain Res. *139*, 197–213.

Barha, C.K., Brummelte, S., Lieblich, S.E., and Galea, L.A.M. (2011). Chronic restraint stress in adolescence differentially influences hypothalamic-pituitary-adrenal axis function and adult hippocampal neurogenesis in male and female rats. Hippocampus *21*, 1216–1227.

Barnea, A., and Nottebohm, F. (1994). Seasonal recruitment of hippocampal neurons in adult free-ranging black-capped chickadees. Proc. Natl. Acad. Sci. U. S. A. *91*, 11217–11221.

Bednarczyk, M.R., Hacker, L.C., Fortin-Nunez, S., Aumont, A., Bergeron, R., and Fernandes, K.J.L. (2011). Distinct stages of adult hippocampal neurogenesis are regulated by running and the running environment. Hippocampus *21*, 1334–1347.

Bemben, M.A., Shipman, S.L., Hirai, T., Herring, B.E., Li, Y., Badger, J.D., Nicoll, R.A., Diamond, J.S., and Roche, K.W. (2014). CaMKII phosphorylation of neuroligin-1 regulates excitatory synapses. Nat. Neurosci. *17*, 56–64.

Blanchard, D.C., Spencer, R.L., Weiss, S.M., Blanchard, R.J., McEwen, B., and Sakai, R.R. (1995). Visible burrow system as a model of chronic social stress: Behavioral and neuroendocrine correlates. Psychoneuroendocrinology *20*, 117–134.

Blundell, J., Blaiss, C.A., Etherton, M.R., Espinosa, F., Tabuchi, K., Walz, C., Bolliger, M.F., Südhof, T.C., and Powell, C.M. (2010). Neuroligin-1 Deletion Results in Impaired Spatial Memory and Increased Repetitive Behavior. J. Neurosci. *30*, 2115–2129.

Boekhoorn, K., Joels, M., and Lucassen, P.J. (2006). Increased proliferation reflects glial and vascular-associated changes, but not neurogenesis in the presenile Alzheimer hippocampus. Neurobiol. Dis. *24*, 1–14.

Bolam, J.P., Hanley, J.J., Booth, P.A., and Bevan, M.D. (2000). Synaptic organisation of the basal ganglia. J. Anat. *196 (Pt 4)*, 527–542.

Boldrini, M., Fulmore, C.A., Tartt, A.N., Simeon, L.R., Pavlova, I., Poposka, V., Rosoklija, G.B., Stankov, A., Arango, V., Dwork, A.J., et al. (2018). Human Hippocampal Neurogenesis Persists throughout Aging. Cell Stem Cell *22*, 589-599.e5.

Bonhoeffer, T., and Yuste, R. (2002). Spine Motility: Phenomenology, Mechanisms, and Function. Neuron *35*, 1019–1027.

Boyer, C., Schikorski, T., and Stevens, C.F. (1998). Comparison of Hippocampal Dendritic Spines in Culture and in Brain. J. Neurosci. *18*, 5294–5300.

Brummelte, S., and Galea, L.A.M. (2010). Chronic corticosterone during pregnancy and postpartum affects maternal care, cell proliferation and depressive-like behavior in the dam. Horm. Behav. *58*, 769–779.

Burguière, E., Monteiro, P., Feng, G., and Graybiel, A.M. (2013). Optogenetic Stimulation of Lateral Orbitofronto-Striatal Pathway Suppresses Compulsive Behaviors. Science *340*, 1243–1246.

Burguière, E., Monteiro, P., Mallet, L., Feng, G., and Graybiel, A.M. (2015). Striatal circuits, habits, and implications for obsessive–compulsive disorder. Curr. Opin. Neurobiol. *30*, 59–65.

Cabungcal, J.-H., Steullet, P., Morishita, H., Kraftsik, R., Cuenod, M., Hensch, T.K., and Do, K.Q. (2013). Perineuronal nets protect fast-spiking interneurons against oxidative stress. Proc. Natl. Acad. Sci. U. S. A. *110*, 9130–9135.

Cai, Y., Wang, L., Xiao, R., Li, X., He, X., Gao, J., Xu, H., and Fan, X. (2017). Autism-like behavior in the BTBR mouse model of autism is improved by propofol. Neuropharmacology *118*, 175–187.

Cameron, H.A., and Gould, E. (1994). Adult neurogenesis is regulated by adrenal steroids in the dentate gyrus. Neuroscience *61*, 203–209.

Carayol, J., Sacco, R., Tores, F., Rousseau, F., Lewin, P., Hager, J., and Persico, A.M. (2011). Converging evidence for an association of ATP2B2 allelic variants with autism in male subjects. Biol. Psychiatry *70*, 880–887.

Centers for Disease Control and Prevention (CDC) (2013). Autism spectrum disorders (ASDs): data and statistics. (Centers for Disease Control and Prevention (CDC)).

Chang, H.T., Wilson, C.J., and Kitai, S.T. (1982). A Golgi study of rat neostriatal neurons: light microscopic analysis. J. Comp. Neurol. *208*, 107–126.

Chao, H.-T., Chen, H., Samaco, R.C., Xue, M., Chahrour, M., Yoo, J., Neul, J.L., Gong, S., Lu, H.-C., Heintz, N., et al. (2010). Dysfunction in GABA signalling mediates autism-like stereotypies and Rett syndrome phenotypes. Nature *468*, 263–269.

Chawana, R., Alagaili, A., Patzke, N., Spocter, M.A., Mohammed, O.B., Kaswera, C., Gilissen, E., Bennett, N.C., Ihunwo, A.O., and Manger, P.R. (2014). Microbats appear to have adult hippocampal neurogenesis, but post-capture stress causes a rapid decline in the number of neurons expressing doublecortin. Neuroscience *277*, 724–733.

Chen, C.-C., Huang, C.-C., and Hsu, K.-S. (2016). Chronic Social Stress Affects Synaptic Maturation of Newly Generated Neurons in the Adult Mouse Dentate Gyrus. Int. J. Neuropsychopharmacol. *19*.

Cheng, C.-H., Lin, C.-T., Lee, M.-J., Tsai, M.-J., Huang, W.-H., Huang, M.-C., Lin, Y.-L., Chen, C.-J., Huang, W.-C., and Cheng, H. (2015). Local Delivery of High-Dose Chondroitinase ABC in the Sub-Acute Stage Promotes Axonal Outgrowth and Functional Recovery after Complete Spinal Cord Transection. PLOS ONE *10*, e0138705.

Cope, E.C., Briones, B.A., Brockett, A.T., Martinez, S., Vigneron, P.-A., Opendak, M., Wang, S.S.-H., and Gould, E. (2016). Immature Neurons and Radial Glia, But Not Astrocytes or Microglia, Are Altered in Adult Cntnap2 and Shank3 Mice, Models of Autism. ENeuro *3*.

Cornew, L., Roberts, T.P.L., Blaskey, L., and Edgar, J.C. (2012). Resting-State Oscillatory Activity in Autism Spectrum Disorders. J. Autism Dev. Disord. *42*, 1884–1894.

Cowan, R.L., Wilson, C.J., Emson, P.C., and Heizmann, C.W. (1990). Parvalbumin-containing GABAergic interneurons in the rat neostriatum. J. Comp. Neurol. *302*, 197–205.

Crawley, J.N. (2012). Translational animal models of autism and neurodevelopmental disorders. Dialogues Clin. Neurosci. *14*, 293–305.

Czéh, B., Michaelis, T., Watanabe, T., Frahm, J., Biurrun, G. de, Kampen, M. van, Bartolomucci, A., and Fuchs, E. (2001). Stress-induced changes in cerebral metabolites, hippocampal volume, and cell proliferation are prevented by antidepressant treatment with tianeptine. Proc. Natl. Acad. Sci. *98*, 12796–12801.

Czéh, B., Müller-Keuker, J.I.H., Rygula, R., Abumaria, N., Hiemke, C., Domenici, E., and Fuchs, E. (2007). Chronic Social Stress Inhibits Cell Proliferation in the Adult Medial Prefrontal Cortex: Hemispheric Asymmetry and Reversal by Fluoxetine Treatment. Neuropsychopharmacology *32*, 1490–1503.

Danielson, N.B., Kaifosh, P., Zaremba, J.D., Lovett-Barron, M., Tsai, J., Denny, C.A., Balough, E.M., Goldberg, A.R., Drew, L.J., Hen, R., et al. (2016). Distinct Contribution of Adult-Born Hippocampal Granule Cells to Context Encoding. Neuron *90*, 101–112.

David, D.J., Samuels, B.A., Rainer, Q., Wang, J.-W., Marsteller, D., Mendez, I., Drew, M., Craig, D.A., Guiard, B.P., Guilloux, J.-P., et al. (2009). Neurogenesis-Dependent and -Independent Effects of Fluoxetine in an Animal Model of Anxiety/Depression. Neuron *62*, 479–493.

Dayer, A.G., Cleaver, K.M., Abouantoun, T., and Cameron, H.A. (2005). New GABAergic interneurons in the adult neocortex and striatum are generated from different precursors. J. Cell Biol. *168*, 415–427.

D'Cruz, A.-M., Ragozzino, M.E., Mosconi, M.W., Shrestha, S., Cook, E.H., and Sweeney, J.A. (2013). Reduced behavioral flexibility in autism spectrum disorders. Neuropsychology *27*, 152–160.

De Kloet, E.R., and Reul, J.M. (1987). Feedback action and tonic influence of corticosteroids on brain function: a concept arising from the heterogeneity of brain receptor systems. Psychoneuroendocrinology *12*, 83–105.

De Kloet, E.R., Vreugdenhil, E., Oitzl, M.S., and Joëls, M. (1998). Brain corticosteroid receptor balance in health and disease. Endocr. Rev. *19*, 269–301.

De Miguel, Z., Haditsch, U., Palmer, T.D., Azpiroz, A., and Sapolsky, R.M. (2018). Adult-generated neurons born during chronic social stress are uniquely adapted to respond to subsequent chronic social stress. Mol. Psychiatry.

Deacon, R.M.J. (2006). Digging and marble burying in mice: simple methods for in vivo identification of biological impacts. Nat. Protoc. *1*, 122–124.

Dennis, C.V., Suh, L.S., Rodriguez, M.L., Kril, J.J., and Sutherland, G.T. (2016). Human adult neurogenesis across the ages: An immunohistochemical study. Neuropathol. Appl. Neurobiol. *42*, 621–638.

Devan, B.D., Hong, N.S., and McDonald, R.J. (2011). Parallel associative processing in the dorsal striatum: Segregation of stimulus–response and cognitive control subregions. Neurobiol. Learn. Mem. *96*, 95–120.

Dityatev, A., Brückner, G., Dityateva, G., Grosche, J., Kleene, R., and Schachner, M. (2007). Activity-dependent formation and functions of chondroitin sulfate-rich extracellular matrix of perineuronal nets. Dev. Neurobiol. *67*, 570–588.

Ellegood, J., and Crawley, J.N. (2015). Behavioral and Neuroanatomical Phenotypes in Mouse Models of Autism. Neurother. J. Am. Soc. Exp. Neurother. *12*, 521–533.

Eriksson, P.S., Perfilieva, E., Björk-Eriksson, T., Alborn, A.-M., Nordborg, C., Peterson, D.A., and Gage, F.H. (1998). Neurogenesis in the adult human hippocampus. Nat. Med. *4*, 1313–1317.

Ernst, A., Alkass, K., Bernard, S., Salehpour, M., Perl, S., Tisdale, J., Possnert, G., Druid, H., and Frisén, J. (2014). Neurogenesis in the Striatum of the Adult Human Brain. Cell *156*, 1072–1083.

Faini, G., Aguirre, A., Landi, S., Lamers, D., Pizzorusso, T., Ratto, G.M., Deleuze, C., and Bacci, A. (2018). Perineuronal nets control visual input via thalamic recruitment of cortical PV interneurons. ELife *7*.

Falconer, E.M., and Galea, L.A.M. (2003). Sex differences in cell proliferation, cell death and defensive behavior following acute predator odor stress in adult rats. Brain Res. *975*, 22–36.

Fanselow, M.S., and Dong, H.-W. (2010). Are the dorsal and ventral hippocampus functionally distinct structures? Neuron *65*, 7–19.

Feldman, D.E. (2009). Synaptic mechanisms for plasticity in neocortex. Annu. Rev. Neurosci. *32*, 33–55.

Fenlon, L.R., Liu, S., Gobius, I., Kurniawan, N.D., Murphy, S., Moldrich, R.X., and Richards, L.J. (2015). Formation of functional areas in the cerebral cortex is disrupted in a mouse model of autism spectrum disorder. Neural Develop. *10*, 10.

Ferragud, A., Haro, A., Sylvain, A., Velázquez-Sánchez, C., Hernández-Rabaza, V., and Canales, J.J. (2010). Enhanced habit-based learning and decreased neurogenesis in the adult hippocampus in a murine model of chronic social stress. Behav. Brain Res. *210*, 134–139.

Fu, M., Yu, X., Lu, J., and Zuo, Y. (2012). Repetitive motor learning induces coordinated formation of clustered dendritic spines in vivo. Nature *483*, 92–95.

Fujioka, A., Fujioka, T., Ishida, Y., Maekawa, T., and Nakamura, S. (2006). Differential effects of prenatal stress on the morphological maturation of hippocampal neurons. Neuroscience *141*, 907–915.

Gandal, M.J., Edgar, J.C., Ehrlichman, R.S., Mehta, M., Roberts, T.P.L., and Siegel, S.J. (2010). Validating γ oscillations and delayed auditory responses as translational biomarkers of autism. Biol. Psychiatry *68*, 1100–1106.

Garthe, A., Roeder, I., and Kempermann, G. (2016). Mice in an enriched environment learn more flexibly because of adult hippocampal neurogenesis. Hippocampus *26*, 261–271.

Gatome, C.W., Mwangi, D.K., Lipp, H.-P., and Amrein, I. (2010). Hippocampal Neurogenesis and Cortical Cellular Plasticity in Wahlberg's Epauletted Fruit Bat: A Qualitative and Quantitative Study. Brain. Behav. Evol. *76*, 116–127.

Gazzaley, A., Kay, S., and Benson, D.L. (2002). Dendritic spine plasticity in hippocampus. Neuroscience *111*, 853–862.

Gdalyahu, A., Lazaro, M., Penagarikano, O., Golshani, P., Trachtenberg, J.T., and Gescwind, D.H. (2015). The Autism Related Protein Contactin-Associated Protein-Like 2 (CNTNAP2) Stabilizes New Spines: An In Vivo Mouse Study. PLoS ONE *10*.

Geinisman, Y. (2000). Structural Synaptic Modifications Associated with Hippocampal LTP and Behavioral Learning. Cereb. Cortex *10*, 952–962.

Gertler, T.S., Chan, C.S., and Surmeier, D.J. (2008). Dichotomous Anatomical Properties of Adult Striatal Medium Spiny Neurons. J. Neurosci. *28*, 10814–10824.

Gipson, C.D., and Olive, M.F. (2017). Structural and functional plasticity of dendritic spines – root or result of behavior? Genes Brain Behav. *16*, 101–117.

Gittis, A.H., Nelson, A.B., Thwin, M.T., Palop, J.J., and Kreitzer, A.C. (2010). Distinct roles of GABAergic interneurons in the regulation of striatal output pathways. J. Neurosci. Off. J. Soc. Neurosci. *30*, 2223–2234.

Gittis, A.H., Hang, G.B., LaDow, E.S., Shoenfeld, L.R., Atallah, B.V., Finkbeiner, S., and Kreitzer, A.C. (2011). Rapid target-specific remodeling of fast-spiking inhibitory circuits after loss of dopamine. Neuron *71*, 858–868.

Glasper, E.R., Llorens-Martin, M.V., Leuner, B., Gould, E., and Trejo, J.L. (2010). Blockade of insulin-like growth factor-I has complex effects on structural plasticity in the hippocampus. Hippocampus *20*, 706–712.

Golgi, C. (1898). Intorno alle strutture delle cellule nervose. Boll. Soc. Med-chir. Pavia, 1, 1–14.

González-Tapia, D., González-Ramírez, M.M., Vázquez-Hernández, N., and González-Burgos, I. (2017). Motor learning induces plastic changes in Purkinje cell dendritic spines in the rat cerebellum. Neurol. Barc. Spain.

Goshen, I., Kreisel, T., Ben-Menachem-Zidon, O., Licht, T., Weidenfeld, J., Ben-Hur, T., and Yirmiya, R. (2008). Brain interleukin-1 mediates chronic stress-induced depression in mice via adrenocortical activation and hippocampal neurogenesis suppression. Mol. Psychiatry *13*, 717–728.

Gould, E., and Tanapat, P. (1997). Lesion-induced proliferation of neuronal progenitors in the dentate gyrus of the adult rat. Neuroscience *80*, 427–436.

Gould, E., McEwen, B.S., Tanapat, P., Galea, L.A.M., and Fuchs, E. (1997). Neurogenesis in the Dentate Gyrus of the Adult Tree Shrew Is Regulated by Psychosocial Stress and NMDA Receptor Activation. J. Neurosci. *17*, 2492–2498.

Gould, E., Tanapat, P., McEwen, B.S., Flügge, G., and Fuchs, E. (1998). Proliferation of granule cell precursors in the dentate gyrus of adult monkeys is diminished by stress. Proc. Natl. Acad. Sci. *95*, 3168–3171.

Gould, E., Beylin, A., Tanapat, P., Reeves, A., and Shors, T.J. (1999a). Learning enhances adult neurogenesis in the hippocampal formation. Nat. Neurosci. *2*, 260–265.

Gould, E., Reeves, A.J., Fallah, M., Tanapat, P., Gross, C.G., and Fuchs, E. (1999b). Hippocampal neurogenesis in adult Old World primates. Proc. Natl. Acad. Sci. *96*, 5263–5267.

Gould, E., Beylin, A., Tanapat, P., Reeves, A., and Shors, T.J. (1999c). Learning enhances adult neurogenesis in the hippocampal formation. Nat. Neurosci. *2*, 260–265.

Grassi Zucconi, G., Cipriani, S., Balgkouranidou, I., and Scattoni, R. (2006). 'One night' sleep deprivation stimulates hippocampal neurogenesis. Brain Res. Bull. *69*, 375–381.

Greisen, M.H., Altar, C.A., Bolwig, T.G., Whitehead, R., and Wörtwein, G. (2005). Increased adult hippocampal brain-derived neurotrophic factor and normal levels of neurogenesis in maternal separation rats. J. Neurosci. Res. *79*, 772–778.

Guzman, S.J., Schlögl, A., and Schmidt-Hieber, C. (2014). Stimfit: quantifying electrophysiological data with Python. Front. Neuroinformatics *8*.

Guzmán-Marín Ruben, Suntsova Natalia, Stewart Darya R., Gong Hui, Szymusiak Ronald, and McGinty Dennis (2004). Sleep Deprivation Reduces Proliferation of Cells in the Dentate Gyrus of the Hippocampus in Rats. J. Physiol. *549*, 563–571.

Haber, S.N., Fudge, J.L., and McFarland, N.R. (2000). Striatonigrostriatal pathways in primates form an ascending spiral from the shell to the dorsolateral striatum. J. Neurosci. Off. J. Soc. Neurosci. *20*, 2369–2382.

Han, S., Tai, C., Jones, C.J., Scheuer, T., and Catterall, W.A. (2014). Enhancement of Inhibitory Neurotransmission by GABAA Receptors Having α2,3-Subunits Ameliorates Behavioral Deficits in a Mouse Model of Autism. Neuron *81*, 1282–1289.

Harris, K.M., and Stevens, J.K. (1989). Dendritic spines of CA 1 pyramidal cells in the rat hippocampus: serial electron microscopy with reference to their biophysical characteristics. J. Neurosci. *9*, 2982–2997.

Hastings, N.B., and Gould, E. (1999). Rapid extension of axons into the CA3 region by adult-generated granule cells. J. Comp. Neurol. *413*, 146–154.

Heine, V.M., Maslam, S., Zareno, J., Joëls, M., and Lucassen, P.J. (2004). Suppressed proliferation and apoptotic changes in the rat dentate gyrus after acute and chronic stress are reversible. Eur. J. Neurosci. *19*, 131–144.

Hill, M.N., Kambo, J.S., Sun, J.C., Gorzalka, B.B., and Galea, L.A.M. (2006). Endocannabinoids modulate stress-induced suppression of hippocampal cell proliferation and activation of defensive behaviours. Eur. J. Neurosci. *24*, 1845–1849.

Hillerer, K.M., Neumann, I.D., Couillard-Despres, S., Aigner, L., and Slattery, D.A. (2013). Sex-dependent regulation of hippocampal neurogenesis under basal and chronic stress conditions in rats. Hippocampus *23*, 476–487.

Hollander, E., Greenwald, S., Neville, D., Johnson, J., Hornig, C.D., and Weissman, M.M. (1996). Uncomplicated and comorbid obsessive-compulsive disorder in an epidemiologic sample. Depress. Anxiety *4*, 111–119.

Hong, S.L., Cossyleon, D., Hussain, W.A., Walker, L.J., Barton, S.J., and Rebec, G.V. (2012). Dysfunctional Behavioral Modulation of Corticostriatal Communication in the R6/2 Mouse Model of Huntington's Disease. PLOS ONE *7*, e47026.

Hunnicutt, B.J., Jongbloets, B.C., Birdsong, W.T., Gertz, K.J., Zhong, H., and Mao, T. (2016). A comprehensive excitatory input map of the striatum reveals novel functional organization. ELife *5*, e19103.

Hwang, I.K., Yoo, K.-Y., Li, H., Choi, J.H., Kwon, Y.-G., Ahn, Y., Lee, I.S., and Won, M.H. (2007). Differences in Doublecortin Immunoreactivity and Protein Levels in the Hippocampal Dentate Gyrus Between Adult and Aged Dogs. Neurochem. Res. *32*, 1604–1609.

Jasinska, M., Siucinska, E., Jasek, E., Litwin, J.A., Pyza, E., and Kossut, M. (2016). Effect of Associative Learning on Memory Spine Formation in Mouse Barrel Cortex. Neural Plast. *2016*.

Jiang, Y., and Ehlers, M.D. (2013). Modeling Autism by SHANK Gene Mutations in Mice. Neuron *78*, 8–27.

Jin Kunlin, Minami Manabu, Xie Lin, Sun Yunjuan, Mao Xiao Ou, Wang Yaoming, Simon Roger P., and Greenberg David A. (2004). Ischemia-induced neurogenesis is preserved but reduced in the aged rodent brain. Aging Cell *3*, 373–377.

Kang, J., and Kim, E. (2015). Suppression of NMDA receptor function in mice prenatally exposed to valproic acid improves social deficits and repetitive behaviors. Front. Mol. Neurosci. *8*.

Kaplan, M.S., and Bell, D.H. (1984). Mitotic neuroblasts in the 9-day-old and 11-month-old rodent hippocampus. J. Neurosci. *4*, 1429–1441.

Kaplan, M.S., and Hinds, J.W. (1977). Neurogenesis in the adult rat: electron microscopic analysis of light radioautographs. Science *197*, 1092–1094.

Kazdoba, T.M., Leach, P.T., and Crawley, J.N. (2016). Behavioral phenotypes of genetic mouse models of autism. Genes Brain Behav. *15*, 7–26.

Kempermann, G., Kuhn, H.G., and Gage, F.H. (1997). More hippocampal neurons in adult mice living in an enriched environment. Nature *386*, 493–495.

Kempermann, G., Gage, F.H., Aigner, L., Song, H., Curtis, M.A., Thuret, S., Kuhn, H.G., Jessberger, S., Frankland, P.W., Cameron, H.A., et al. (2018). Human Adult Neurogenesis: Evidence and Remaining Questions. Cell Stem Cell *23*, 25–30.

Kheirbek, M.A., Tannenholz, L., and Hen, R. (2012). NR2B-Dependent Plasticity of Adult-Born Granule Cells is Necessary for Context Discrimination. J. Neurosci. *32*, 8696–8702.

Kim, J.J., and Fanselow, M.S. (1992). Modality-specific retrograde amnesia of fear. Science *256*, 675–677.

Kim, K.C., Gonzales, E.L., Lázaro, M.T., Choi, C.S., Bahn, G.H., Yoo, H.J., and Shin, C.Y. (2016). Clinical and Neurobiological Relevance of Current Animal Models of Autism Spectrum Disorders. Biomol. Ther. *24*, 207–243.

Kirby, E.D., Friedman, A.R., Covarrubias, D., Ying, C., Sun, W.G., Goosens, K.A., Sapolsky, R.M., and Kaufer, D. (2012). Basolateral amygdala regulation of adult hippocampal neurogenesis and fear-related activation of newborn neurons. Mol. Psychiatry *17*, 527–536.

Kita, H. (1993). Chapter 4 GABAergic circuits of the striatum. In Progress in Brain Research, G.W. Arbuthnott, and P.C. Emson, eds. (Elsevier), pp. 51–72.

Kita, H., Kosaka, T., and Heizmann, C.W. (1990). Parvalbumin-immunoreactive neurons in the rat neostriatum: a light and electron microscopic study. Brain Res. *536*, 1–15.

Knoth, R., Singec, I., Ditter, M., Pantazis, G., Capetian, P., Meyer, R.P., Horvat, V., Volk, B., and Kempermann, G. (2010). Murine Features of Neurogenesis in the Human Hippocampus across the Lifespan from 0 to 100 Years. PLOS ONE *5*, e8809.

Kötter, R. (1994). Postsynaptic integration of glutamatergic and dopaminergic signals in the striatum. Prog. Neurobiol. *44*, 163–196.

Kouser, M., Speed, H.E., Dewey, C.M., Reimers, J.M., Widman, A.J., Gupta, N., Liu, S., Jaramillo, T.C., Bangash, M., Xiao, B., et al. (2013). Loss of predominant Shank3 isoforms results in hippocampus-dependent impairments in behavior and synaptic transmission. J. Neurosci. Off. J. Soc. Neurosci. *33*, 18448–18468.

Kozorovitskiy, Y., and Gould, E. (2004). Dominance Hierarchy Influences Adult Neurogenesis in the Dentate Gyrus. J. Neurosci. *24*, 6755–6759.

Kozorovitskiy, Y., Gross, C.G., Kopil, C., Battaglia, L., McBreen, M., Stranahan, A.M., and Gould, E. (2005). Experience induces structural and biochemical changes in the adult primate brain. Proc. Natl. Acad. Sci. *102*, 17478–17482.

Kuhlman, S.J., O'Connor, D.H., Fox, K., and Svoboda, K. (2014). Structural Plasticity within the Barrel Cortex during Initial Phases of Whisker-Dependent Learning. J. Neurosci. *34*, 6078–6083.

Lagace, D.C., Donovan, M.H., DeCarolis, N.A., Farnbauch, L.A., Malhotra, S., Berton, O., Nestler, E.J., Krishnan, V., and Eisch, A.J. (2010). Adult hippocampal neurogenesis is functionally important for stress-induced social avoidance. Proc. Natl. Acad. Sci. *107*, 4436–4441.

Langen, M., Schnack, H.G., Nederveen, H., Bos, D., Lahuis, B.E., de Jonge, M.V., van Engeland, H., and Durston, S. (2009). Changes in the developmental trajectories of striatum in autism. Biol. Psychiatry *66*, 327–333.

Langen, M., Kas, M.J.H., Staal, W.G., van Engeland, H., and Durston, S. (2011). The neurobiology of repetitive behavior: Of mice…. Neurosci. Biobehav. Rev. *35*, 345–355.

Langen, M., Bos, D., Noordermeer, S.D.S., Nederveen, H., van Engeland, H., and Durston, S. (2014). Changes in the Development of Striatum Are Involved in Repetitive Behavior in Autism. Biol. Psychiatry *76*, 405–411.

Larrain-Valenzuela, J., Zamorano, F., Soto-Icaza, P., Carrasco, X., Herrera, C., Daiber, F., Aboitiz, F., and Billeke, P. (2017). Theta and Alpha Oscillation Impairments in Autistic Spectrum Disorder Reflect Working Memory Deficit. Sci. Rep. *7*.

Lauber, E., Filice, F., and Schwaller, B. (2016). Prenatal Valproate Exposure Differentially Affects Parvalbumin-Expressing Neurons and Related Circuits in the Cortex and Striatum of Mice. Front. Mol. Neurosci. *9*.

Leasure, J.L., and Decker, L. (2009). Social isolation prevents exercise-induced proliferation of hippocampal progenitor cells in female rats. Hippocampus *19*, 907–912.

Lee, C.H., Yoo, D.Y., Park, O.K., Park, J.H., Yi, S.S., Yoon, Y.S., Won, M.-H., and Hwang, I.K. (2011). Effects of Adrenalectomy and Replacement Therapy of Corticosterone on Cell Proliferation and Neuroblast Differentiation in the Rat Dentate Gyrus. Neurochem. Res. *36*, 1767–1775.

Lee, H., Leamey, C.A., and Sawatari, A. (2012). Perineuronal Nets Play a Role in Regulating Striatal Function in the Mouse. PLOS ONE *7*, e32747.

Lee, K., Holley, S.M., Shobe, J.L., Chong, N.C., Cepeda, C., Levine, M.S., and Masmanidis, S.C. (2017). Parvalbumin Interneurons Modulate Striatal Output and Enhance Performance during Associative Learning. Neuron *93*, 1451-1463.e4.

Lemaire, V., Koehl, M., Moal, M.L., and Abrous, D.N. (2000). Prenatal stress produces learning deficits associated with an inhibition of neurogenesis in the hippocampus. Proc. Natl. Acad. Sci. *97*, 11032–11037.

Lensjø, K.K., Lepperød, M.E., Dick, G., Hafting, T., and Fyhn, M. (2017). Removal of Perineuronal Nets Unlocks Juvenile Plasticity Through Network Mechanisms of Decreased Inhibition and Increased Gamma Activity. J. Neurosci. Off. J. Soc. Neurosci. *37*, 1269–1283.

Leuner, B., Falduto, J., and Shors, T.J. (2003). Associative memory formation increases the observation of dendritic spines in the hippocampus. J. Neurosci. Off. J. Soc. Neurosci. *23*, 659–665.

Leuner, B., Gould, E., and Shors, T.J. (2006). Is there a link between adult neurogenesis and learning? Hippocampus *16*, 216–224.

Leuner, B., Glasper, E.R., and Mirescu, C. (2007). A Critical Time for New Neurons in the Adult Hippocampus. J. Neurosci. *27*, 5845–5846.

Leuner, B., Glasper, E.R., and Gould, E. (2010). Sexual Experience Promotes Adult Neurogenesis in the Hippocampus Despite an Initial Elevation in Stress Hormones. PLOS ONE *5*, e11597.

Lewis, M., and Kim, S.-J. (2009). The pathophysiology of restricted repetitive behavior. J. Neurodev. Disord. *1*, 114–132.

Lin, Y.-T., Chen, C.-C., Huang, C.-C., Nishimori, K., and Hsu, K.-S. (2017). Oxytocin stimulates hippocampal neurogenesis via oxytocin receptor expressed in CA3 pyramidal neurons. Nat. Commun. *8*, 537.

Ling, C., Zuo, M., Alvarez-Buylla, A., and Cheng, M.F. (1997). Neurogenesis in juvenile and adult ring doves. J. Comp. Neurol. *379*, 300–312.

Llorens-Martín, M.V., Rueda, N., Martínez-Cué, C., Torres-Alemán, I., Flórez, J., and Trejo, J.L. (2007). Both increases in immature dentate neuron number and decreases of immobility time in the forced swim test occurred in parallel after environmental enrichment of mice. Neuroscience *147*, 631–638.

Lloyd, S.A., Balest, Z.R., Corotto, F.S., and Smeyne, R.J. (2010). Cocaine selectively increases proliferation in the adult murine hippocampus. Neurosci. Lett. *485*, 112–116.

Luzzati, F., De Marchis, S., Fasolo, A., and Peretto, P. (2006). Neurogenesis in the Caudate Nucleus of the Adult Rabbit. J. Neurosci. *26*, 609–621.

Ma, L., Qiao, Q., Tsai, J.-W., Yang, G., Li, W., and Gan, W.-B. (2016). Experience-dependent plasticity of dendritic spines of layer 2/3 pyramidal neurons in the mouse cortex. Dev. Neurobiol. *76*, 277–286.

MacDowell, C.J., and Buschman, T.J. (2020). Low-Dimensional Spatio-Temporal Dynamics Underlie Cortex-Wide Neural Activity. BioRxiv 2020.01.05.895177.

Mahmmoud, R.R., Sase, S., Aher, Y.D., Sase, A., Gröger, M., Mokhtar, M., Höger, H., and Lubec, G. (2015). Spatial and Working Memory Is Linked to Spine Density and Mushroom Spines. PLoS ONE *10*.

Malberg, J.E., and Duman, R.S. (2003). Cell Proliferation in Adult Hippocampus is Decreased by Inescapable Stress: Reversal by Fluoxetine Treatment. Neuropsychopharmacology *28*, 1562–1571.

Marín-Burgin, A., Mongiat, L.A., Pardi, M.B., and Schinder, A.F. (2012). Unique Processing During a Period of High Excitation/Inhibition Balance in Adult-Born Neurons. Science *335*, 1238–1242.

McEwen, B.S., De Kloet, E.R., and Rostene, W. (1986). Adrenal steroid receptors and actions in the nervous system. Physiol. Rev. *66*, 1121–1188.

McHugh, S.B., Fillenz, M., Lowry, J.P., Rawlins, J.N.P., and Bannerman, D.M. (2011). Brain tissue oxygen amperometry in behaving rats demonstrates functional dissociation of dorsal and ventral hippocampus during spatial processing and anxiety. Eur. J. Neurosci. *33*, 322–337.

Meyza, K.Z., and Blanchard, D.C. (2017). The BTBR mouse model of idiopathic autism - Current view on mechanisms. Neurosci. Biobehav. Rev. *76*, 99–110.

Miller, H.L., Ragozzino, M.E., Cook, E.H., Sweeney, J.A., and Mosconi, M.W. (2015). Cognitive set shifting deficits and their relationship to repetitive behaviors in autism spectrum disorder. J. Autism Dev. Disord. *45*, 805–815.

Mirescu, C., Peters, J.D., and Gould, E. (2004). Early life experience alters response of adult neurogenesis to stress. Nat. Neurosci. *7*, 841–846.

Mirescu, C., Peters, J.D., Noiman, L., and Gould, E. (2006). Sleep deprivation inhibits adult neurogenesis in the hippocampus by elevating glucocorticoids. Proc. Natl. Acad. Sci. U. S. A. *103*, 19170–19175.

Moldrich, R.X., Leanage, G., She, D., Dolan-Evans, E., Nelson, M., Reza, N., and Reutens, D.C. (2013). Inhibition of histone deacetylase in utero causes sociability deficits in postnatal mice. Behav. Brain Res. *257*, 253–264.

Monteiro, B.M.M., Moreira, F.A., Massensini, A.R., Moraes, M.F.D., and Pereira, G.S. (2014). Enriched environment increases neurogenesis and improves social memory persistence in socially isolated adult mice. Hippocampus *24*, 239–248.

Moreno-Jiménez, E.P., Flor-García, M., Terreros-Roncal, J., Rábano, A., Cafini, F., Pallas-Bazarra, N., Ávila, J., and Llorens-Martín, M. (2019). Adult hippocampal neurogenesis is abundant in neurologically healthy subjects and drops sharply in patients with Alzheimer's disease. Nat. Med. *25*, 554–560.

Moser, M.-B., and Moser, E.I. (1998). Functional differentiation in the hippocampus. Hippocampus *8*, 608–619.

Moser, E., Moser, M.B., and Andersen, P. (1993). Spatial learning impairment parallels the magnitude of dorsal hippocampal lesions, but is hardly present following ventral lesions. J. Neurosci. Off. J. Soc. Neurosci. *13*, 3916–3925.

Moser, M.B., Trommald, M., and Andersen, P. (1994). An increase in dendritic spine density on hippocampal CA1 pyramidal cells following spatial learning in adult rats suggests the formation of new synapses. Proc. Natl. Acad. Sci. *91*, 12673–12675.

Moser, M.B., Moser, E.I., Forrest, E., Andersen, P., and Morris, R.G. (1995). Spatial learning with a minislab in the dorsal hippocampus. Proc. Natl. Acad. Sci. *92*, 9697–9701.

Mouri, A., Ukai, M., Uchida, M., Hasegawa, S., Taniguchi, M., Ito, T., Hida, H., Yoshimi, A., Yamada, K., Kunimoto, S., et al. (2018). Juvenile social defeat stress exposure persistently impairs social behaviors and neurogenesis. Neuropharmacology *133*, 23–37.

Moy, S.S., Nadler, J.J., Young, N.B., Perez, A., Holloway, L.P., Barbaro, R.P., Barbaro, J.R., Wilson, L.M., Threadgill, D.W., Lauder, J.M., et al. (2007). Mouse behavioral tasks relevant to autism: phenotypes of 10 inbred strains. Behav. Brain Res. *176*, 4–20.

Muller, D., Toni, N., and Buchs, P.-A. (2000). Spine changes associated with long-term potentiation. Hippocampus *10*, 596–604.

Murakoshi, H., and Yasuda, R. (2012). Postsynaptic signaling during plasticity of dendritic spines. Trends Neurosci. *35*, 135–143.

National Institute of Mental Health (NIMH) (2017). Autism Spectrum Disorder (ASD). (National Institute of Mental Health (NIMH)).

von Nicolai, C., Engler, G., Sharott, A., Engel, A.K., Moll, C.K., and Siegel, M. (2014). Corticostriatal coordination through coherent phase-amplitude coupling. J. Neurosci. Off. J. Soc. Neurosci. *34*, 5938–5948.

Nicolini, C., and Fahnestock, M. (2018). The valproic acid-induced rodent model of autism. Exp. Neurol. *299*, 217–227.

Nilsson, M., Perfilieva, E., Johansson, U., Orwar, O., and Eriksson, P.S. (1999). Enriched environment increases neurogenesis in the adult rat dentate gyrus and improves spatial memory. J. Neurobiol. *39*, 569–578.

Nishiyama, J., and Yasuda, R. (2015). Biochemical computation for spine structural plasticity. Neuron *87*, 63–75.

Oomen, C.A., Soeters, H., Audureau, N., Vermunt, L., van Hasselt, F.N., Manders, E.M.M., Joëls, M., Lucassen, P.J., and Krugers, H. (2010). Severe early life stress hampers spatial learning and neurogenesis, but improves hippocampal synaptic plasticity and emotional learning under high-stress conditions in adulthood. J. Neurosci. Off. J. Soc. Neurosci. *30*, 6635–6645.

Opendak, M., Offit, L., Monari, P., Schoenfeld, T.J., Sonti, A.N., Cameron, H.A., and Gould, E. (2016). Lasting Adaptations in Social Behavior Produced by Social Disruption and Inhibition of Adult Neurogenesis. J. Neurosci. *36*, 7027–7038.

Packard, M.G., and Knowlton, B.J. (2002). Learning and memory functions of the Basal Ganglia. Annu. Rev. Neurosci. *25*, 563–593.

Pantazopoulos, H., and Berretta, S. (2016). In Sickness and in Health: Perineuronal Nets and Synaptic Plasticity in Psychiatric Disorders.

Parent, J.M. (2003). Injury-Induced Neurogenesis in the Adult Mammalian Brain. The Neuroscientist *9*, 261–272.

Parent, J.M., Yu, T.W., Leibowitz, R.T., Geschwind, D.H., Sloviter, R.S., and Lowenstein, D.H. (1997). Dentate Granule Cell Neurogenesis Is Increased by Seizures and Contributes to Aberrant Network Reorganization in the Adult Rat Hippocampus. J. Neurosci. *17*, 3727–3738.

Peça, J., Feliciano, C., Ting, J.T., Wang, W., Wells, M.F., Venkatraman, T.N., Lascola, C.D., Fu, Z., and Feng, G. (2011). Shank3 mutant mice display autistic-like behaviours and striatal dysfunction. Nature *472*, 437–442.

Penadés, R., Catalán, R., Andrés, S., Salamero, M., and Gastó, C. (2005). Executive function and nonverbal memory in obsessive-compulsive disorder. Psychiatry Res. *133*, 81–90.

Peñagarikano, O., Abrahams, B.S., Herman, E.I., Winden, K.D., Gdalyahu, A., Dong, H., Sonnenblick, L.I., Gruver, R., Almajano, J., Bragin, A., et al. (2011). Absence of CNTNAP2 leads to epilepsy, neuronal migration abnormalities, and core autism-related deficits. Cell *147*, 235–246.

Pereira, A.C., Huddleston, D.E., Brickman, A.M., Sosunov, A.A., Hen, R., McKhann, G.M., Sloan, R., Gage, F.H., Brown, T.R., and Small, S.A. (2007). An in vivo correlate of exercise-induced neurogenesis in the adult dentate gyrus. Proc. Natl. Acad. Sci. *104*, 5638–5643.

Pérez-Cañellas, M.M., and García-Verdugo, J.M. (1996). Adult neurogenesis in the telencephalon of a lizard: a [3H]thymidine autoradiographic and bromodeoxyuridine immunocytochemical study. Brain Res. Dev. Brain Res. *93*, 49–61.

Perez-Sanchez, F., Molowny, A., Garcia-Verdugo, J.M., and Lopez-Garcia, C. (1989). Postnatal neurogenesis in the nucleus sphericus of the lizard, Podarcis hispanica. Neurosci. Lett. *106*, 71–75.

Pham, K., Nacher, J., Hof, P.R., and McEwen, B.S. (2003). Repeated restraint stress suppresses neurogenesis and induces biphasic PSA-NCAM expression in the adult rat dentate gyrus. Eur. J. Neurosci. *17*, 879–886.

Praag, H. van, Kempermann, G., and Gage, F.H. (1999). Running increases cell proliferation and neurogenesis in the adult mouse dentate gyrus. Nat. Neurosci. *2*, 266–270.

van Praag, H., Schinder, A.F., Christie, B.R., Toni, N., Palmer, T.D., and Gage, F.H. (2002). Functional neurogenesis in the adult hippocampus. Nature *415*, 1030–1034.

Ramón y Cajal, S. (1891). Comunicacion acerca de la significación fisiológica de las expansiones protoplásmicas y nerviosas de la sustancia gris. Primer Congr. Méd.-Farm. Reg. Valencia 671–679.

Rankin-Gee, E.K., McRae, P.A., Baranov, E., Rogers, S., Wandrey, L., and Porter, B.E. (2015). Perineuronal net degradation in epilepsy. Epilepsia *56*, 1124–1133.

Restivo, L., Vetere, G., Bontempi, B., and Ammassari-Teule, M. (2009). The formation of recent and remote memory is associated with time-dependent formation of dendritic spines in the hippocampus and anterior cingulate cortex. J. Neurosci. Off. J. Soc. Neurosci. *29*, 8206–8214.

Rhodes, J.S., van Praag, H., Jeffrey, S., Girard, I., Mitchell, G.S., Garland, T., and Gage, F.H. (2003). Exercise increases hippocampal neurogenesis to high levels but does not improve spatial learning in mice bred for increased voluntary wheel running. Behav. Neurosci. *117*, 1006–1016.

Robertson, B.-A., Rathbone, L., Cirillo, G., D'Eath, R.B., Bateson, M., Boswell, T., Wilson, P.W., Dunn, I.C., and Smulders, T.V. (2017). Food restriction reduces neurogenesis in the avian hippocampal formation. PLOS ONE *12*, e0189158.

Rodgers, J., Glod, M., Connolly, B., and McConachie, H. (2012). The relationship between anxiety and repetitive behaviours in autism spectrum disorder. J. Autism Dev. Disord. *42*, 2404–2409.

Rosenbrock, H., Koros, E., Bloching, A., Podhorna, J., and Borsini, F. (2005). Effect of chronic intermittent restraint stress on hippocampal expression of marker proteins for synaptic plasticity and progenitor cell proliferation in rats. Brain Res. *1040*, 55–63.

Roullet, F.I., Lai, J.K.Y., and Foster, J.A. (2013). In utero exposure to valproic acid and autism--a current review of clinical and animal studies. Neurotoxicol. Teratol. *36*, 47–56.

Sahay, A., Scobie, K.N., Hill, A.S., O'Carroll, C.M., Kheirbek, M.A., Burghardt, N.S., Fenton, A.A., Dranovsky, A., and Hen, R. (2011). Increasing adult hippocampal neurogenesis is sufficient to improve pattern separation. Nature *472*, 466–470.

Sale, A., Maya Vetencourt, J.F., Medini, P., Cenni, M.C., Baroncelli, L., De Pasquale, R., and Maffei, L. (2007). Environmental enrichment in adulthood promotes amblyopia recovery through a reduction of intracortical inhibition. Nat. Neurosci. *10*, 679–681.

Sánchez-Vidaña, D.I., Chan, N.-M.J., Chan, A.H.L., Hui, K.K.Y., Lee, S., Chan, H.-Y., Law, Y.S., Sze, M.Y., Tsui, W.-C.S., Fung, T.K.H., et al. (2016). Repeated treatment with oxytocin promotes hippocampal cell proliferation, dendritic maturation and affects socio-emotional behavior. Neuroscience *333*, 65–77.

Schlessinger, A.R., Cowan, W.M., and Gottlieb, D.I. (1975). An autoradiographic study of the time of origin and the pattern of granule cell migration in the dentate gyrus of the rat. J. Comp. Neurol. *159*, 149–175.

Seese, R.R., Maske, A.R., Lynch, G., and Gall, C.M. (2014). Long-term memory deficits are associated with elevated synaptic ERK1/2 activation and reversed by mGluR5 antagonism in an animal model of autism. Neuropsychopharmacol. Off. Publ. Am. Coll. Neuropsychopharmacol. *39*, 1664–1673.

Segal, M. (2001). Rapid plasticity of dendritic spine: hints to possible functions? Prog. Neurobiol. *63*, 61–70.

Seki, T., and Arai, Y. (1995). Age-related production of new granule cells in the adult dentate gyrus. Neuroreport *6*, 2479–2482.

Selemon, L.D., and Goldman-Rakic, P.S. (1985). Longitudinal topography and interdigitation of corticostriatal projections in the rhesus monkey. J. Neurosci. Off. J. Soc. Neurosci. *5*, 776–794.

Sforazzini, F., Bertero, A., Dodero, L., David, G., Galbusera, A., Scattoni, M.L., Pasqualetti, M., and Gozzi, A. (2016). Altered functional connectivity networks in acallosal and socially impaired BTBR mice. Brain Struct. Funct. *221*, 941–954.

Sharott, A., Doig, N.M., Mallet, N., and Magill, P.J. (2012). Relationships between the firing of identified striatal interneurons and spontaneous and driven cortical activities in vivo. J. Neurosci. Off. J. Soc. Neurosci. *32*, 13221–13236.

Shin, N.Y., Lee, T.Y., Kim, E., and Kwon, J.S. (2014). Cognitive functioning in obsessive-compulsive disorder: a meta-analysis. Psychol. Med. *44*, 1121–1130.

Simon, M., Czéh, B., and Fuchs, E. (2005). Age-dependent susceptibility of adult hippocampal cell proliferation to chronic psychosocial stress. Brain Res. *1049*, 244–248.

Skaar, D.A., Shao, Y., Haines, J.L., Stenger, J.E., Jaworski, J., Martin, E.R., DeLong, G.R., Moore, J.H., McCauley, J.L., Sutcliffe, J.S., et al. (2005). Analysis of the RELN gene as a genetic risk factor for autism. Mol. Psychiatry *10*, 563–571.

Slaker, M., Churchill, L., Todd, R.P., Blacktop, J.M., Zuloaga, D.G., Raber, J., Darling, R.A., Brown, T.E., and Sorg, B.A. (2015). Removal of perineuronal nets in the medial prefrontal cortex impairs the acquisition and reconsolidation of a cocaine-induced conditioned place preference memory. J. Neurosci. Off. J. Soc. Neurosci. *35*, 4190–4202.

Sliwowska, J.H., Barker, J.M., Barha, C.K., Lan, N., Weinberg, J., and Galea, L. a. M. (2010). Stress-induced suppression of hippocampal neurogenesis in adult male rats is altered by prenatal ethanol exposure. Stress Amst. Neth. *13*, 301–313.

Sompol, P., Liu, X., Baba, K., Paul, K.N., Tosini, G., Iuvone, P.M., and Ye, K. (2011). N-acetylserotonin promotes hippocampal neuroprogenitor cell proliferation in sleep-deprived mice. Proc. Natl. Acad. Sci. *108*, 8844–8849.

Song, J., Sun, J., Moss, J., Wen, Z., Sun, G.J., Hsu, D., Zhong, C., Davoudi, H., Christian, K.M., Toni, N., et al. (2013). Parvalbumin interneurons mediate neuronal circuitry–neurogenesis coupling in the adult hippocampus. Nat. Neurosci. *16*, 1728–1730.

Sorg, B.A., Berretta, S., Blacktop, J.M., Fawcett, J.W., Kitagawa, H., Kwok, J.C.F., and Miquel, M. (2016). Casting a Wide Net: Role of Perineuronal Nets in Neural Plasticity. J. Neurosci. *36*, 11459–11468.

Sorrells, S.F., Paredes, M.F., Cebrian-Silla, A., Sandoval, K., Qi, D., Kelley, K.W., James, D., Mayer, S., Chang, J., Auguste, K.I., et al. (2018). Human hippocampal neurogenesis drops sharply in children to undetectable levels in adults. Nature.

Spalding, K.L., Bergmann, O., Alkass, K., Bernard, S., Salehpour, M., Huttner, H.B., Boström, E., Westerlund, I., Vial, C., Buchholz, B.A., et al. (2013). Dynamics of Hippocampal Neurogenesis in Adult Humans. Cell *153*, 1219–1227.

Stanfield, B.B., and Trice, J.E. (1988). Evidence that granule cells generated in the dentate gyrus of adult rats extend axonal projections. Exp. Brain Res. *72*, 399–406.

Steiner, H., and Tseng, K.Y. (2010). Handbook of Basal Ganglia Structure and Function (Academic Press).

Stephenson, D.T., O'Neill, S.M., Narayan, S., Tiwari, A., Arnold, E., Samaroo, H.D., Du, F., Ring, R.H., Campbell, B., Pletcher, M., et al. (2011). Histopathologic characterization of the BTBR mouse model of autistic-like behavior reveals selective changes in neurodevelopmental proteins and adult hippocampal neurogenesis. Mol. Autism *2*, 7.

Steullet, P., Cabungcal, J.-H., Cuénod, M., and Do, K.Q. (2014). Fast oscillatory activity in the anterior cingulate cortex: dopaminergic modulation and effect of perineuronal net loss. Front. Cell. Neurosci. *8*.

Stranahan, A.M., Khalil, D., and Gould, E. (2006). Social isolation delays the positive effects of running on adult neurogenesis. Nat. Neurosci. *9*, 526–533.

Strüber, M., Jonas, P., and Bartos, M. (2015). Strength and duration of perisomatic GABAergic inhibition depend on distance between synaptically connected cells. Proc. Natl. Acad. Sci. *112*, 1220–1225.

Sun, L., Grützner, C., Bölte, S., Wibral, M., Tozman, T., Schlitt, S., Poustka, F., Singer, W., Freitag, C.M., and Uhlhaas, P.J. (2012). Impaired gamma-band activity during perceptual organization in adults with autism spectrum disorders: evidence for dysfunctional network activity in frontal-posterior cortices. J. Neurosci. Off. J. Soc. Neurosci. *32*, 9563–9573.

Swaab, D.F., and Uylings, H.B.M. (1988). Potentialities and pitfalls in the use of human brain material in molecular neuroanatomy. In Molecular Neuroanatomy, (Amsterdam: Elsevier), pp. 403–416.

Tanapat, P., Hastings, N.B., Rydel, T.A., Galea, L.A., and Gould, E. (2001). Exposure to fox odor inhibits cell proliferation in the hippocampus of adult rats via an adrenal hormone-dependent mechanism. J. Comp. Neurol. *437*, 496–504.

Thomas, R.M., Urban, J.H., and Peterson, D.A. (2006). Acute exposure to predator odor elicits a robust increase in corticosterone and a decrease in activity without altering proliferation in the adult rat hippocampus. Exp. Neurol. *201*, 308–315.

Thomas, R.M., Hotsenpiller, G., and Peterson, D.A. (2007). Acute Psychosocial Stress Reduces Cell Survival in Adult Hippocampal Neurogenesis without Altering Proliferation. J. Neurosci. *27*, 2734–2743.

Toni, N., Teng, E.M., Bushong, E.A., Aimone, J.B., Zhao, C., Consiglio, A., van Praag, H., Martone, M.E., Ellisman, M.H., and Gage, F.H. (2007). Synapse formation on neurons born in the adult hippocampus. Nat. Neurosci. *10*, 727–734.

Toni, N., Laplagne, D.A., Zhao, C., Lombardi, G., Ribak, C.E., Gage, F.H., and Schinder, A.F. (2008). Neurons born in the adult dentate gyrus form functional synapses with target cells. Nat. Neurosci. *11*, 901–907.

Tronel, S., Fabre, A., Charrier, V., Oliet, S.H.R., Gage, F.H., and Abrous, D.N. (2010). Spatial learning sculpts the dendritic arbor of adult-born hippocampal neurons. Proc. Natl. Acad. Sci. *107*, 7963–7968.

Tung, A., Takase, L., Fornal, C., and Jacobs, B. (2005). Effects of sleep deprivation and recovery sleep upon cell proliferation in adult rat dentate gyrus. Neuroscience *134*, 721–723.

Turner, K.C., Frost, L., Linsenbardt, D., McIlroy, J.R., and Müller, R.-A. (2006). Atypically diffuse functional connectivity between caudate nuclei and cerebral cortex in autism. Behav. Brain Funct. BBF *2*, 34.

Uhlhaas, P.J., and Singer, W. (2012). Neuronal Dynamics and Neuropsychiatric Disorders: Toward a Translational Paradigm for Dysfunctional Large-Scale Networks. Neuron *75*, 963–980.

Van Bokhoven, P., Oomen, C.A., Hoogendijk, W.J.G., Smit, A.B., Lucassen, P.J., and Spijker, S. (2011). Reduction in hippocampal neurogenesis after social defeat is long-lasting and responsive to late antidepressant treatment. Eur. J. Neurosci. *33*, 1833–1840.

Veenema, A.H., de Kloet, E.R., de Wilde, M.C., Roelofs, A.J., Kawata, M., Buwalda, B., Neumann, I.D., Koolhaas, J.M., and Lucassen, P.J. (2007). Differential effects of stress on adult hippocampal cell proliferation in low and high aggressive mice. J. Neuroendocrinol. *19*, 489–498.

Vivar, C., Peterson, B.D., and van Praag, H. (2016). Running rewires the neuronal network of adult-born dentate granule cells. NeuroImage *131*, 29–41.

Wang, J., Barstein, J., Ethridge, L.E., Mosconi, M.W., Takarae, Y., and Sweeney, J.A. (2013). Resting state EEG abnormalities in autism spectrum disorders. J. Neurodev. Disord. *5*, 24.

Wang, X., Tao, J., Qiao, Y., Luo, S., Zhao, Z., Gao, Y., Guo, J., Kong, J., Chen, C., Ge, L., et al. (2018). Gastrodin Rescues Autistic-Like Phenotypes in Valproic Acid-Induced Animal Model. Front. Neurol. *9*.

Wei, D., Dinh, D., Lee, D., Li, D., Anguren, A., Moreno-Sanz, G., Gall, C.M., and Piomelli, D. (2016). Enhancement of Anandamide-Mediated Endocannabinoid Signaling Corrects Autism-Related Social Impairment. Cannabis Cannabinoid Res. *1*, 81–89.

Winner, B., Desplats, P., Hagl, C., Klucken, J., Aigner, R., Ploetz, S., Laemke, J., Karl, A., Aigner, L., Masliah, E., et al. (2009). Dopamine receptor activation promotes adult neurogenesis in an acute Parkinson model. Exp. Neurol. *219*, 543–552.

Wiskott, L., Rasch, M.J., and Kempermann, G. (2006). A functional hypothesis for adult hippocampal neurogenesis: avoidance of catastrophic interference in the dentate gyrus. Hippocampus *16*, 329–343.

Wolf, S.A., Melnik, A., and Kempermann, G. (2011). Physical exercise increases adult neurogenesis and telomerase activity, and improves behavioral deficits in a mouse model of schizophrenia. Brain. Behav. Immun. *25*, 971–980.

Wong, E.Y.H., and Herbert, J. (2004). The corticoid environment: a determining factor for neural progenitors' survival in the adult hippocampus. Eur. J. Neurosci. *20*, 2491–2498.

Wong, E.Y.H., and Herbert, J. (2006). Raised circulating corticosterone inhibits neuronal differentiation of progenitor cells in the adult hippocampus. Neuroscience *137*, 83–92.

Workman, J.L., Raineki, C., Weinberg, J., and Galea, L.A.M. (2015). Alcohol and pregnancy: effects on maternal care, HPA axis function, and hippocampal neurogenesis in adult females. Psychoneuroendocrinology *57*, 37–50.

Wu, M.V., Shamy, J.L., Bedi, G., Choi, C.-W.J., Wall, M.M., Arango, V., Boldrini, M., Foltin, R.W., and Hen, R. (2014). Impact of Social Status and Antidepressant Treatment on Neurogenesis in the Baboon Hippocampus. Neuropsychopharmacology *39*, 1861–1871.

Yamada, J., Ohgomori, T., and Jinno, S. (2015). Perineuronal nets affect parvalbumin expression in GABAergic neurons of the mouse hippocampus. Eur. J. Neurosci. *41*, 368–378.

Yanes, C., Monzon-Mayor, M., Ghandour, M.S., de Barry, J., and Gombos, G. (1990). Radial glia and astrocytes in developing and adult telencephalon of the lizard Gallotia galloti as revealed by immunohistochemistry with anti-GFAP and anti-vimentin antibodies. J. Comp. Neurol. *295*, 559–568.

Yang, E.-J., Ahn, S., Lee, K., Mahmood, U., and Kim, H.-S. (2016). Early Behavioral Abnormalities and Perinatal Alterations of PTEN/AKT Pathway in Valproic Acid Autism Model Mice. PLOS ONE *11*, e0153298.

Yang, S., Cacquevel, M., Saksida, L.M., Bussey, T.J., Schneider, B.L., Aebischer, P., Melani, R., Pizzorusso, T., Fawcett, J.W., and Spillantini, M.G. (2015). Perineuronal net digestion with chondroitinase restores memory in mice with tau pathology. Exp. Neurol. *265*, 48–58.

Yin, H.H., and Knowlton, B.J. (2006). The role of the basal ganglia in habit formation. Nat. Rev. Neurosci. *7*, 464–476.

Yin, H.H., Knowlton, B.J., and Balleine, B.W. (2004). Lesions of dorsolateral striatum preserve outcome expectancy but disrupt habit formation in instrumental learning. Eur. J. Neurosci. *19*, 181–189.

Yuste, R. (2011). Dendritic Spines and Distributed Circuits. Neuron *71*, 772–781.

Zhao, C., Teng, E.M., Summers, R.G., Ming, G., and Gage, F.H. (2006). Distinct Morphological Stages of Dentate Granule Neuron Maturation in the Adult Mouse Hippocampus. J. Neurosci. *26*, 3–11.